Spring 3-28-2013

Actomyosin Contractility in Nonmuscle Cells

Nilushi Lakmali Dasanayake
Washington University in St. Louis

WASHINGTON UNIVERSITY IN ST LOUIS

Department of Physics

Dissertation Examination Committee:
Anders Carlsson, Chair
Phillip Bayly
Petra Levine
Zohar Nussinov
Yan Mei Wang
Ralf Wessel

Actomyosin Contractility in Nonmuscle Cells

by

Nilushi Lakmali Dasanayake

A dissertation presented to the
Graduate School of Arts and Sciences
of Washington University in
partial fulfillment of the
requirements for the degree
of Doctor of Philosophy

May 2013

St. Louis, Missouri

Contents

List of Figures

List of Tables

Acknowledgements

I wish to express my most sincere gratitude and appreciation to my advisor, Prof. Anders Carlsson for paving the way for this achievement. His knowledge, understanding, patience and guidance were truly exceptional and it wouldn't have been possible for me to accomplish this without his generous support.

Also I like to thank The Physics Department and National Institutes of Health (Grant R01 GM086882) for providing financial support.

Next I would like to thank Prof. Ralf Wessel, Prof. Yan Mei Wang, Prof. Zohar Nussinov, Prof. Phillip Bayly and Prof. Petra Levine for comprising my dissertation committee and also for providing great support, especially during the scheduling of my defense. Special thanks goes to Prof. Ralf Wessel and Prof. Yan Mei Wang for serving on my progress report committee and for giving advice and helpful comments.

I also want to take this opportunity to thank my loving parents Jayantha Fonseka and Dayakanthi Maddage for embracing me with love and being there for me through all the ups and downs. You made me who I am today, with boundless caring, with incommensurable effort and unconstrained enthusiasm regarding every little thing

about me, and I am ever so grateful for everything.

I also especially want to thank my brother Dinusha Lakmal Fonseka, my sister-in-law Chanika Gunarathne, my loving niece Yashitha Dilmi Fonseka and my cousin Anusha Kumari for your caring, love and great affection. I am extremely fortunate to have all of you in my life.

Further, I want to thank my parents in law, D. M. Ratnayake and Soma Ekanayake and also two brothers in-law, Charaka and Nalaka Dasanayake for accepting me as a daughter and a sister, and for giving me so much love and caring from the very first day we met.

I would like to thank all the professors at the Department of Physics, at the University of Peradeniya for helping me build a solid foundation of knowledge during my undergraduate studies. My special thanks to Dr. R. P. U. Karunasiri for being an excellent teacher and his guidance and support especially when applying to graduate school. If not for his advice, I would not even have thought of applying.

Next I would like to thank our friends from St. Louis, Lasitha Senadheera and Himasha Hadunge for taking great care of us when we first came to the US and helping us blend in successfully at the beginning. We will forever be thankful to you two for everything and for the friendship we share. Also my gratitude goes to Janaki and Bandula Guruge. I cannot be more thankful for the support you two gave us in last five years. I must mention that the help you gave during my parents in law's visit, throughout my pregnancy and during, and after the time of our daughter's birth

were truly unforgettable. We felt reassured because of your caring, understanding and friendship. I also thank Thanura Elvitigala and Hiranda Dodanwela for being dear friends to us and offering help whenever we needed. Finally I want to thank Waruni Jayawardane and Amila Weerasinghe for their extraordinary friendship. For all the help you two gave from the birth of our daughter to the end of my thesis work, thank you very much.

I would also like to mention here my friends from high school and college, especially Himali Indika Batagalla, Sanari Anasuya Fernando and Nasrul Aamina Zainudeen. Your friendship helped me keep going in difficult situations and I thank you from the depth of my heart for always being there for me.

I want to thank Simin Mahmoodifar and Dandan Hu for being the best office mates ever. Your company helped me keep my spirits high through the cold winters and steamy summers we spent together.

My special thanks also goes to all the members of the staff in the Physics Department. Specially Julia Hamilton, Tammy White, Sarah Hedly, Christina Saldivar, Debra Barco, Alison Verbeck and late Bob Poli, for their immense support, as well as Dr. Sai Iyer for his quick responses and very helpful advice on all the technical issues I had and also Marry for being such a good friend to me.

I also wish to thank Anatoly Zlotnik for proof reading my acknowledgement.

Finally I take this opportunity to thank my daughter Nethuli Pahanya Dasanayake, your are my inspiration and you give me strength to take my life forward, and my

husband, my soul mate, Isuru Sammana Dasanayake for his indispensable love, caring, support and for walking the extra mile with me. I thank you for doing everything for setting the background to make this a reality.

ABSTRACT OF THE DISSERTATION

Actomyosin Contractility in Nonmuscle Cells

by

Nilushi L. Dasanayake

Doctor of Philosophy in Physics

Washington University in St. Louis, 2013

Professor Anders E. Carlsson, Chair

Forces and stresses generated by the action of myosin minifilaments are analyzed via simulation of their motion in idealized computer-generated random, isotropic actin networks and bundles. The networks and bundles are generated as random collections of actin filaments in two dimensions with constrained orientations, crosslinked and attached to fixed walls (four walls for isotropic networks, two for bundles). Minifilaments are placed on actin filament pairs and allowed to move and deform the network so that it exerts forces on the walls. The stresses are overwhelmingly contractile in both cases, because minifilament equilibrium positions having contractile stress have lower energy than those for expansive stress. Mini-filaments rotate into these energetically stable contractile configurations. This process is aided by the bending of actin filaments, which accomodates mini-filament rotation. The presence of force chains leads to unexpectedly large stresses especially in the random networks. Stresses for bundles are greater than those for isotropic networks, and antiparallel filaments gener-

ate more tension than parallel filaments. The forces transmitted by the actin network to the walls of the simulation cell often exceed the tension in the minifilament itself.

Chapter 1

Introduction

The cytoskeleton of a eukaryotic cell consists of three types of protein polymers: actin, microtubules and intermediate filaments. They form the cytoplasmic matrix, which has viscous as well as elastic properties. The cytoskeleton provides physical support to the cell in a way similar to how the skeleton supports our body. It is also responsible for cellular motility, while providing tracks for numerous proteins that aid cell movement as well as those that transport various organelles or cellular cargo inside the cytoplasm. Many important phenomena sustaining life depend on cellular motility. Examples include the growth of a fertilized egg past its single cell stage, active cell shape changes in the embryo during growth, the motion of white blood cells triggered by invasion of an invading microorganism, and muscle contraction [13]. Molecular machines made up of protein motors and protein polymers are responsible for these biological movements. In many cases, these molecular motors move along

the tracks made up of the protein polymers making up the cytoskeleton.

Actomyosin contractility is a cytoskeletal phenomenon observed in many muscle as well as non-muscle cells. It generates pulling forces through mutual sliding of actin and myosin II filaments. This myosin II dependent contraction is essential for producing forces responsible for many biological processes such as cell migration, adhesion, cytokinesis, endocytosis, and axonal growth, as well as more complex motile processes influencing synaptic plasticity, embryonic axis patterning, and immune response [14].

Force generation by myosin on actin is generally believed to require parallel or nearly parallel arrangement of actin filaments. Retraction of the trailing edge of a cell during cell migration depends on the action of non-muscle myosin II located towards the rear of the cell [15], where actin filaments are longer and more parallel than those at the leading edge of the cell. Also, stress fibers that exert forces on the cell's environment are made up of actin filaments that are almost parallel bundles. Moreover traction studies of cells provide strong evidence for correspondence between myosin distribution and contraction [16, 17]. However the actin filament arrangements in cells are often disordered and it is not known how contraction is generated in such cases.

In this study we are trying to come up with a plausible mechanism of contractility observed in these actomyosin systems that lack ordered arrangement of filaments.

1.1 Actin

1.1.1 Structure

Actin is a globular protein with a weight of about 42 kDa. Monomeric actin (G-actin) polymerizes to form two-stranded helical filaments. This filamentous or polymeric actin is called F-actin. Actin filaments participate in many important cellular processes including muscle contraction, cell motility, cell division and cytokinesis, vesicle and organelle movement, cell signaling, and the establishment and maintenance of cell junctions and cell shape [14]. Many of these processes are mediated by extensive and intimate interactions of actin with cellular membranes. With the interaction of many other proteins, actin filaments form higher-order structures such as stress fibers, dendritic lamellar arrays, cortical networks, filopodial bundles, and contractile rings depending on their position in the cell.

Fig. 1.1 is a ribbon representation of an actin monomer. A hypothetical vertical line divides the actin monomer into two domains, a "large" left side and a "small" right side. These two domains are further divided into two subdomains each. The small domain consists of subdomains 1 and 2 and the large domain is comprised of subdomains 3 and 4. Subdomain 2 is the lightest and this introduces a polarity to actin. The two ends are called the barbed end (the side of subdomains 1 and 3) and the pointed end (side of subdomains 2 and 4). This polarity is key to the mechanism of actin assembly in cells.

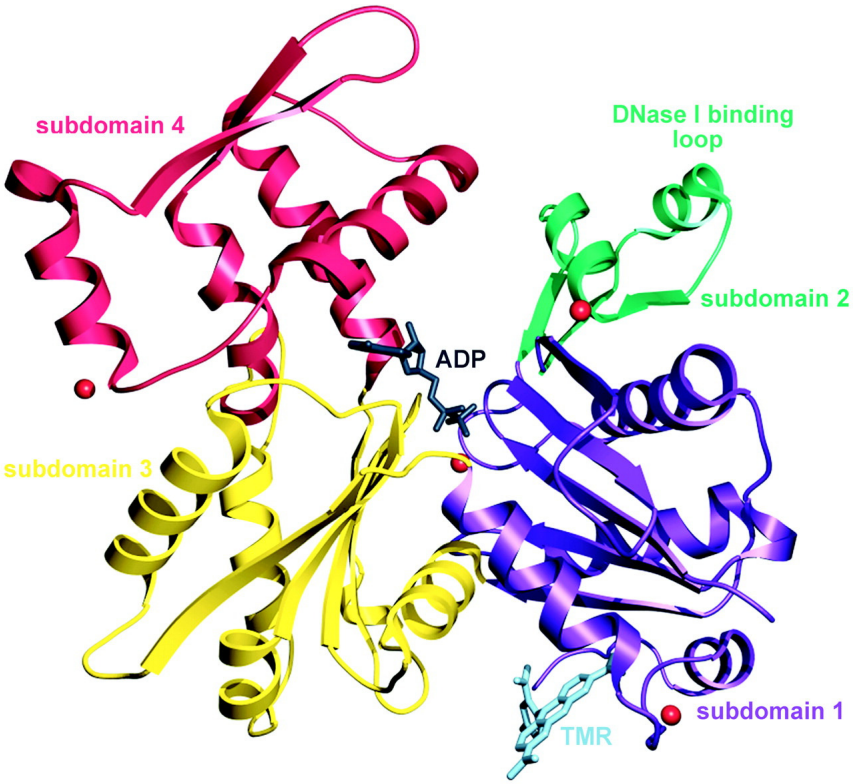

Figure 1.1: Monomeric actin, ribbon representation of an un-complexed actin monomer in the ADP state. Figure taken from [1].

1.1.2 Dynamic nature

Dynamic behavior is an important character of actin filaments. Depending on the requirements of the cell, actin is used in strenuous structural tasks requiring stability as well as in more dynamic continually renewing assemblies. For example, in actin bundles in microvilli, a collection of specialized actin-binding proteins stabilize the filament, forming a more permanent structure, whereas at the leading edge of a typical

moving cell, filaments are continuously disassembled and rebuilt. Polymerization of an actin filament is more prominent at barbed end while depolymerization dominates at the pointed end. In a dynamic actin structure at steady state, monomers are added at the barbed end and removed at the pointed end at the same rate, maintaining a constant filament length while the center of the filament moves towards the barbed end. This phenomenon is known as treadmilling.

Treadmilling of actin is controlled by ATP hydrolysis in the filaments as the nucleotide state determines the stability of the actin filament. ATP is bound in the cleft between the two major domains of an actin monomer. A free actin monomer that holds an ATP molecule can bind tightly to growing filaments. After attaching, by association with a water molecule, ATP cleaves its Pi and goes to a ADP-Pi state where the Pi remains in close proximity to the ADP. Since the cleft is closed upon F-ATP association, Pi release is slower than the cleavage. When the Pi is released, the affinity between actins in the ADP state becomes weak, so the subunits disassemble from the filament at this stage. Free actin monomers have low affinity to ADP, hence it releases the ADP, allowing another ATP in the solution to enter. This cycle continues in steady state. The diagram on the right in Fig. 1.2 is a schematic showing the cleavage and release processes [18].

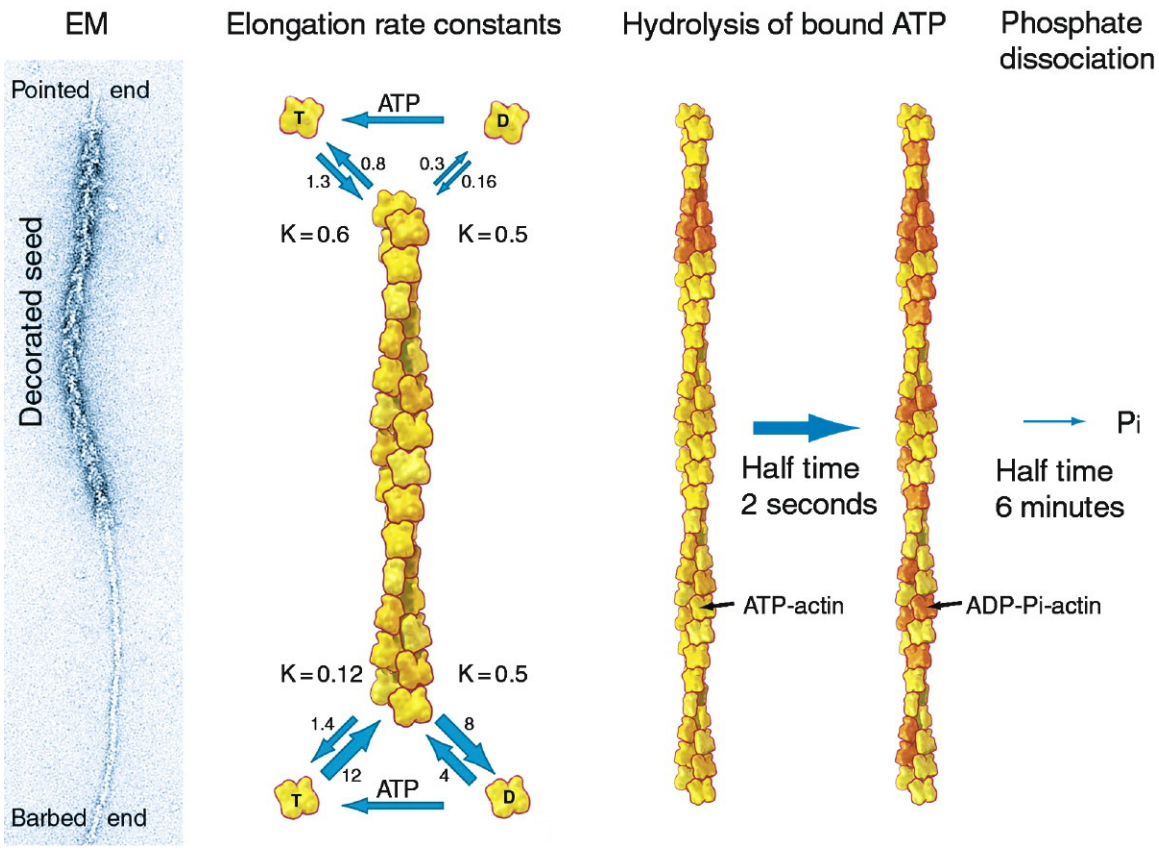

Figure 1.2: Polymerization of an actin filament with, rate constants for association and dissociation of actin monomers at both barbed and pointed ends, Pi cleavage and release. Left most panel shows an electron micrograph of an actin filament decorated by myosin heads. Thin lower tail represents elongation of the actin filament with ATP actin monomers (not decorated with myosin heads). Panel with the heading "Elongation rate constants" shows rate constants for association and dissociation of actin monomers from pointed and barbed ends. Unit of association constant is $\mu M^{-1}s^{-1}$ while that of dissociation constants is s^{-1}. K represents the ratio of the dissociation rate constant to the association rate constant and hence it has units μM. Right most panels show the Pi cleavage and release and the former is faster while the later takes longer time.

There are three major models of ATP hydrolysis that have been used to interpret experimental data: (i) Random ATP hydrolysis. ATP is assumed to be hydrolyzed at a rate that is independent of the type of nucleotide bound to adjacent filament subunits [19]. (ii) Cooperative hydrolysis. The rate of ATP hydrolysis is thought to depend on the type of nucleotide bound to adjacent subunits [20]. (iii) Sequential hydrolysis. ATP assumed to be hydrolyzed only at the interface between ATP-subunits and ADP-subunits [21]. Recent work [22] suggests that by considering available experimental evidence it is not possible to exclude cooperative hydrolysis even though most workers have assumed random hydrolysis. Novel experimental techniques and methods should be used to foster new ideas and knowledge on this still unclear but crucial issue.

1.2 Myosin II

Myosins constitute a large superfamily of actin-dependent molecular motors that play an important role in cellular processes that require force and translocation [23, 2, 24]. Phylogenetic analyses have categorized myosins in eukaryotic cells into more than 15 different classes. However they are broadly divided into two groups as conventional myosins and unconventional myosins. Class II myosins that are found in muscle and non-muscle cells belong to the conventional myosins as they were the only myosins known for decades [25]. All the other classes of myosins fall under unconventional

myosins.

1.2.1 Structure

Myosin II is a key player in actin dependent contraction and moves towards the positive or the barbed end of actin filaments. Due to this directional movement of myosins, they propel the sliding of, or produce tension on, actin filaments. This requires energy, which is provided by the hydrolysis of ATP, and requires myosins to have catalytic sites with ATPase activity [2]. Non-muscle myosin II (NM II) is a hexamer composed of two heavy chains, two essential light chains, and two myosin regulatory light chains. Its structure has three functional subdomains: (i) The globular head or motor domain which contains the binding site for actin and ATP. This globular head is also known as the crossbridge in muscle myosin II. (II) The neck domain that binds two $20kDa$ regulatory light chains (RLCs) that regulate NM II activity and two $17kDa$ essential light chains (ELCs) that stabilize the heavy chain structure (III) The tail domain which serves to anchor and position the motor domain so that it can interact with actin. The anchoring part is a $230kDa$ heavy chain, a long α-helical coiled coil, which forms an extended rod-shape that effects dimerization between the heavy chains and terminates in a relatively short non-helical tail as shown in Fig. 1.3 a).

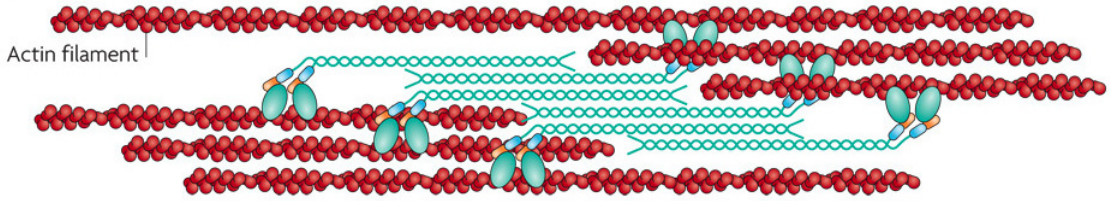

Figure 1.3: Non muscle myosin II assembly. NM II dimers interact through their tail domains and form filaments such that the head domains are at the ends of filaments. These are known as mini-filaments and are typically 0.4 μm in size. Figure taken from [2]

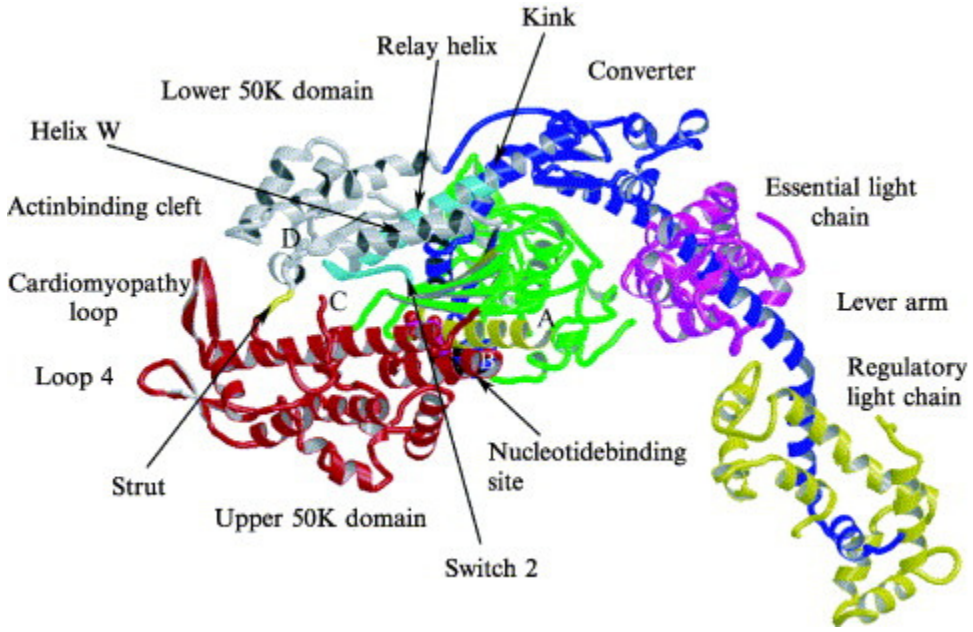

Figure 1.4: Ribbon representation of the S-1 fragment of the myosin II molecule. Lower $50kDa$ domain (grey) and upper $50kDa$ domian (red) compose the actin binding surface. Nucleotide binding site is at the bottom of the actin binding cleft. Figure taken from [3]

.

S-1 is a fragment of NM II that contains the motor domain and neck but lacks the rod domain and is unable to dimerize Fig. 1.4. Heavy meromyosin (HMM) is a fragment that contains the motor domain, neck and enough of the rod to effect dimerization.

Myosin II molecules assemble into bipolar filaments through interactions between their rod domains. Myosin filaments in non muscle cells are known as mini-filaments and in muscle cells these structures are called thick filaments. The main difference is the size and hence the amount of myosin heads attached in each configuration. A mini-filament usually has about 30-40 myosin heads and the length is about 0.4 μm whereas thick filaments usually have about 300 myosin heads attached and can be about 3 μm long. These filaments bind to actin through their head domains and the ATPase activity of the head enables a conformational change (known as power stroke) that moves actin filaments in an anti-parallel manner. Bipolar myosin filaments also work as crosslinks to bind actin filaments together in thick bundles that form cellular structures such as stress fibers. Fig. 1.5 is an electron micrograph of a platelet myosin minifilament.

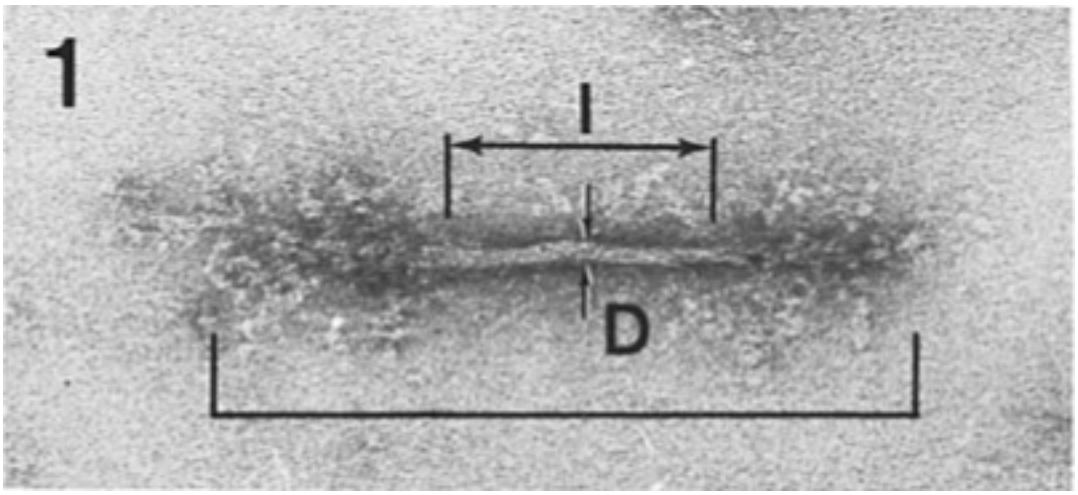

Figure 1.5: An electron micrograph of a myosin II minifilament. The bracket indicates the length of the minifilament which was 400 nm. Image is at a magnification $\times$ 150,000. Figure taken from [4]

Since myosin is found mostly in aggregated state or in the filament form, it is difficult to measure forces and displacements due to a single myosin molecule. However Ref. [5] showed that the force applied by a myosin molecule is on the order of piconewtons and the displacement of actin filaments due to a single power stroke is a couple of nanometers. There, to measure these single molecular measurements, a low concentration of HMM was allowed to interact with a single actin filament. The experimental setup is shown in Fig. 1.6.

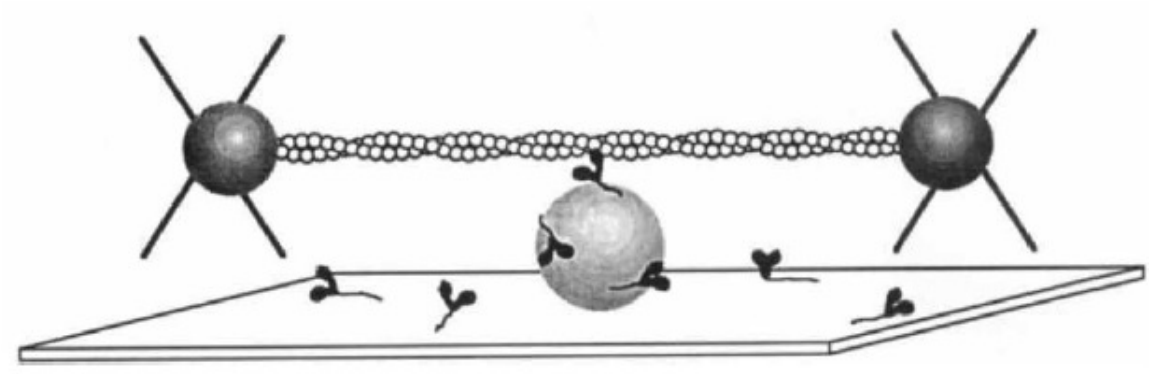

Figure 1.6: Schematic diagram of the experimental setup used to measure displacement due to myosin II function. Silica bead (light colored bead in the middle) coated with N-ethylmaleimide is firmly attached to a cover slip. Both the bead and the coverslip are coated with HMM. The dark colored beads keep the actin filament (represented as a double helix) stretched and fixed in space with the aid of optical traps. The actin filament has been brought close to the silica bead to allow HMM to attach and generate forces on the actin filament. Figure taken from [5].

The displacement of one of the beads was detected using a high resolution position detector and since the spring constant of the traps were known, the forces were calculated using the displacement measurements using the fact that the force is proportional to the displacement for a given power stroke. Force measurements are shown in Fig. 1.7.

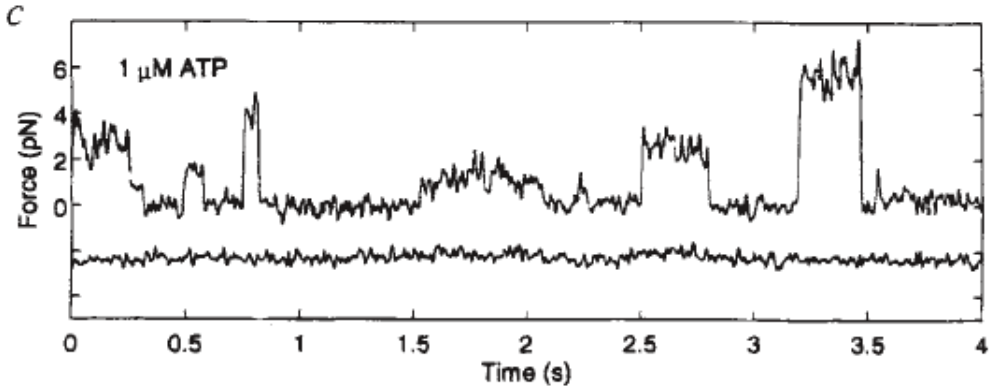

Figure 1.7: Upper trace represents the force applied on the actin filament along its length. The lower trace shows the force applied on the filament perpendicular direction. Figure taken from [5].

No force was applied on the filament in the transverse direction and the force on a given actin filament was always in one direction along the length. The observed average step size here was 11 nm while the average force produced by a single myosin molecule was about $3 - 4$ pN.

1.3 Muscle Contraction

Muscles are made up of tubular muscle cells known as muscle fibers or myofibers. These myofibers are composed of tubular myofibrils. The building blocks of myofibrils are sarcomeres. Fig. 1.8 shows the components of a muscle. A sarcomere consists of mainly actin and myosin II proteins. Sarcomeric organization in striated muscles

has a highly ordered structure to aid efficient contraction. The resting length of a sarcomere in muscle is about $2 - 3\mu m$ [26]

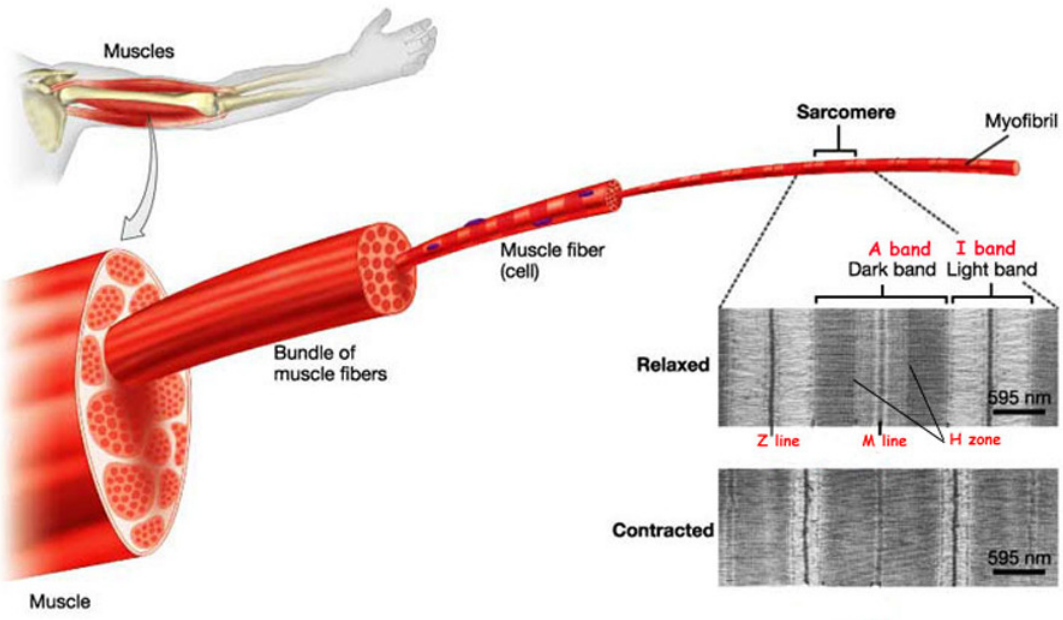

Figure 1.8: Anatomy of the striated muscle. On the right is an electron micrograph (EM) of a sarcomere. Figure taken from [6]

1.3.1 Structure of the sarcomere

Fig. 1.9 shows a schematic diagram of a filament arrangement in sarcomere. There, actin filaments are arranged in order such that all the pointed ends are pointing inwards. These actin filaments are called thin filaments and the myosin filaments are called thick filaments. Due to this special arrangement, when the myosin heads

become active, they try to move toward the barbed ends resulting in contraction of the entire structure. Depending on the composition, the sarcomere is divided into different regions. Thin filaments are attached to the Z line which is the dark line shown in the EM of Fig. 1.8. The region between two Z lines is defined as the sarcomere. Surrounding the Z line is the I band. It is named the I band since this area is "Isotropic" as only thin filaments reside there but not thick filaments. Similarly, the A band is the "Anisotropic" region where the thin filaments and thick filaments both reside. The length of the A band is equal to that of a thick filament. The H band is the lighter region within the A band (see the EM in Fig. 1.8), it is the middle section where only the thick filaments are. The M line defines the middle of the sarcomere and consists of thick filament crosslinking molecules that keep the structure stable 1.9.

1.3.2 Function of the sarcomere

The myosin head or the crossbridge is the active component in muscle contraction. This process is fueled by ATP hydrolysis. When the muscle is at rest, ATP is bound to the myosin head. The myosin head has a low energy configuration and cannot bind to actin filaments at this stage. However ATP can hydrolyze to become ADP and an inorganic phosphate group. This is a dissipative process and the energy released here is stored in the myosin head transforming it to a high energy state. At this point, the myosin head is ready attach to actin and to do work using the stored energy similar

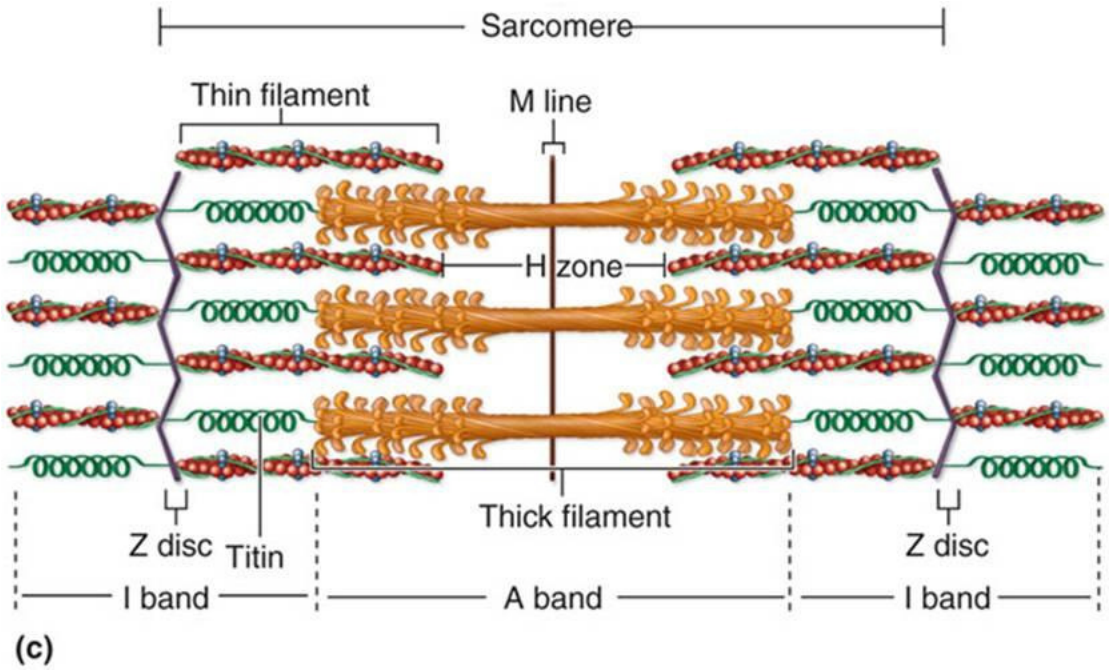

Figure 1.9: Sarcomere arrangement in muscle contraction. Depending on the composition, the sarcomere is divided into different regions. (http://www.studyblue.com/notes/note/n/chapter-10-muscle-tissue/deck/1176893)

to a stretched spring. In sarcomeres actin thin filaments are associated with a protein called tropomyosin. Tropomyosins blocks the myosin binding site on actin as shown in Fig. 1.10 a). A protein called troponin is attached to tropomyosin. When Ca^{+2} ions associate with troponins, a structural change occurs in tropomyosins which moves them away, uncovering myosin binding sites on actin thin filaments (Fig. 1.10b). At this point, excited myosin heads attach to exposed binding sites on thin filaments while releasing the phosphate [3]. The energy stored in the myosin head is used for the power stroke which causes the myosin head to return to its starting configuration.

This movement involves the swinging of the light chain binding region through an angle of $\sim 70^{\circ}$ while translocating the bound actin filament $\sim 10nm$ towards its pointed end direction [29]. ADP is released during this movement.

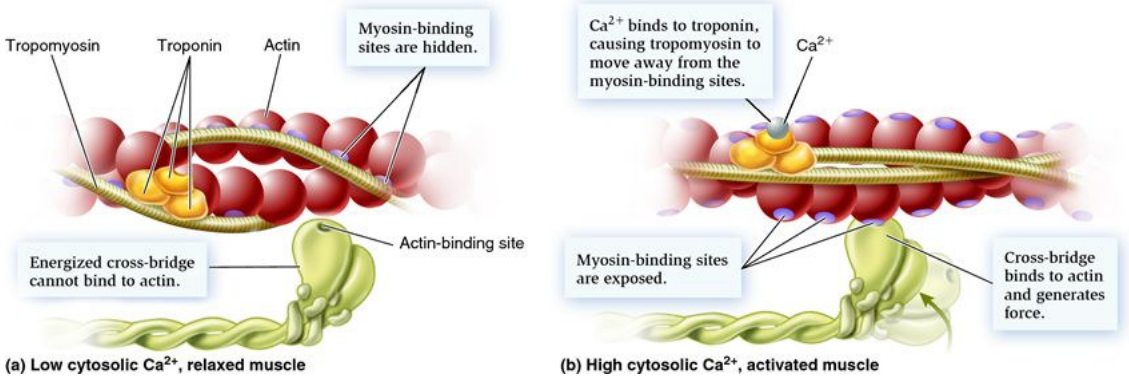

Figure 1.10: Binding of the myosin head to actin thin filaments in muscle contraction. a) Before Ca^{+2} association b) After Ca^{+2} association. (http://biology-forums.com/index.php?action=gallery;sa=view;id=1189)

This nucleotide free state in the actomyosin complex is known as the "rigor" state. Myosins have very high affinity to actin in rigor. The binding of an ATP to the ATPase site in the myosin heads dissociates the actomyosin complex readily. Hydrolysis of this ATP brings the myosin head again to the upright excited state which is ready to bind to actin. If the Ca^{+2} ions are still available to expose the myosin binding site, the cycle continues. The Ca^{+2} concentration in muscles is regulated by the sarcoplasmic reticulum, a unique form of endoplasmic reticulum in the sarcoplasm. The sarcoplasm exists in the region between the muscle fibers in muscle tissues [30].

1.4 Background on Myosin II in Non-Muscle Cells

Despite the fairly complete understanding of the mechanism behind muscle contraction, the microscopic origin of contraction in non-muscle cells is yet unknown. Remarkably, even without an ordered arrangement, myosin II in actin networks provides mostly contractile stress as opposed to extensile stress. Evidence for this phenomenon can be found in many biological processes such as tail retraction during cell migration, pinching off the mother cell into two in cytokinesis that leads to cell division, and in remodeling the matrix during wound healing. During cell migration, the front of the cell moves forward mainly by actin polymerization, whereas in the cell rear, an abundance of myosin II is found. Interaction of these myosins with actin produces contraction, which facilitates the retraction of the cell from the substrate, allowing the cell to move forward. In cytokinesis [31], preceded by mitosis, an actomyosin ring is formed around the center of the cell. With the consumption of ATP, the myosins start to pull on actin, resulting in contraction of the ring. With contraction, the diameter of the ring decreases while pinching the cell off. Similarly in wound healing [32], myosin II and actin preferentially accumulate, and a stable contractile actomyosin ring is formed, around the wound. Due to the contraction of the ring, the corners of a wound round up as contracting actin pull its edges in. Breakage of this contractile ring prevents proper closure of the wound.

However we still lack a qualitative understanding of myosin-based force genera-

tion in disordered actin structures. The minimum requirements for contractility in these actomyosin structures remain to be determined. In other words, the dominant mechanism which converts the motion of myosin heads toward barbed ends of actin filaments into contraction has not been established. Furthermore, the relationship between the molecular-level forces exerted by a myosin mini-filament, and the macroscopic stress, is not known. Some previous studies have tried to address these questions. Application of hydrodynamic theory to linear actin bundles suggested that contraction occurs only if mini-filaments reaching the barbed end stay there [8, 33]. Other calculations treating one dimensional bundles found that nonlinearities such as buckling are required for contractility [34, 9, 10]. Reference [9] also suggested that having linkers with non-identical unloaded velocities is important for generating these nonlinearities, which in turn lead to contractility. Below we summarize the models that have been proposed to date.

1.4.1 Existing theoretical models

Ref. [8] describes a model that could be applied to simple one dimensional structures such as stress fibers. They considered a linear bundle of aligned polar filaments distributed along the x-axis, each of which has length l. Only two types of filament interactions were considered. Fig. 1.12 is a schematic representation of the motor-filament interactions. Motors are assumed to move towards the barbed (plus) ends and the arrows indicate the direction of filament motion. Table 1.1 defines the

notation they used in the model:

Table 1.1: Notation used

$C^+(x)$	Number density of filaments with their center at position x with plus end pointing to the right.
$C^-(x)$	Number density of filaments with their center at position x with plus end pointing to the left.
J^{+-}, J^{-+}	Active filament currents created by the activity of motors connected between antiparallel filaments.
J^{++}, J^{--}	Active filament currents created by the activity of motors connected between parallel filaments.
$\upsilon^{\pm\pm}$	Effective relative velocity between parallel filaments a distance ξ (parallel to to filaments) apart induced by events of motor activity
$\upsilon^{\pm\mp}$	Effective relative velocity between antiparallel filaments. a distance ξ apart induced by events of motor activity
D	Diffusion coefficient of actin filaments

For the conservation of filament number,

$$\begin{aligned} \partial_t C^+ &= D\partial_x^2 C^+ - \partial_x J^{++} - \partial_x J^{+-} \\ \partial_t C^- &= D\partial_x^2 C^- - \partial_x J^{--} - \partial_x J^{-+} \end{aligned} \tag{1.1}$$

Using the fact that the direction of filament motion induced by a motor depends only on the filaments relative orientation, they used general symmetry arguments to write expressions for filament currents without referring to any specific interaction mechanism.

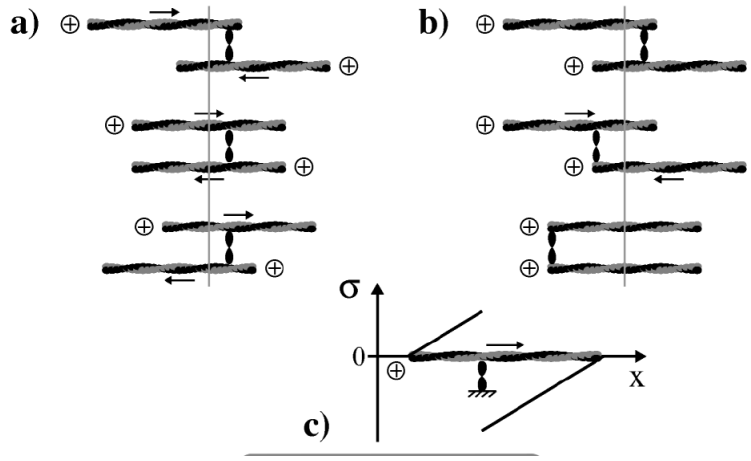

Figure 1.11: Relative displacements for parallel and antiparallel filaments with respective to center of gravity for the filament pair, represented by the vertical line in the middle for each case. (a) Interaction between antiparallel filaments that slide in opposing directions. (b) Relative motion between parallel filaments occurs if a motor binds to the plus end. In that case they tend to align their plus ends. (c) Tension profile σ along a filament driven by a point force. Figure taken from [8].

symmetry arguments:

I. In the absence of external forces, momentum conservation requires that the center of gravity remains fixed when filaments are displaced.

$$v^{\pm\pm}(\xi) = -v^{\pm\pm}(-\xi)$$

$$v^{+-}(\xi) = -v^{-+}(-\xi)$$

II. Invariance of the system with respect to inversion of space gives:

$$\upsilon^{++}(\xi) = -\upsilon^{--}(-\xi)$$

For simplicity, the authors took

$$\upsilon^{-+}(\xi) = -\upsilon^{+-}(-\xi) = \beta \tag{1.2}$$

$$\upsilon^{++}(\xi) = \upsilon^{--}(\xi) = \alpha \; sign(\xi)$$

where α and β are constants and $sign(\xi) = \pm 1$, based on sign of ξ. Hence the currents that describe the dynamics of the model were as follows:

$$\begin{aligned} J^{\pm\pm}(x) &= \alpha \int_0^l d\xi \; [c^{\pm}(x+\xi) - c^{\pm}(x-\xi)]c^{\pm}(x), \\ J^{\pm\mp}(x) &= \mp\beta \int_{-l}^l d\xi \; c^{\mp}(x+\xi)c^{\pm}(x) \end{aligned} \tag{1.3}$$

By calculating the average tension in the bundle they showed that positive tension or contraction occurs for all $\alpha > 0$. Hence the main conclusions were: 1) Interaction of parallel filaments induces unstable behavior and is responsible for active contraction and tension in the bundle, under the assumption that a mini-filament stays attached when it reaches the barbed end. 2) Interaction of antiparallel filaments leads to filament sorting.

Ref. [9] developed a more detailed model of contraction in bundles, based on the experiments of Ref. [34]. The main assumptions they made here were: I) completely

parallel actin filaments are cross-linked by myosin II motors and passive cross-linkers, and II) that the motors will leave actin once they reached the barbed end. The parallel experiment showed evidence of telescopic contraction, so they specifically tried to come up with an explanation for the mechanism underlying telescopic contraction of disordered actomyosin bundles. While emphasizing the fact that movement of myosin along actin alone doesn't favor contraction or extension they conducted a systematic study of the possible role of less obvious effects such as complicated bundle topologies and their interplay with linkers' nonlinear force-velocity relationships. Their calculations identified two factors as necessary requirements for contractility. They are: I) linkers with non-identical unloaded velocities that generate stresses inside the bundle and II) actin nonlinear elastic behavior allowing the compressive stresses to collapse the bundle while resisting stretching by extensile stresses. They further illustrated this mechanism by studying an example of a simple bundle with randomly distributed motors and showed that wormlike chain nonlinear elasticity gives rise to contractility rather than to extensibility.

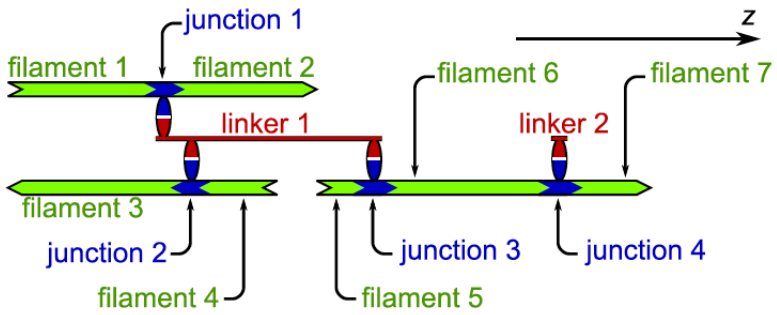

Figure 1.12: A schematic illustration of a sample bundle. Actin filament units are represented in green, linkers in red and the junctions in blue. The model does not impose any restrictions on the number of actin filaments a given linker can connect to or on the polarity of the actin filaments they can connect to. Figure taken from [9].

Very little work has addressed the relationship between the macroscopic stress and the tension in the mini-filament. Ref. [35] treated the action of a myosin mini-filament as a force dipole acting on two nearby points on actin filaments, predicting that the maximum tension at the contractile ring depends on the length of the bipolar mini-filament, the length of the actin polymer, and the circumference of the ring, for a contractile ring geometry during cytokinesis. However with the available measured values, this estimates 20 - 30 fold lower forces than those obtained using measured membrane tensions. Nonetheless, the author mentioned that through crosslinking, the effective length of the actin filaments could be much longer, and according to the model predictions, longer actin filaments do indeed increase the maximum stress gen-

erated. Existing experiments support the this idea of having extra passive crosslinkers in the contractile ring [36, 37]. Moreover, the local pulling force of these dipoles propagates through the cytoskeleton to much larger distances compared to the actin filament length, with the help of cooperative effects, actin inextensibility and crosslinkers keeping these actins intact through the cytoskeleton.

1.4.2 Experimental evidence for acto-myosin contraction

Apart from the theoretical models described above, there are many *in vivo* as well as *in vitro* experiments that have been carried out using both reconstituted model systems and cytoplasmic extracts. These experiments observe mostly contraction but in some cases expansion. Ref. [10] is an example of an experiment that observed contraction exclusively. There, a reconstituted simplified model system consisting of F-actin taken from rabbit skeletal muscle, muscle myosin-II taken from chicken skeletal muscle, and crosslinker α-actinin was used. The observations were compared with those of a cytoplasmic extract (taken from *Xenopus* eggs) under identical environments. In order to examine contractility, small droplets of the sample containing a fixed concentration of F-actin and varying concentrations of myosin-II and α-actinin were placed on a non-adsorbing oil layer, as shown in Fig. 1.13.

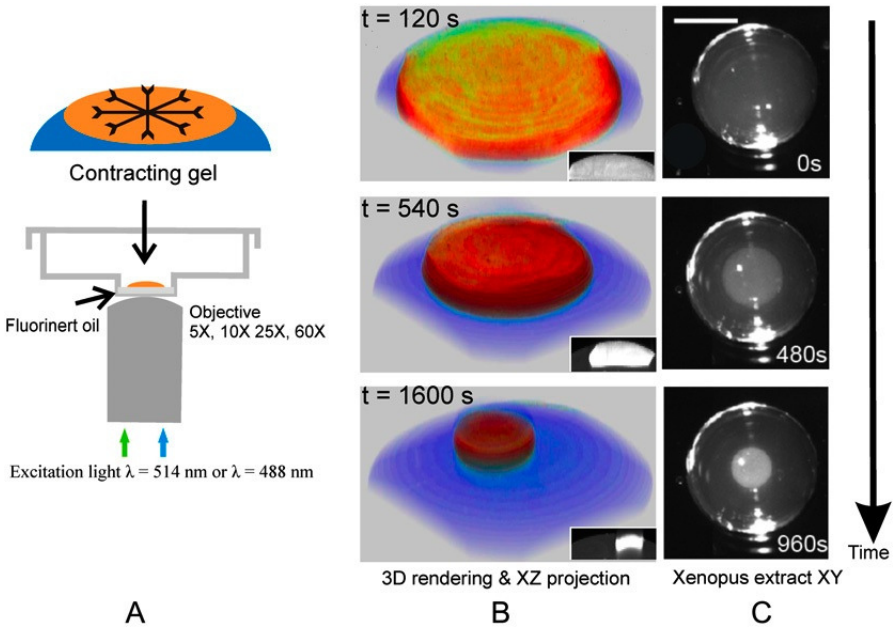

Figure 1.13: Experimental setup and time lapse images of contracting gels. (a) A schematic representation of the experimental setup. Sample droplet was placed in a dish with a recessed center, on top of an inert fluorocarbon oil layer. (b) three dimensional view of XY confocal slices of the fluorescently labeled F-actin network represented in orange color. Blue area was the water medium. Insets on each image correspond to XZ projections across the gel. (c) *Xenopus* cytoplasmic extract deposited within a layer of mineral oil. Dark field images taken at different times show the contraction of the gel with time. Figure taken from [10]

With time, the networks detached from the droplet surface and contracted inwards. Typically these networks had shrunk to about 5% of their initial volume.

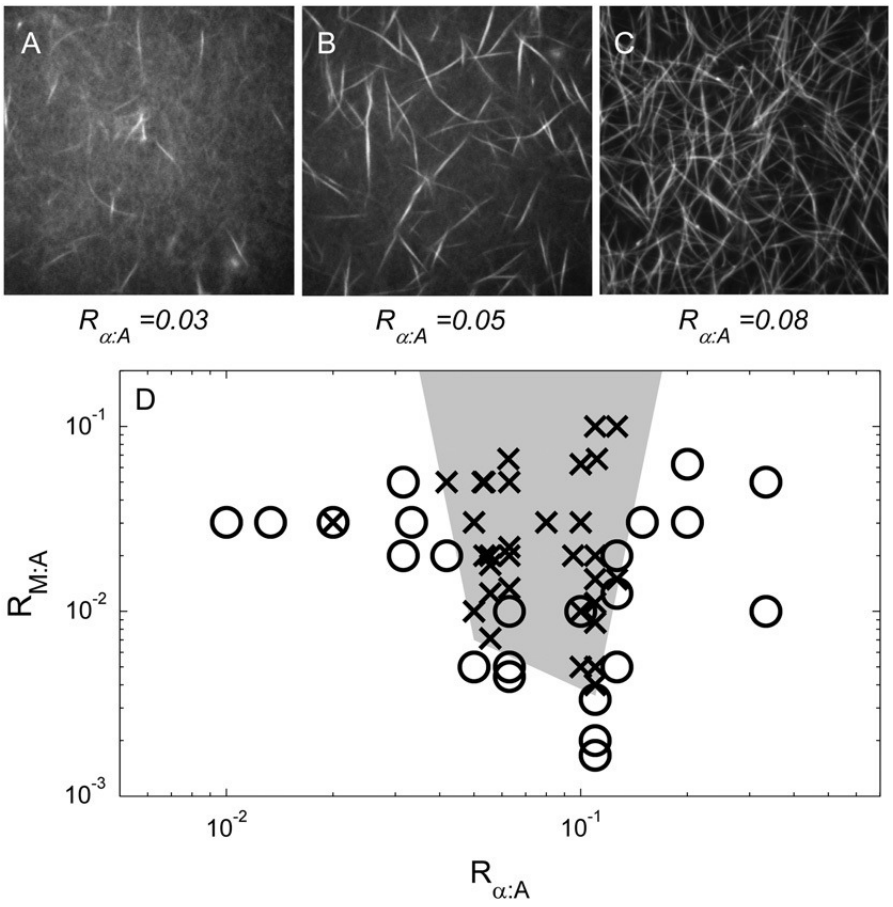

Figure 1.14: Actin filament bundling due to crosslinker α-actinin and the concentrations of myosin-II and α-actinin that generate contraction. (a)-(c) Variation of bundle formation and microstructure of the network formation with different α-actinin concentrations. Bundles in the figure are about 5 μm long. $R_{\alpha:A}$ is α-actinin to actin molar ratio. (d) Dependence of contractility on myosin-II and crosslinker molar concentrations. Open circles represent non contracting concentrations whereas crosses represent contracting concentrations. Shaded area was the region with contracting myosin-II concentrations and α-actinin concentrations. $R_{M:A}$: myosin to actin molar ratio. Figure taken from [10].

The following were the main observations of this experiment:

I. Contraction was observed above a threshold myosin-II motor concentrations.

Contraction only occurred above a myosin to actin molar ratio of 0.003. This was equivalent to having about 1 myosin thick filament (A thick filament is assumed to have about 300 myosin molecules) per 30 actin filaments.

II. Contraction was observed in a window of crosslinker concentration.

It was observed that the contraction occurred only when the α-actinin to actin molar ratio was between 0.04-0.1. A molar ratio of 0.05 is equivalent to about 90 α-actinin dimers per actin filament.

The main mechanism of contraction here was that myosin filaments pull neighboring actin bundles together to form aggregated structures. Hence the pore size of the bundled network was important for this mechanism to function. The average actin filament length was found to be around 5 μm. The pore size that was required to attain contraction was at most about 3 μm, roughly the size of a myosin thick filament. The claim was that if the bundles were too far apart, the myosin filaments cannot latch on to two different bundles to produce contraction. A minimum crosslinker concentration was required to obtain this pore size and that is why the networks did not contract when α-actinin to actin molar ratio was below 0.04. Also, during the experiment, changes to the size or the shape of the bundles were not observed. Hence the contraction mechanism operated by thick filaments acting on two different

bundles and not by filament gliding within individual bundles. Further, no change in the network geometry was observed after myosin II molecules were added to the assay containing actin and α-actinin before adding ATP to solution. However it was evident that the contraction started with a time lag after the myosins were added and that the contraction velocity was proportional to the myosin concentration until it saturated at a myosin to actin molar ratio of 0.05. The initial delay for the onset of contraction occured because during this time the function of the motors was building up tension without much affecting the existing network architecture. For the reconstituted network the initial contraction velocity of the network edge was around $3 - 8\ \mu m s^{-1}$ and then it decayed roughly exponentially. For cytoplasmic extracts these velocities were initially around $1 - 2\ \mu m s^{-1}$ and also decayed exponentially. These were about an order of magnitude larger than the *in vitro* measurements done in Ref. [11] (discussed below), which were about $0.1 - 1\ \mu m s^{-1}$.

The other important measurement was the maximum tension produced by these gels. As shown in Fig. 1.15, the gel was placed in glass capillaries between two drops of mineral oil. It was observed that first the networks moved away from the walls and then the gel contraction deformed the oil-water interface while pulling the two oil droplets together. At a maximum tension of about 1 μN or 100 nN per filament the top oil droplet broke completely collapsing the gel. This was the observable maximum tension exerted from the network. This could be an underestimate as it was limited by the maximum tension the oil droplet could withstand.

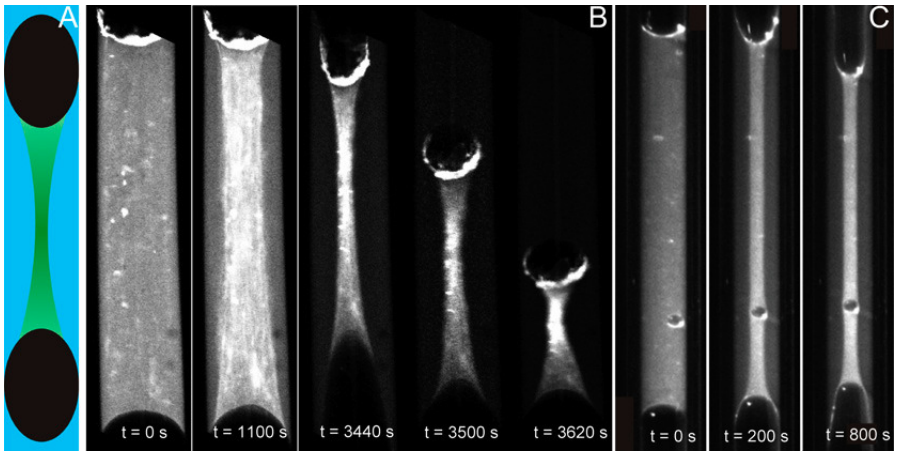

Figure 1.15: Measurement of generated maximum contractile force for both reconstituted networks and cytoplasmic extracts. (a) A schematic representation of the setup where the contracting gel is sandwiched between two oil droplets. (b) Confocal images of the model system during contraction. (c) Dark field images of the cytoplasmic extract during contraction. Figure taken from [10].

However in some rare cases, the contraction stalled at this force before the droplet collapsed. Hence this value might legitimately represent the maximum tension generated by the network. Finally it was speculated that the symmetry breaking at the air-gel interface or the gel periphery may have played a role in observing contraction exclusively in these experiments. The reasoning behind this argument was that the contraction always started at the air-gel interface and proceeded inwards. This is visible in the insets of Fig. 1.13. (b) The symmetry breaking occurred as the F-actin bundles within the gel were subjected to isotropic tension while the bundles at

the periphery of the gel experienced a large unbalanced tension from the bulk that exceeded the force required to detach the gel from the air-gel interface.

Interestingly, another experiment [11] basically similar to Ref. [10] reported both contraction and expansion. However there were differences in the constituents as well as the network geometry. For example, in Ref. [11] F-actin solutions were pre mixed with heavy meromyosin (HMM) molecules in the absence of ATP. The authors mentioned that some of these heads might have formed thick filaments and hence it was a mixture of individual HMM molecules and thick filaments. However in Ref. [10] the myosins formed 3 μm long thick filaments. To generate the bundled structure Ref. [11] added inert polymer methylcellulose. Methylcellulose in HMM mixed F-actin solutions formed loosely packed large bundles with varying lengths from 30 μm up to and over 100 μm. In contrast, Ref. [10] had α-actinin as crosslinkers and average length of an actin bundle was about 5 μm.

In Ref. [11], when bundles were allowed to interact with a glass slide coated with HMM, they disintegrated with time, indicating that filaments in these initial bundles had random polarity. This was because as myosin heads try to move toward the barbed ends of actin filaments, if the actin filaments within the bundle were sorted according to the polarity, the displacement would be in one direction for all the filaments and the bundle would displace in that direction without disintegrating. After adding different HMM concentrations, the changes in the bundle geometry and positions were observed to determine the effect of HMM on F-actin bundles. The

following were the main observations:

I. At low HMM concentrations elongation of the bundles was observed.

When the HMM and actin concentrations were 0.1 μM and 0.8 μM respectively, the bundles elongated with time. Also HMMs were found localized at the center of the resulting bud like formations.

II. At high HMM concentrations, contraction of bundles was observed.

Contraction was observed when the HMM concentration was above 1 μM while the actin concentration was 1 μM. Moreover at the end of contraction, aster-like structures were formed and HMM were localized in the middle of those asters.

III. Polarity sorting of actin filaments occurred within bundles during both contraction and elongation.

Fig. 1.16 gives examples of these phenomena. Frame B shows contraction of a bundle over time. At 54 s, the bundles deform into asters. The actin and HMM concentrations in these images are 1 $\mu M$and 5 μM respectively. The bundles had shortened to about one-third of their initial length before they collapsed into smaller aster formations. These small asters then merged to form a larger aster with arm-like extensions made up of polarized actin bundles. Frame D is a sequence of images where the arms of such an aster were allowed to interact with a cover slip coated with HMM to investigate polarity.

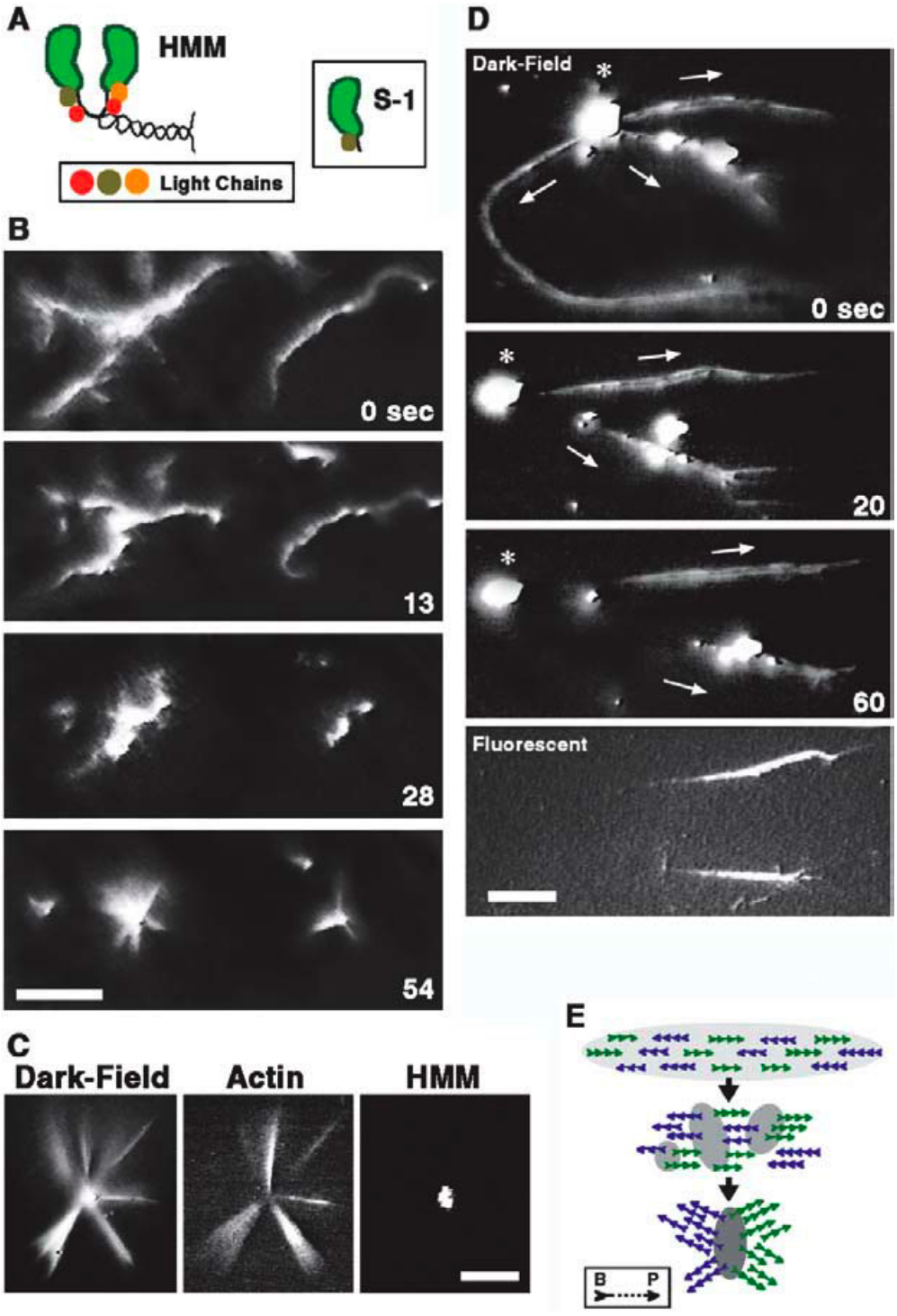

Figure 1.16: (Caption on next page)

Figure 1.16: (Previous page.) Contraction of actin bundles with time and formation of aster shaped structures in HMM-actin mixture. (A) A schematic diagram of the HMM and the S-1 sub fragment structure. It shows that the HMM has enough of a tail to dimerize whereas the S-1 sub fragment does not. (B) Dark field images showing contraction of two actin bundles with time. (C) Left panel is a dark field image of an aster like structure. Middle and right panels are fluorescent images showing actin and HMM localization respectively. (D) Dark field images (the first three panels) of an aster with three arms put in contact with a coverslip coated with HMM to investigate the polarity of actin bundles that formed arm-like structures. The asterisk indicates the center of the aster and arrows show the direction of movement of arms with time. The last panel is a fluorescent image of actin filaments taken at almost the same time as panel three. (E) Schematic of steps during contraction including filament sorting and aster formation. Figure taken from [11]

Images show that with time, the arms moved away from the center (arrows indicate the direction of the movement of the bundles) indicating that almost all the filaments within those bundles had their pointed ends pointing outwards. This was again due to the fact that myosin heads try to move towards the barbed ends of the actin filaments and because all the barbed ends were pointing toward the center of the bud like structure, actin filaments moved outward with the myosin movement. Hence these images provide evidence for uniform polarity within these structures. Contraction was believed to be originated here by the relative sliding between antiparallel actin

filaments induced by the function of HMM.

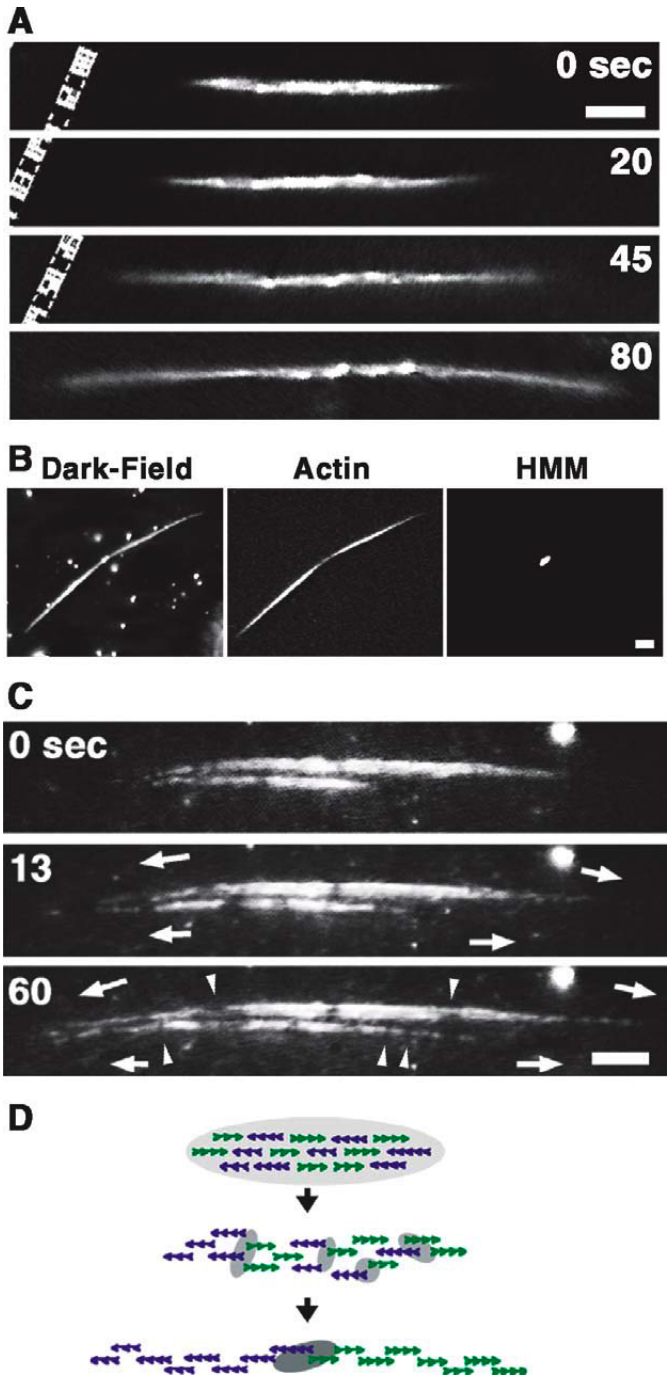

Figure 1.17: (Caption on next page)

Figure 1.17: (Previous page) Elongation of actin bundles with time in HMM-actin mixture. (A) Time lapse dark field images of an actin bundle that elongated due to the function of HMM. The bundle became slightly thinner and the length almost doubled after 80 seconds. (B) Localization of HMM in the center of the elongated bundle and the distribution of actin filaments. The left panel is a dark field image showing the bud like structure formed after elongation. Center and right panels show fluorescent images of actin and HMM respectively. (c) Sequence of dark field images showing the motion of elongated bundles after allowing them to contact a myosin coated cover slip. Arrows indicate the direction of movement. (D) Schematic illustration of polarity sorting and formation of localized patches of HMM, and the fusion of those at the end during the bundle elongation process. Figure taken from [11].

At low HMM concentrations, below 0.2 μM, elongation of filament bundles was observed. Fig. 1.17 (frame A) shows one such case. It was found that the bundles elongated up to about twice the initial length and formed bud-like structures, again with HMM localized at the center (Fig. 1.17 frame B). Similar to the case of aster arms, to investigate the polarity of the bundles after elongation, they were put in contact with HMM coated cover slips. Fig. 1.17 (frame C) shows most of these bundles again glided outwards indicating that they also had their pointed ends pointing outwards. However in a few cases shearing of bundles was observed, indicating that filament sorting might not be efficient during elongation at lower HMM

concentrations compared to that during contraction with high HMM concentrations.

Finally Fig. 1.18 summarizes the mechanisms proposed by the authors for contractility in these *in vitro* experiments.

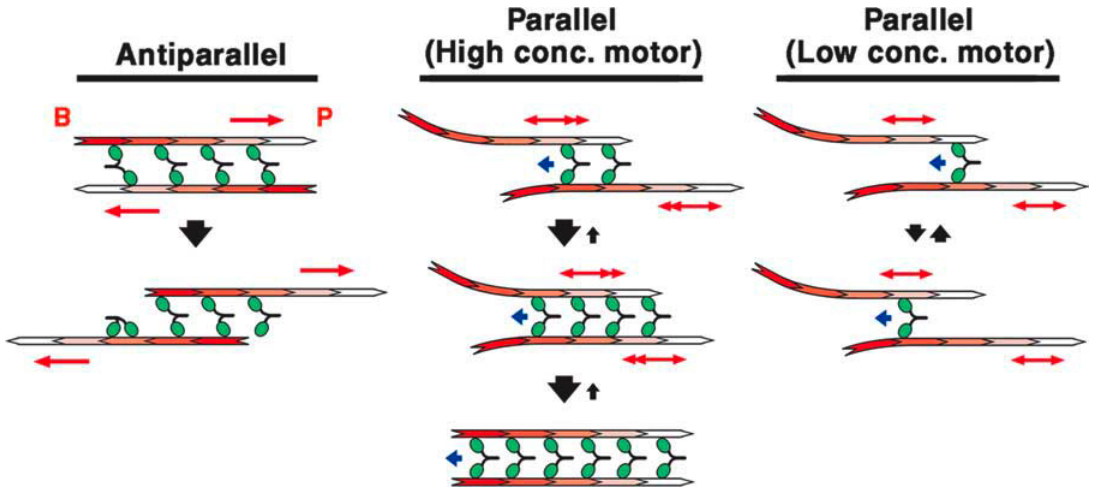

Figure 1.18: Model describing the sliding movements that can occur between two parallel actin filaments. B and P represented the barbed and pointed ends respectively. HMM dimers are colored in green and red arrows indicate the direction of motion for actin filaments. Blue arrows indicate the expected direction of motion for myosin motors. Left panel shows the mechanism that operates between anti-parallel filaments while the center and the right panels show the mechanisms for parallel actin filaments, for high and low motor concentrations respectively. Figure taken from [11].

In these mechanisms, the overlapping distance between two parallel filaments within a bundle plays an important role in determining the contraction or expansion that takes place. For example, as shown in the leftmost sketch of Fig. 1.18,

for interacting anti-parallel filaments, due to the function of active HMM molecules the overlap distance within the filaments decreases. Hence in the case shown for antiparallel filaments, despite the HMM concentration in solution, elongation occurs. However the authors did not consider the case with two overlapping pointed ends. In this case the overlap distance will increase and contraction will occur depending on the amount of HMM present.

In the case of two interacting parallel filaments, a high HMM concentration produced contraction. This was because the function of active HMM molecules between these filaments caused the overlap distance to increase with time, and hence more and more HMM molecules were required to attach and generate forces to overcome the external resistance for sliding. If not enough HMM molecules are present in the solution, the motors will slide along the parallel filaments without producing any filament sliding (Fig. 1.18 right sketch). Hence assuming initial random polarity within bundles, at lower HMM concentrations elongation dominates while at high HMM concentrations contraction becomes prominent.

In summary, the study in Ref. [11] differs considerably from [10] as in Ref. [11], due to the presence of methylcellulose, the bundles were loosely packed. In addition, HMM molecules were able to attach to bind two actin filaments within the same bundle and generate relative sliding. On the other hand in Ref. [10], actin filaments within bundles were relatively tightly bound together and myosin-II was present in aggregates or as thick filaments. These were relatively similar in length to the actin

filaments that were in the solution and were mostly found to interact with and apply tension on different bundles rather than on different actin filaments within the same bundle.

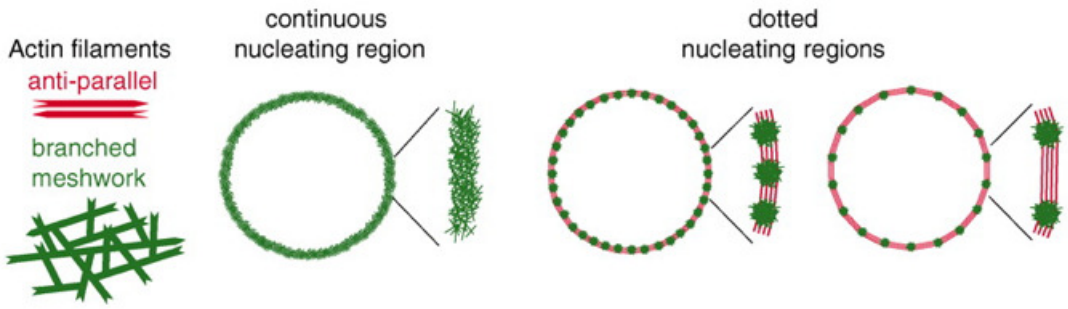

Figure 1.19: Schematic representation of actin networks nucleating continuously and in discrete dots around a ring shape. These nucleating sites had a branched meshwork of actin which was represented in green. In discrete structures between the nucleating region, anti-parallel actin filaments were formed and these are represented in red. The number of dots in nucleating regions is inversely proportional to the amount of anti-parallel filaments in the structure. Figure taken from [12].

Finally a more recent study [12] showed that filament polarity is an important player in generating contractility. It was observed that contraction occurs in antiparallel actin bundles while no change was observed in parallel bundles. Also, the contraction velocity was proportional to the amount of anti-parallel bundles present. Fig. 1.19 shows the bundle structures produced with varying ratios of nucleating regions with branched meshworks to anti-parallel bundles. To these bundles they

added pointed end directed motor, myosin VI (HMM) molecules in the presence of ATP. Fig. 1.20 clearly shows that the contraction velocity increased with the amount of anti-parallel bundles present.

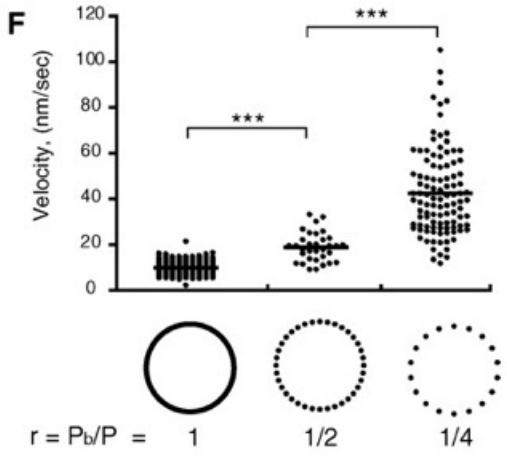

Figure 1.20: Variation of contraction velocity with amount of anti-parallel filaments present after the addition of myosin (HMM). Ratio $r = P_b/P$ represents the ratio between the total length of nucleating regions to perimeter of the ring structure. Hence the lower the ratio r, the higher the amount of anti-parallel filaments in the structure. Figure taken from [12].

However, these observations contradict those in Ref. [11], where they observed contraction only in the case of parallel actin filaments. The difference in observations might be because in Ref. [12] bundles were connected at their ends to the meshwork structure and hence, as described in Ref. [11], filaments may not have been free to move in such a way to decrease overlap distance and result in contraction. Also as

mentioned earlier, the investigation of contractility in antiparallel bundles seemed incomplete in Ref. [11].

In conclusion, it is evident that myosin-II in actin networks is able to generate contractile stress mostly in well connected or crosslinked actin networks. The requirement of passive crosslinkers such as α-actinin or filamin to aid contractility has been emphasized in many recent experiments including the ones described above [38, 39, 10]. In contrast, a recent study [40] shows that actin and smooth muscle myosin thick filaments alone can generate contraction above a certain threshold of myosin concentration. However, the authors explicitly mention that in previous experiments which required extra passive crosslinkers, the myosin to actin ratio $R_{M:A}$ was $\leq$ 0.05, whereas in their experiment $R_{M:A} \geq 0.75$. This was estimated to be more than four thick filaments per actin filament. Further, they showed that actin filaments and myosin thick filaments form contractile elements that work in series to transfer forces generated in these units to cellular length scales while resulting in telescopic contraction of actomyosin bundles. Existing theoretical models describe the contractility under certain assumptions but a detailed description of the microscopic origin of contractility in acto-myosin networks is still missing. Here in this work we are trying to come up with a model that describes the contractility with a small number of well justified set of assumptions, and also to show how contractility depends on the network structure.

Chapter 2

Contractility in Random Networks

2.1 Introduction

Myosin II, in combination with polymerized actin, produces contractile stresses in non-muscle cells by moving directionally along actin filaments or polarized actin bundles. These stresses are important for cell retraction during migration and for pinching-off during cytokinesis. Myosin II generally forms "minifilaments" - bipolar polymers of tens of molecules with active heads at both ends [41], which move toward the "barbed" ends of actin filaments and away from the "pointed" ends. Recent experiments have shown that *in vitro* actin-minifilament systems in a layer geometry with extra crosslinkers [10] or in a bundle geometry without extra crosslinkers [9] generate contraction. In muscles, contraction follows straightforwardly from the ordered actin-myosin arrangement. But in the disordered actin networks of non-muscle

cells, the reason for contractilion is not clear. Minifilaments moving on filament pairs with outward-pointing barbed ends should generate contraction, while motion toward inward-pointing barbed ends should lead to expansion. There is no structural evidence that the former case is more common. Several calculations [42, 38, 43, 35] have treated myosin and/or myosin minifilaments as contractile force dipoles. Support for this approach comes from 1) a hydrodynamic theory of a linear actin bundle [8, 33], which found contraction if myosins reaching the end of an actin filament remain there, and 2) calculations for one-dimensional bundles [44, 9] and an active-gel model [45] suggesting that nonlinearities such as buckling are crucial for contraction. However, there are no detailed calculations of the effect of the actin network structure on the stress.

Here we evaluate the effects of the network structure via simulation of myosin minifilament motion through a random two-dimensional actin network. We find overwhelmingly contractile stress, because the contractile local myosin equilibria are more stable than the expansive ones. This effect is independent of assumptions made about myosin behavior at filament ends, and does not require buckling or nonlinear network elasticity. The calculated network stresses can be much greater than suggested by the minifilament size and force, because force chains transmit the myosin force to larger distances.

This chapter is based on and extends, an article published as N. L. Dasanayake, P. J. Michalski and A. E. Carlsson, "General Mechanism of Actomyosin Contractilty",

Phys. Rev. Lett. 107:118101, 2011.

2.2 Model

Our simulations build on the method of Ref. [46]. We first generate a two-dimensional random network, whose filaments represent either single actin filaments or parallel bundles of actin filaments. We place filaments with random positions and orientations in a $5\mu m \times 5\mu m$ simulation cell (see Fig. 2.1). This size is likely an upper limit for biological relevance because localized adhesions pin the actin network to the substrate and thus act as rigid boundaries. Filaments extending outside the simulation cell are cropped. Static crosslinks are placed at filament intersections. Next the network is scanned for pairs of points on different filaments that could be linked by myosin minifilaments. At pairs of points whose distance is within 10% of the average equilibrium minifilament length $\overline{L}_m$, the two ends of a minifilament are placed and new, mobile crosslinks are created. This is the network's equilibrium state in the absence of ATP-induced myosin motion.

The system is then relaxed according to an energy function containing the stretching ($E_{stretch}$) and bending (E_{bend}) energies of actin filaments and bundles, the minifilament stretching energy E_m, and the ATP-driven motor energy E_{motor} moving myosin heads toward barbed ends. $E_{stretch}$ and E_{bend} are based on the lengths and relative

angles of the filament segments between crosslinks ("rods"):

$$E_{stretch} = \mu \sum_{i=0}^{N_r} (\Delta L_i)^2 / 2L_i^0, \tag{2.1}$$

where μ is the stretching modulus, ΔL_i is a rod's length change, L_i^0 is its initial length, and N_r is the number of rods;

$$E_{bend} = \kappa \sum_{j=0}^{N_c} (\Delta\theta_j)^2 / 2\overline{L}_j, \tag{2.2}$$

where κ is the bending modulus, $\Delta\theta_j$ is the angle between the two rods on the same filament meeting at the crosslink j, and $\overline{L}_j$ is the average of the two rod lengths. Further,

$$E_m = \gamma[(L_m)^2 - (L_m^0)^2]^2/2, \tag{2.3}$$

where γ is a constant, and $L_m^0(L_m)$ is the minifilament's initial (final) length. Finally,

$$E_{motor} = (M_1 + M_2)\delta F_{ATP} \tag{2.4}$$

where M_j is the distance of myosin head j from the barbed end of its filament, in units of the step size δ, and F_{ATP} is the myosin stall force. At crosslinks, filaments rotate freely.

Although the method and results are broadly applicable, we consider the case of single (unbundled) actin filaments for concreteness. Then $\kappa = k_B T l_p$, where $l_p \simeq 15\mu m$ [39]. Because use of the experimental value of μ (45 nN [47]) leads to slow convergence of the elastic relaxation, we use a smaller value $\mu = 600\ pN$, which is still

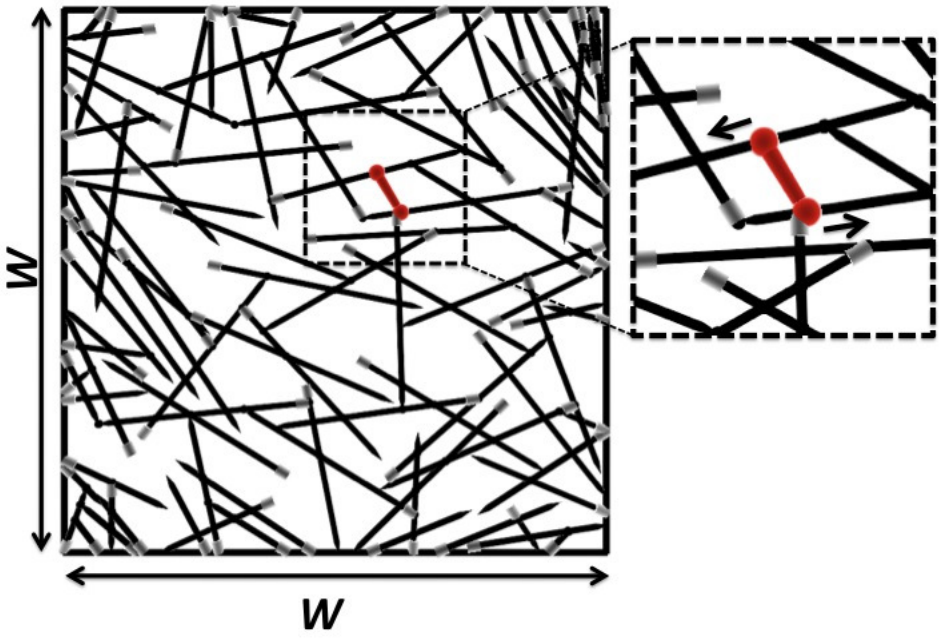

Figure 2.1: Network as generated before relaxation. Region around minifilament (dumbbell) is enlarged and arrows show the direction of myosin motion (toward the barbed end). Arrowheads at ends of actin filaments represent pointed end; barbed end is drawn in grey. Here $W = 5\mu m$.

large enough that filament stretching is negligible compared to bending. We choose an actin filament length of 2 μm, based on typical values away from the leading edge of cells, and $\overline{L}_m = 0.4\ \mu m$ [41]; γ is varied over a range $60 - 120\ pN/\mu m^3$. We vary F_{ATP} over a range on the order of pN, which corresponds to myosin heads with a low duty ratio.

We evolve each random network to a stable steady state minimizing the total

energy $E_{tot} = E_{stretch} + E_{bend} + E_m + E_{motor}$. Myosion motion is treated separately from elastic relaxation because it is slower. For each set of values of M_j, the elastic degrees of freedom are relaxed using a nonlinear conjugate-gradient method which gives finite (rather than infinitesimal) crosslink and minifilament displacements. The myosin heads then move via a steepest-descent algorithm driven by the derivatives $\partial E_{tot}/\partial M_{1,2}$, until all of the forces have reached a specificed tolerance. Calculation of forces is described in detail in section 2.3. Although the energies in the model are quadratic functions of L_m and $\Delta\theta$, the energy-minimization solution can yield nonlinear displacements. We evaluate the spatially-averaged wall stress

$$\sigma_{wall} = -\sum_i (\vec{f_i} \cdot \vec{r_i})/2W^2. \tag{2.5}$$

where $\vec{f_i}$ is the force exerted by a rod on the wall, $\vec{r_i}$ is the position of a rod-wall contact point, and the sum is over all contact points. This formula for the stress is chosen because it gives the derivative of the total energy with respect to uniform hydrostatic expansion or contraction. We make varying assumptions regarding the motion of myosin heads past crosslinks and at filament tips.

2.3 Methods

Below is the detailed elastic energy and force calculations.

2.3.1 Energy and force due to stretching of actin rods

The stretching energy was calculated using a simple quadratic formula that depends on the initial and final length of the rods. The total energy due to stretching of actin rods can be written as:

$$E_{stretch} = \mu \sum_{i=0}^{N_r} (\Delta L_i)^2 / 2L_i^0, \tag{2.6}$$

where,

μ = Stretching modulus of actin
N_r = Total number of rods in the system
L_i^0 = Initial length of a rod
L_i = Final length of a rod

This energy generates two types of forces. 1) Physical forces on crosslinks which determine their equilibrium at fixed M values. and 2) Generalized forces which cause the M values to change. For a single rod, the force due to stretching, the physical force $F_{stretch}$ on a crosslink was calculated by taking the derivative of $E_{stretch}$ with respective to L_i^0.

$$\begin{aligned} F_{stretch} &= -\frac{\partial E}{\partial \Delta L_i} \\ &= -\mu \frac{\Delta L_i}{L_i^0} \end{aligned} \tag{2.7}$$

The generalized forces for mini-filaments attached to actin filaments were obtained by calculating the stretching energy of the two segments of the same rod (on either side of the mini-filament end) separately. Here, the mini-filament motion causes

the length of each segment to vary. Therefore, based on the number of subunits in each section, we use following formula to estimate new initial length for each segment.

$$l^0_{new} = \frac{\alpha}{\alpha_0} l^0 \tag{2.8}$$

where

α	=	Current number of subunits
α_0	=	Initial number of subunits
l^0	=	Length of a segment right after the mini-filament attaches before taking any steps
l^0_{new}	=	Estimated initial length of a segment after mini-filament has taken a step

To calculate $F_{stretch}$ on these rod segments we calculated the derivative of the energy with respective to α.

$$\Delta l = l - l^0_{new} = l - \frac{\alpha}{\alpha_0} l^0$$

$$\begin{aligned} \frac{\partial E}{\partial \alpha} &= \frac{\partial}{\partial \alpha}\left[\frac{\mu}{2}\frac{(\Delta l)^2}{l^0_{new}}\right] \\ &= \frac{\mu}{2}\left[\frac{2l^0_{new}\Delta l(\partial \Delta l/\partial \alpha) - (\Delta l)^2(\partial l^0_{new}/\partial \alpha)}{{l^0_{new}}^2}\right] \end{aligned}$$

substituting

$$\frac{\partial \Delta l}{\partial \alpha} = -\frac{l^0}{\alpha_0} \text{ and } \frac{\partial l^0_{new}}{\partial \alpha} = \frac{l^0}{\alpha_0}$$

$$\frac{\partial E}{\partial \alpha} = \frac{\mu}{2}\left[\frac{2(\frac{\alpha}{\alpha_0}l^0)(\Delta l)(-\frac{l^0}{\alpha_0}) - (\Delta l)^2(\frac{l^0}{\alpha_0})}{(\frac{\alpha l^0}{\alpha_0})^2}\right] \tag{2.9}$$

Since

$$F_{stretch}^{(gen)} = -\frac{\partial E}{\partial \alpha}$$

$$F_{stretch}^{(gen)} = \frac{\mu}{2}\left[\frac{2\Delta l l_{new}^{0} + (\Delta l)^2}{\alpha l_{new}^{0}}\right] \tag{2.10}$$

2.3.2 Energy and force due to bending of actin rods

The bending energy is calculated between neighboring rods at a crosslink that belong to same original filament. It depends on the relative angle between rods and their mean length. We set the bending spring constant for dangling ends equal to zero for computational efficiency (we found that this affected the calculations, tensions and forces by less than 5%.) The total bending energy of the system is:

$$E_{bend} = \kappa \sum_{j=0}^{N_c} (\Delta\theta_j)^2 / 2\overline{L}_j, \tag{2.11}$$

where

κ	=	Bending modulus of actin
N_c	=	Total number of crosslinks in the system
$\Delta\theta$	=	Angle between the rods
$\overline{L}_j$	=	Mean length of two rods considered

As shown in Fig. 2.2, to calculate the bending force at one end of a rod, the derivative of energy is taken with respective to the coordinates of the point of interest (at (x_1, z_1) for the calculation shown below) and $\Delta\theta$ was written by using the dot product.

$$\Delta\theta = \cos^{-1}\left[\frac{\vec{\ell}\,.\,\vec{\ell\,'}}{\ell\ell'}\right] \tag{2.12}$$

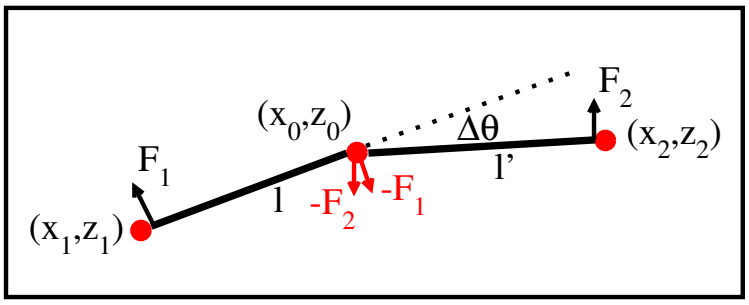

Figure 2.2: Schematic diagram of an actin filament bent at a crosslink (at position (x_0, z_0)). Length of two rods are ℓ and $\acute{\ell}$. Forces that act on actin rods and neighboring crosslinks are shown in black arrows and forces on the crosslink are shown in red. F_1 is the total force on the first rod calculated at position (x_1, z_1), $F_1 = \sqrt{F_{x_1}^2 + F_{z_1}^2}$ and F_2 is the total force on the second rod calculated at (x_2, z_2), $F_2 = \sqrt{F_{x_2}^2 + F_{z_2}^2}$.

$$F_{x_1} = -\frac{\partial E_{bend}}{\partial x_1}$$

$$F_{x_1} = -\frac{\kappa}{2}\left\{\frac{\partial}{\partial x_1}\left[\cos^{-1}\left(\frac{\vec{\ell}\cdot\vec{\acute{\ell}}}{\ell\acute{\ell}}\right)\right]^2 \times \frac{1}{\bar{\ell}} + \left[\cos^{-1}\left(\frac{\vec{\ell}\cdot\vec{\acute{\ell}}}{\ell\acute{\ell}}\right)\right]^2 \times \frac{\partial}{\partial x_1}\frac{1}{\bar{\ell}}\right\} \tag{2.13}$$

Taking

$$\beta = \left[\frac{\vec{\ell}\cdot\vec{\acute{\ell}}}{\ell\acute{\ell}}\right],$$

and using the fact that

$$\bar{\ell} = \frac{\ell + \acute{\ell}}{2},$$

we have

$$F_{x_1} = -\frac{\kappa}{2}\left\{\frac{-2\cos^{-1}\beta}{\sqrt{1-\beta^2}} \times \frac{\partial\beta}{\partial x_1} + (-2)(\ell+\acute{\ell})^{-2} \times \frac{\partial\ell}{\partial x_1}\right\} \tag{2.14}$$

Then writing β and ℓ in terms of position coordinates and taking their derivatives with respective to x_1 gives

$$\beta = \frac{(x_1 - x_0)(x_0 - x_2) + (z_1 - z_0)(z_0 - z_2)}{\sqrt{[(x_1 - x_0)^2 + (z_1 - z_0)^2]\,[(x_2 - x_0)^2 + (z_2 - z_0)^2]}}$$

$$\frac{\partial \beta}{\partial x_1} = \frac{\ell\acute{\ell}(x_0 - x_2) - [(x_1 - x_0)(x_0 - x_2) + (z_1 - z_0)(z_0 - z_2)](x_1 - x_0)(\acute{\ell}/\ell)}{(\ell\acute{\ell})^2}$$

$$\ell = \sqrt{[(x_1 - x_0)^2 + (z_1 - z_0)^2]}$$

and

$$\frac{\partial \ell}{\partial x_1} = \frac{(x_1 - x_0)}{\ell},$$

Therefore,

$$F_{x_1} = \frac{\kappa}{2}\frac{2\Delta\theta}{\sqrt{1-\beta^2}}\frac{l\acute{l}(x_0 - x_2) - [(x_1 - x_0)(x_0 - x_2) + (z_1 - z_0)(z_0 - z_2)](x_1 - x_0)(\acute{\ell}/\ell)}{(\ell\acute{\ell})^2} \tag{2.15}$$

$$+ \frac{\kappa}{2}(\Delta\theta)^2\frac{(x_1 - x_0)}{2\bar{\ell}^2\ell}$$

similarly,

$$F_{z_1} = \frac{\kappa}{2}\frac{2\Delta\theta}{\sqrt{1-\beta^2}}\frac{\ell\acute{\ell}(z_0 - z_2) - [(x_1 - x_0)(x_0 - x_2) + (z_1 - z_0)(z_0 - z_2)](z_1 - z_0)(\acute{\ell}/\ell)}{(\ell\acute{\ell})^2} \tag{2.16}$$

$$+ \frac{\kappa}{2}(\Delta\theta)^2\frac{(z_1 - z_0)}{2\bar{\ell}^2\ell}$$

2.3.3 Energy and force due to stretching of a mini-filament

We take

$$E_m = \gamma[(L_m)^2 - (L_m^0)^2]^2/2, \tag{2.17}$$

where γ is a constant, and $L_m^0(L_m)$ is the minifilament's initial (final) length. Writing the mini-filament length in terms of the coordinates,

$$E_m = \gamma[(x_s - x_e)^2 + (z_s - z_e)^2 - (L_m^0)^2]^2/2 \tag{2.18}$$

where (x_s, z_s) and (x_e, z_e) are the starting and ending coordinates of the mini-filament respectively.

$$F_{x_s} = -\frac{\partial E_m}{\partial x_s} = (-1) \times \gamma[(x_s - x_e)^2 + (z_s - z_e)^2 - (L_m^0)^2] \times 2(x_s - x_e)$$

Hence

$$F_{x_s} = -2\gamma(x_s - x_e)[(L_m)^2 - (L_m^0)^2], \tag{2.19}$$

and similarly

$$F_{z_s} = -2\gamma(z_s - z_e)[(L_m)^2 - (L_m^0)^2]. \tag{2.20}$$

2.3.4 Motor Energy / Energy from ATP hydrolysis

$$E_{motor} = (M_1 + M_2)\delta F_{ATP} \tag{2.21}$$

where M_j is the distance of myosin head j from the barbed end of its filament, in units of the step size δ, and F_{ATP} is the myosin stall force. M_j's are dimensionless

and δ has units of length. Here the driving force is simply the stall force ($\frac{\partial E_{motor}}{\partial \alpha} = \delta F_{ATP}$).

2.3.5 Mini-filament stopping criterion

As the mini-filament proceeds toward the barbed end, it deforms the actin network. The deformations are most prominent in the actin filaments the mini-filament is attached to. Due to these deformations, elastic energy builds up in these actin filaments generating forces opposing the deformations. Hence, as the stopping criterion for mini-filaments, we compared the gradient of the elastic energy with respect to the change in the subunit number (to which the mini-filament is attached) to energy from the driving force, E_{ATP}. The exact condition we imposed was, the mini-filament will come to equilibrium on the actin filament if,

$$\frac{dE_{total}}{d\alpha} < 10^{-6}\ pN\mu m \tag{2.22}$$

For $dE_{total}/d\alpha$ we only considered the contribution from the stretching of the actin rods and the energy from the driving force. The total collection of variables consists of the crosslink positions plus the α values (one for each end of the mini-filament). Changing α modifies the equilibrium rod lengths but does not move the crosslinks, so it does not affect the bending energies.

Hence using Eq. 2.10, the energy change due to the movement of mini-filament

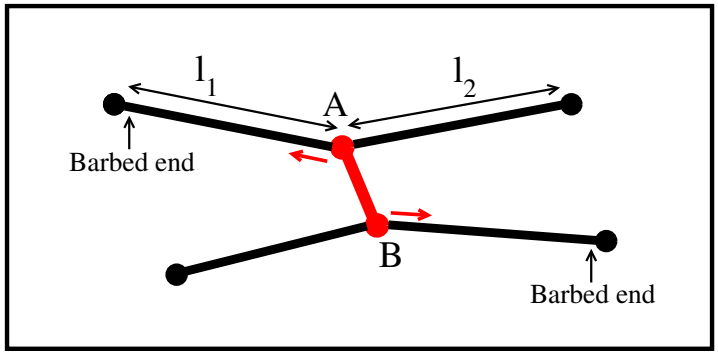

Figure 2.3: Snap shot of a mini filament during its movement towards barbed end. Red arrows indicate the direction of movement of each mini-filament end (A and B). ℓ_1 and ℓ_2 are the lengths of actin rod sections that mini-filament end A is attached. ℓ_1 is gradually decreasing while ℓ_2 is increasing as end A moves toward the barbed end.

end A (in Fig. 2.3), towards the barbed end is

$$\frac{dE_{Elastic}}{d\alpha} = \frac{\mu}{2}\left[\frac{-2\Delta l_1 l^0_{1new} - (\Delta l_1)^2}{\alpha\ l^0_{1new}}\right] + \frac{\mu}{2}\left[\frac{2\Delta l_2 l^0_{2new} + (\Delta l_2)^2}{(1-\alpha)\ l^0_{2new}}\right] \tag{2.23}$$

Fig. 2.4 shows the numerical derivative of total energy with respect to changing subunit number vs the derivative of the analytical expression we derived only considering stretching of actin filaments for ten mini-filament steps. It confirms the accuracy of the method.

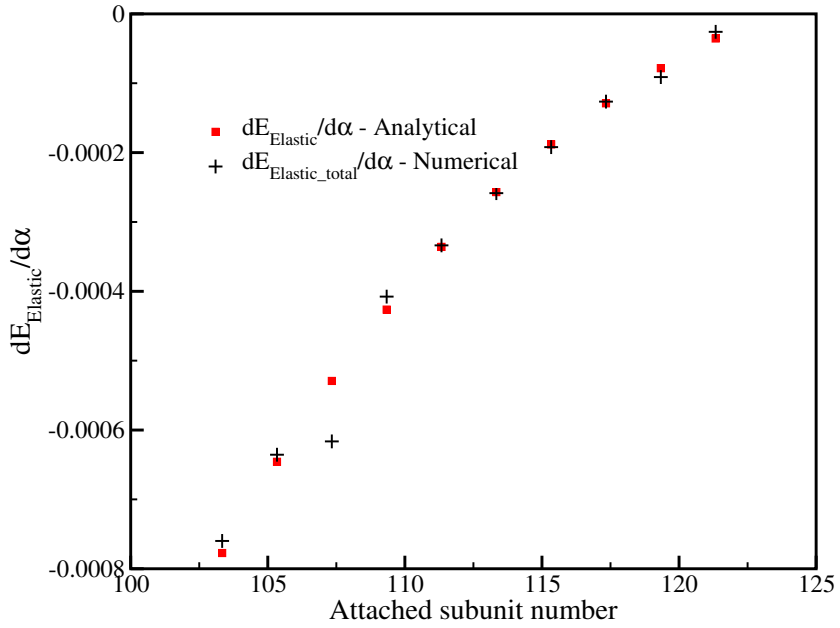

Figure 2.4: Numerical derivative of $dE_{Elastic\_total}/d\alpha$ vs analytical approximation to $dE_{Elastic}/d\alpha$ derived considering only stretching of actin filaments. X-axis shows the subunit number the mini-filament is attached to, counted from the barbed end. Y-axis shows the derivative of the elastic energy with respect to the change in subunit number.

When calculating the numerical derivative of total energy, we first allowed one end of the mini-filament to re-attach to a subunit closer to the barbed end from its initial equilibrium state (or take a step of n subunits, where we treat n as a floating point number). Then the network was allowed to relax and total energy (E_{tot1}) was calculated after the minimization. After that, in a new run, the same mini-filament was allowed to attach at a point $n + 10^{-8}$ closer to the barbed end from the initial position and allowed to relax. The total energy (E_{tot2}) was calculated after relaxation.

Finally the numerical total energy derivative was calculated as below.

$$\frac{\partial E_{total}^{numerical}}{\partial \alpha} = -\frac{E_{tot2} - E_{tot1}}{10^{-8}}$$

2.3.6 Derivation of σ_{th}

Here we obtain an approximate expression for the stress on the fixed boundary of a two-dimensional actin network due to an active myosin minifilament, as shown in Fig. 2.5 (a). We treat the minifilament as a force dipole. To simplify our calculations we consider a circular region and assume that the effect of the force dipole is equivalent to that of a uniform inward pressure P along a boundary at a radius a that is half the size of the force dipole (see Fig. 2.5(b)). For generality, we first consider a layered system having two different elastic moduli inside and outside $r = a$: κ , G from $r = 0$ to $r = a$ and κ^o and G^o from $r = a$ to $r = b$; later we will treat the myosin-actin system as a special case.

Table 2.1: Notation Used

κ, κ^o	Bulk modulus of the material
G, G^o	Shear modulus of the material
$\vec{U}(\vec{r})$	Displacement vector at position r
U_r	Radial component of the displacement vector
η_{ij}	ij^{th} component of the strain tensor
σ_{ij}	ij^{th} component of the stress tensor

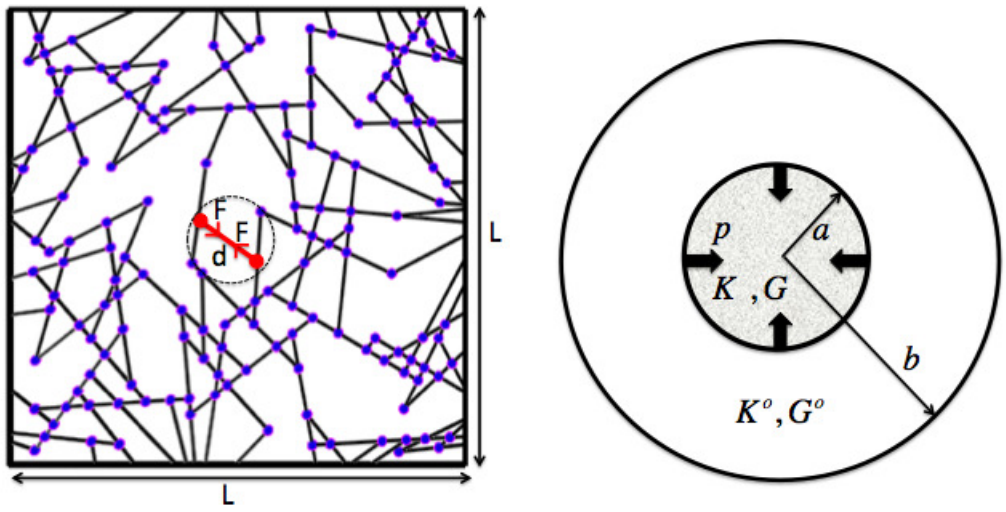

(a) (b)

Figure 2.5: (a) An actin network with a myosin minifilament (dumbbell) represented as a force dipole acting on the network. (b) Circularly layered system with different material properties in two regions. (Here a and b in (b) correspond to $d/2$ and $L/2$ in (a) respectively).

The boundary conditions for the displacement U and the stress σ are as follows. Because of the assumption of a fixed boundary, $U_r(r = b) = 0$, and because there is no singularity at the origin, $U_r(r = 0)$ is finite. Furthermore, because there are no gaps in the material, $U_r(r = a^+) = U_r(r = a^-)$. Finally, the application the pressure at $r = a$ leads to a discontinuity in σ, so that $\sigma_{rr}(r = a^+) - \sigma_{rr}(r = a^-) = P$.

To obtain the functional form of the solution, we note that circular symmetry and the absence of body forces imply that $\vec{U}(\vec{r}) = U_r(r)\hat{r}$ and $\vec{\nabla}(\vec{\nabla} \cdot \vec{U}) = 0$ in

both regions. Thus the solution has the form $U_r(r) = Ar + B/r$ for $r < a$ and $U_r(r) = Cr + D/r$ for $a < r < b$, where A, B, C, and D are constants to be determined. The boundary condition that $U_r(r = 0)$ is finite implies that $B = 0$, and the condition that $U_r(r = b) = 0$ implies that $D = -Cb^2$. Then the condition that $U_r(r = a^+) = U_r(r = a^-)$ implies that $Aa = C(a - b^2/a)$ so that $A = -C(b^2/a^2 - 1)$, and the solution becomes

$$U(r) = \begin{cases} -Cr(b^2/a^2 - 1) & \text{for } r < a \\ -Cr(b^2/r^2 - 1) & \text{for } a < r < b \end{cases}$$

To impose the boundary condition that $\sigma_{rr}(r = a^+) - \sigma_{rr}(r = a^-) = P$, we first calculate the strains, using the general result $\eta_{rr} = \frac{\partial U_r}{\partial r}$, $\eta_{\phi\phi} = \frac{U_r}{r}$ and $\eta_{r\phi} = 0$ (Ref. [48], Eq. (1.7)):

$$\begin{aligned} \eta_{rr} &= -C(b^2/a^2 - 1), \eta_{\phi\phi} &= -C(b^2/a^2 - 1) \ (r < a) \\ \eta_{rr} &= C(b^2/r^2 + 1), \eta_{\phi\phi} &= -C(b^2/r^2 - 1) \ (a < r < b) \end{aligned} \tag{2.24}$$

The stress is given in terms of the strain as follows (Ref. [48], Eq. 4.6)):

$$\begin{aligned} \sigma_{rr} &= (\kappa + \tfrac{4}{3}G)\eta_{rr} + (\kappa - \tfrac{2}{3}G)\eta_{\phi\phi} \\ \sigma_{\phi\phi} &= (\kappa + \tfrac{4}{3}G)\eta_{\phi\phi} + (\kappa - \tfrac{2}{3}G)\eta_{rr} \end{aligned} \tag{2.25}$$

Thus for $r < a$

$$\begin{aligned} \sigma_{rr} &= -2C(\kappa + \frac{G}{3})(\frac{b^2}{a^2} - 1) \\ \sigma_{\phi\phi} &= -2C(\kappa + \frac{G}{3})(\frac{b^2}{a^2} - 1) \end{aligned} \tag{2.26}$$

and for $a < r < b$

$$\sigma_{rr} = 2C[\kappa^o + (\frac{1}{3} + \frac{b^2}{r^2})G^o]$$
$$\sigma_{\phi\phi} = 2C[\kappa^o + (\frac{1}{3} - \frac{b^2}{r^2})G^o] \tag{2.27}$$

Then the stress boundary condition, $\sigma_{rr}(r = a^+) - \sigma_{rr}(r = a^-) = P$, implies that

$$2C[\kappa^o + (\frac{1}{3} + \frac{b^2}{a^2})G^o] + 2C(\kappa + \frac{G}{3})(\frac{b^2}{a^2} - 1) = P \tag{2.28}$$

so that

$$C = \frac{P}{2[\kappa^o + (\frac{1}{3} + \frac{b^2}{a^2})G^o + (\kappa + \frac{G}{3})(\frac{b^2}{a^2} - 1)]} \tag{2.29}$$

Finally, for $a < r < b$ we have

$$\sigma_{rr} = \frac{[\kappa^o + (\frac{1}{3} + \frac{b^2}{r^2})G^o]P}{[\kappa^o + (\frac{1}{3} + \frac{b^2}{a^2})G^o + (\kappa + \frac{G}{3})(\frac{b^2}{a^2} - 1)]} \tag{2.30}$$

We now assume that the two regions consist of the same material, so that $\kappa^o = \kappa$. Furthermore, for actin networks, Poisson's ratio is close to 0.5 [49], so that we take $G^0/\kappa \to 0$ and $G/\kappa \to 0$. Finally, we assume that $b >> a$. Then we obtain at $r = a$

$$\sigma_{rr} \simeq \frac{Pa^2}{b^2} \tag{2.31}$$

For the geometry of Fig.1a, we have $a = d/2,\ b = L/2$. Since the magnitude of the contraction induced by a force distribution $f_{vec}(\vec{r})$ is measured by its force dipole moment $\int \vec{r} \cdot f_{vec}(\vec{r}) d^3r$, we choose the value of P to have the same dipole $-Fd$ as the pair of myosin forces. Since the force density associated with P is $-\hat{r}P\delta(r - a)$,

we obtain $-2\pi Pa^2 = -Fd$, so $P = \frac{2F}{\pi d}$. Thus

$$\sigma_{th} = \frac{Fd}{2\pi(L/2)^2} \tag{2.32}$$

2.4 Results

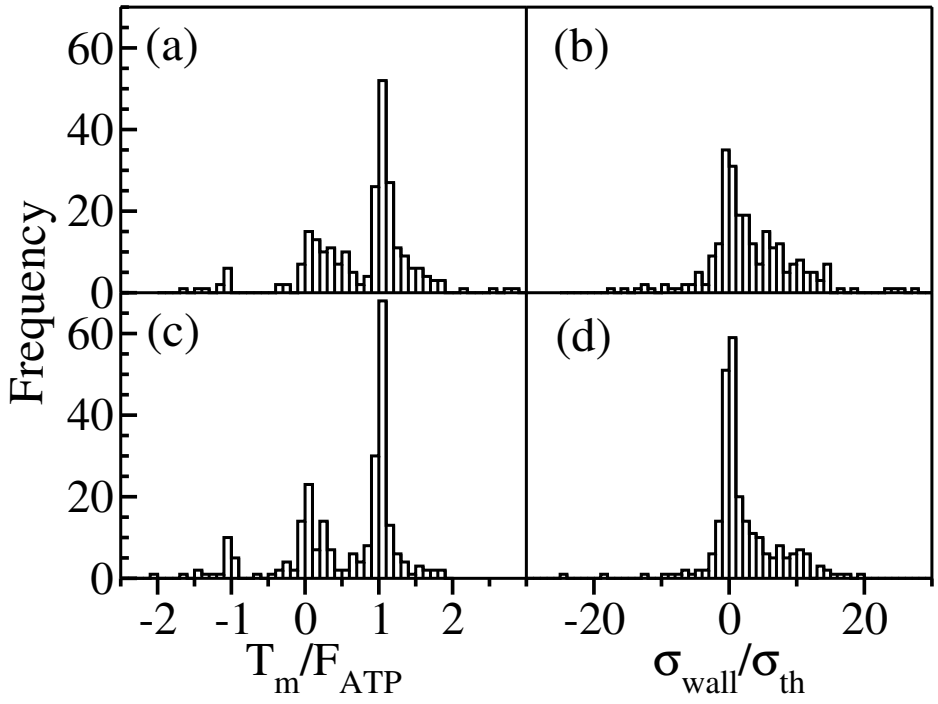

Figure 2.6: Distribution of minifilament tension (a,c) and wall stress (b,d). In a) and b) myosins jump over crosslinks; in c) and d) they are pinned. The mean wall stresses are $3.3\sigma_{th}$ and $2.0\sigma_{th}$ in (b) and (d) respectively. Positive values of T_m and σ_{wall} refer to contraction. Histograms obtained from 251 runs. Frame b) contains one more point at $\sigma_{wall} \simeq 60\sigma_{th}$, which was left out to improve visibility.

Fig. 2.6 shows the distributions of the minifilament tension T_m and σ_{wall} for the case where myosin heads reaching filament tips are pinned there. The wall tension is scaled by an elastic theory prediction $\sigma_{th} = -2fd/\pi W^2$ obtained for a single small force dipole in a 2D circular isotropic elastic patch of area $\pi(W/2)^2$ (see section 2.3 for derivation). In a) and b), where myosin heads move past crosslinks, both T_m and σ_{wall} are overwhelmingly contractile. The values of T_m peak around the myosin stall force F_{ATP}. The fluctuations are caused by the varying angles between the minifilament and the actin filaments, and the pinning of minifilaments at filament tips. In c) and d), stopping myosin heads at crosslinks reduces the fraction of contractile configurations, but leaves the stress mainly contractile; the average T_m is reduced by about 50%. In both cases, the values of σ_{wall} sometimes exceed σ_{th} by as much as an order of magnitude. Allowing myosin heads to leave filament tips enhances the contractile stress by about 50%.

The reason for the dominance of contractile T_m values is seen most clearly when minifilaments come to equilibrium before reaching barbed ends. Contractile minifilament equilibria have lower energy than expansive ones. A minifilament which starts in an expansive-stress configuration tends to rotate and move until it reaches a stable contractile configuration. To clarify this effect, we consider a completely rigid minifilament, interacting with two rigid filaments at a relative angle of ϕ (see Fig. 2.7, inset) and distance of closest approach d (which vanishes in two dimensions). The only energy in this case is E_{motor}. Fig. 2.7 shows its variation as the minifilament moves from

a symmetric equilibrium where it generates expansive stress. The motion is described in terms of $S_{1,2}$, the positions of the ends of the minifilament relative to the crosslink (with the pointed-end direction taken positive); because L_m is fixed, S_1 determines S_2. Simple algebra shows that $E_{motor} = F_{ATP}[\, S_1(1+\cos\phi) + \sqrt{L_m^2 + d^2 - S_1^2 \sin^2\phi}\,]$. This has two extrema, and the one with $S_1 > 0$ (which causes expansive stress) is unstable, as indicated by the energy maxima at the two starting points in Fig. 2.7. From these local maxima, the minifilament rotates in either of two directions breaking the initial symmetry, indicated by the solid and dashed lines. After the minifilament has rotated far enough, both of its ends move in the barbed-end direction, and the minifilament reaches a stable contractile equilibrium. Comparison of Figs. 2.7(a) and 2.7(b) shows that this behavior persists in three dimensions. In our simulation results for minifilaments which equilibrated without becoming stuck, 61 of 62 runs resulted in contractile configurations like those of Fig 2.7(a). In the sole exception, the minifilament stopped in an expansive-stress configuration because the two actin filaments that it impinged became bent enough to allow a local energy minimum.

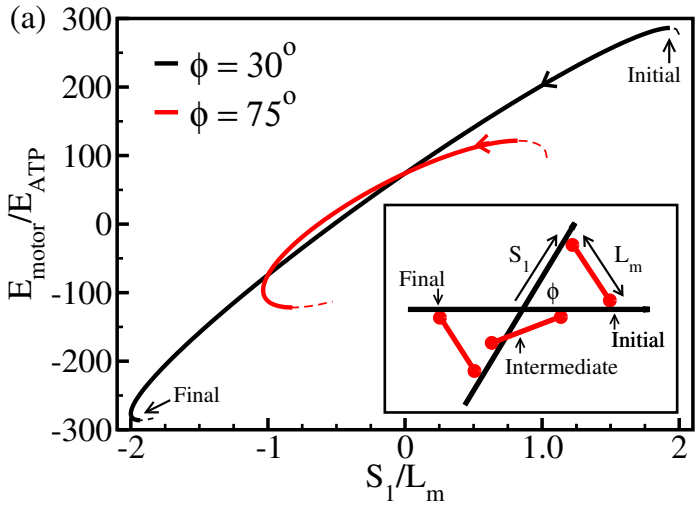

(a)

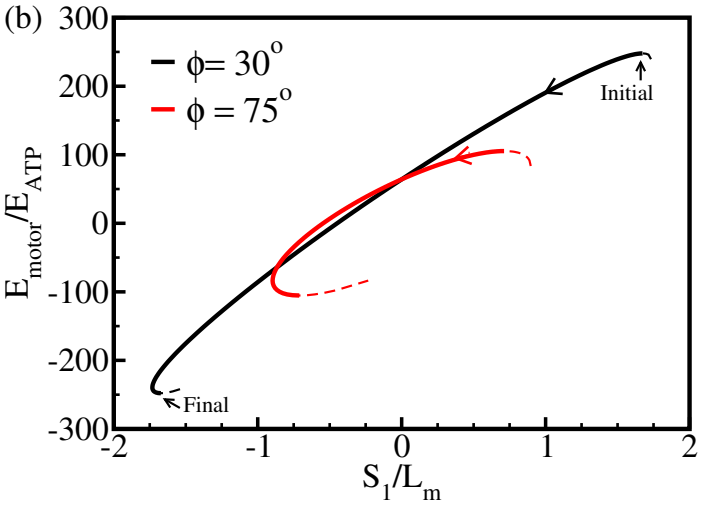

(b)

Figure 2.7: Local equlibria of myosin minifilament moving between rigid actin filaments in two (a) and three (b) dimensions. Inset in (a) shows the geometry; barbed ends are at the left. Here $E_{ATP} = \delta F_{ATP}, F_{ATP} = 1.9\ pN$, $\delta = 5.4\ nm$, $L_m = 0.4\ \mu m$, and in frame (b) $d = 0.2\ \mu m$. Solid lines denote path followed by minifilament; dashed lines denote another possible path.

This effect also implies that minifilaments which become stuck will often have rotated to contractile configurations before becoming stuck. A population of minifilaments starting with equal numbers of contractile and extensile members will then evolve into one biased toward contraction. Thus in 146 of the 188 runs with stuck minifilaments, T_m was contractile at the time of sticking, and all but 6 of these retained the contraction after complete relaxation. Of the remaining 42 runs, 27 transformed from extensile to contractile after sticking, by mechanisms including rotation with one end fixed. The mechanism described here is quite general. It requires large rotations of myosin minifilaments, but not nonlinear actin network elasticity. Only 2% of the runs had extensile myosins with filament bending angles larger than 10°, showing that buckling is not a crucial factor. Furthermore, doubling the filament bending modulus κ, corresponding to reduced nonlinear effects, led to *larger* average values of T_m/F_{ATP}. The mechanism is also independent of specific assumptions regarding the behavior of myosin at filament ends. The main requirement for contractility is that the network structure be sufficiently rigid to support well-defined minifilament energy extrema. This requirement may explain why Ref. [10] found that crosslinkers were needed for contractility.

The very large wall stresses seen in Fig. 2.6 indicate the importance of the network structure. We find that tensile force chains - linked chains of rods under high stress - cause the stress enhancement. These are shown as the thick lines in the relaxed network of Fig. 2.8, which are obtained by finding all connected paths of rods having

tensile strain exceeding a critical value of 0.01%. This mechanism is related to that of Ref. [35], in which force propagation along actin filaments connected to the minifilament enhances the stress; here the effect is greater because chains of filaments, rather than single filaments, are involved. The effect found here may help bridge the gap between measured values of the tension in cytokinesis, and the low theoretical values obtained in Ref. [35].

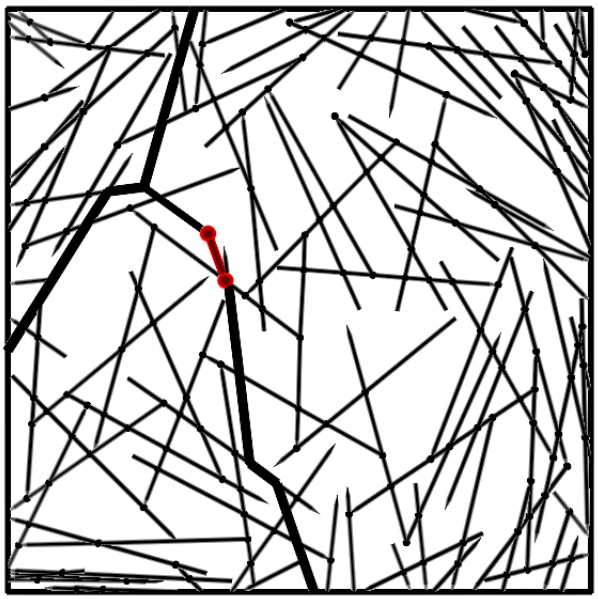

Figure 2.8: Force chain (thick lines) observed after elastic relaxation.

We have evaluated the robustness of the results by varying our input parameters and assumptions. The stresses increase sublinearly with increasing F_{ATP}, but remain contractile and greatly exceed σ_{th}. Doubling γ changes the mean stress by less than 1%; including a crosslink rotation energy comparable to the bending energy changes

it by only about 5%.

2.5 Discussion

The mechanism is general enough to apply when dynamic network effects, such as actin filament treadmilling (barbed-end growth matched by pointed-end depolymerization) and crosslinker dynamics, are included. Since myosin heads move rapidly on actin filaments [50], the minifilaments would equilibrate in a few seconds or less. The time for a filament to treadmill is probably on the order at least tens of seconds. Typical crosslinker lifetimes in cells are on the order of tens of seconds [51, 52]. Therefore the qualitative conclusions reached here should be independent of treadmilling and crosslinker release.

In summary, directional motion of myosin minifilaments along actin network filaments, toward low-energy contractile configurations, produces contractile stresses. This general mechanism requires no specific orientation constraints in the network. Furthermore, the myosin stress is magnified by force chains which transmit force directly to the boundary. Future work should aim to evaluate the stresses more quantitatively in the context of a cellular environment incorporating a three-dimensional branched network structure.

This work was supported by the National Institutes of Health under Grant R01 GM086882.

Appendix

A Evaluating the elastic moduli of networks

For our theoretical calculations, we assumed that the networks we generated were close to isotropic elastic materials. Hence to determine their elastic properties we used two dimensional stress strain relationships for an isotropic elastic material. Fig. A1 shows a simple shear strain (Fig. A1(a)) and affine axial strain (Fig. A1(b)) of a two dimensional square with area $l \times l$. The force applied in each case is F. The change in angle from vertical direction due to shear is γ while the extension of the material due to axial strain is Δx.

A.1 Shear modulus of the networks

For the case shown in Fig. A1(a), the shear modulus G is defined as :

$$\begin{aligned} G &= \frac{\text{shear stress}}{\text{shear strain}} \\ G &= \frac{\tau}{\gamma} \end{aligned} \tag{A-1}$$

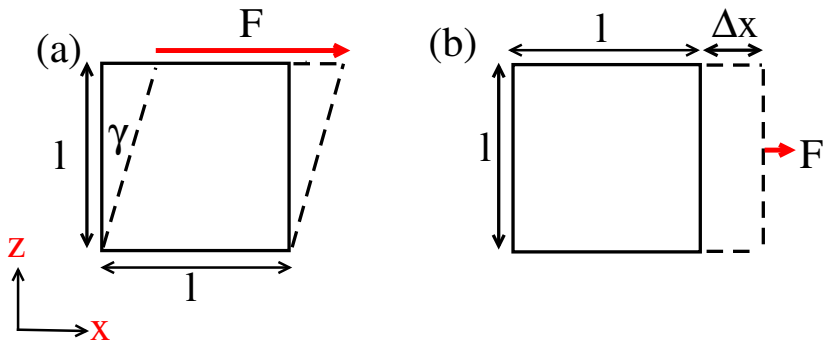

Figure A1: A simple shear strain (a) and an affine axial strain (b)

where $\tau = F/l$. Also the elastic shear strain energy density (U_s - energy per unit area for a two dimensional material) relates to the shear modulus by:

$$U_s = \frac{\tau^2}{2G} \tag{A-2}$$

Hence by Eq. A-1 we have:

$$\begin{aligned} U_s &= \frac{G^2\gamma^2}{2G} \\ G &= \frac{2U_s}{\gamma^2} \end{aligned} \tag{A-3}$$

To evaluate the shear modulus of the random networks, they were sheared by a small angle and then allowed to relax to their new equilibrium positions. Then Eq. A-3 was used to calculate modulus for each network. This was done before adding any mini-filaments to the network. Fig. A2 shows snap shots of a network initially, after shear of 2.8%, and after allowing it to relax.

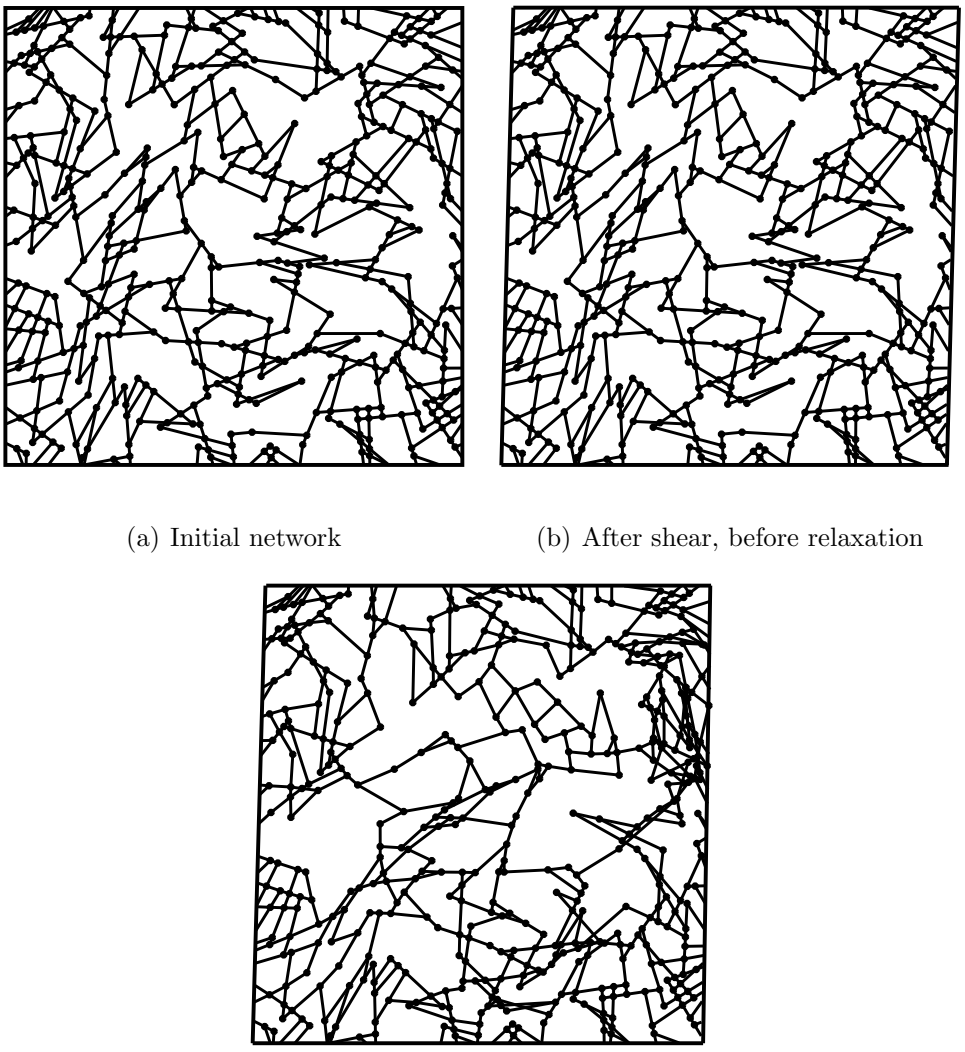

(a) Initial network

(b) After shear, before relaxation

(c) After shear and relaxation

Figure A2: Different stages during the shear of a 1 $\mu m \times 1$ μm network. Here the length of an actin filament is 0.2 μm.(a) Initial network before shear. (b) After shearing by an angle 1.6° which is about 2.8% and before allowing the crosslinks to relax to new equilibrium positions. (c) After allowing the crosslinks to relax to new equilibrium positions.

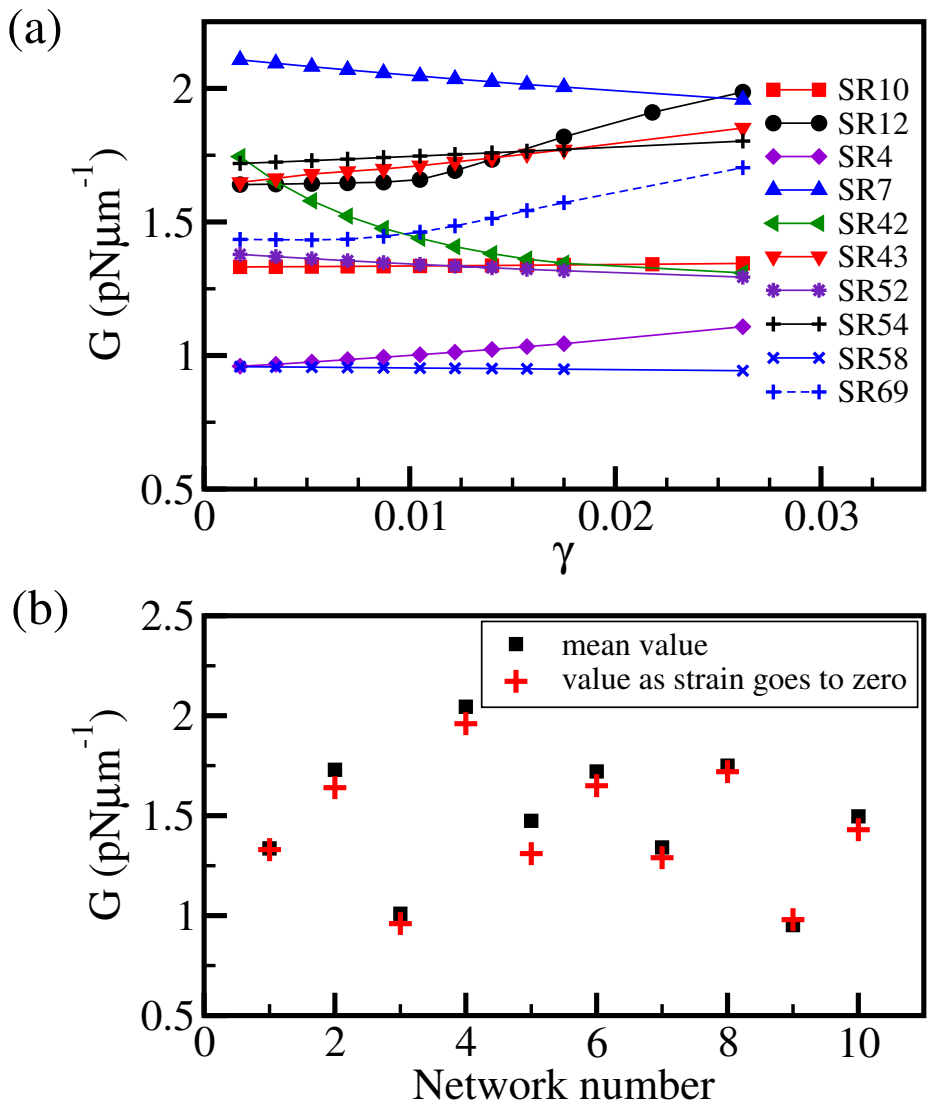

Figure A3: Shear modulus for different random networks. (a) Variation of shear modulus with the angle of shear. Y axis shows the shear modulus in units $pN\mu m^{-1}$ and x-axis shows the applied strain for ten different networks. Legend indicates the value of the random seed for each network. (b) Mean value of shear modulus (black squares) calculated for each network and the red crosses represent the limiting value of the shear modulus as the shear strain goes to zero, calculated from data sets in Fig. A3(a).

Fig. A3 shows the calculated shear modulus for different networks created using different random seeds. Fig. A3(a) shows the variation of the shear modulus in different networks with the angle of shear. Fig. A3(b) shows the mean values of shear modulus using its limiting value as the shear strain goes to zero, calculated from data sets shown in Fig. A3(a). The mean shear modulus for these networks is about $1.5pN\mu m^{-1}$.

A.2 Stretch elastic constant of the networks

For the square area shown in Fig. A1(b), the stretch elastic constant, c_{11} is defined as :

$$\begin{aligned} c_{11} &= \frac{\text{stress}}{\text{strain}} \\ c_{11} &= \frac{F/l}{\Delta x/l} \\ c_{11} &= \frac{F}{\Delta x} \end{aligned} \tag{A-4}$$

Similar to Eq. A-2, the energy density due to axial strain (U_a) relates to stretch elastic constant by:

$$U_a = \frac{(F/l)^2}{2c_{11}} \tag{A-5}$$

Hence by Eq. A-4 we have:

$$\begin{aligned} U_a &= \frac{(c_{11}\Delta x/l)^2}{2c_{11}} \\ c_{11} &= \frac{2U_a}{\eta^2} \end{aligned} \tag{A-6}$$

where $\eta = \Delta x/l$.

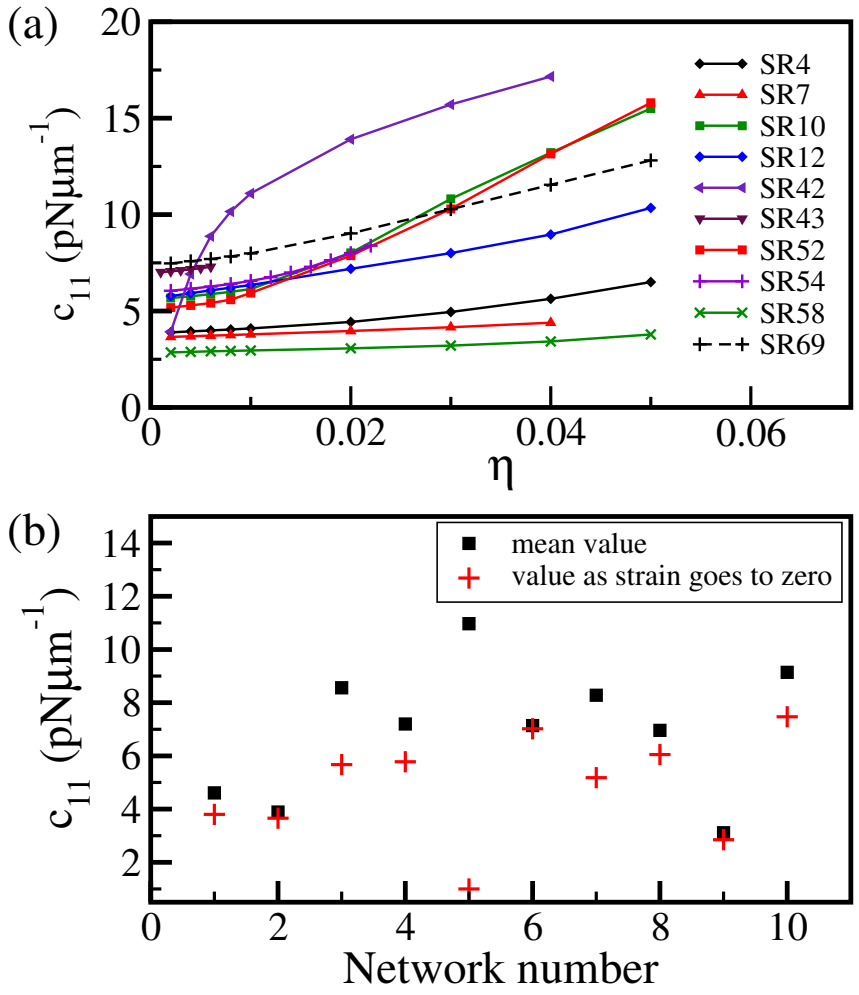

Figure A4: Stretch elastic constant for different random networks. (a)Variation of stretch elastic constant with the axial strain. Y axis shows the stretch elastic constant in units $pN\mu m^{-1}$ and x-axis shows the strain for ten different networks. Legend indicates the value of the random seed for each network. (b) Mean value of stretch elastic constant (black squares) calculated for each network and red plus symbols represent the limiting values of stretch elastic constant as the strain goes to zero, calculated from data sets in Fig. A4(a).

Similar to the shear modulus, stretch elastic constant of the random networks were calculated by first straining the network in the x direction (Fig. A1(b)) and allowing it to relax to its new equilibrium position. Then the energy density due to strain was calculated and the stretch elastic constant for each network was calculated using the relation given in Eq. A-6. Fig. A4(a) shows moduli calculated for ten different networks. The mean value of stretch elastic constant for these networks is about 6 $pN\mu m^{-1}$. Note that for network number 5 in Fig. A4(b) which belongs to the data set SR42 in Fig. A4(a), the values as the strain goes to zero ($\sim 1\ pN\mu m^{-1}$) is an extrapolated number from its data set in Fig. A4(a).

A.3 Greens function approach to mechanical response

In order to evaluate the stability of the networks created, the displacements ($\vec{u}$) of crosslinks induced by active forces ($\vec{F}_{myo}$) were evaluated in terms of the eigenvalues and eigenfunctions of its dynamical matrix $\hat{D}$. At equilibrium, internal forces ($\vec{F}_{int}$) balance external or the active forces. Hence we have,

$$\vec{F}_{myo} + \vec{F}_{int} = 0, \tag{A-7}$$

in steady state, where $\vec{F}_{myo}$ are the forces exerted by the myosins on the crosslinks and $\vec{F}_{int}$ are the internal forces generated by the stretching and bending energies of the network. These internal forces are given by,

$$\vec{F}_{int} = -\hat{D}\vec{u}. \tag{A-8}$$

From linear algebra, the fact that $\hat{D}$ is symmetric implies that

$$\hat{D} = \sum_{\nu} \lambda_\nu |\nu\rangle\langle\nu| \tag{A-9}$$

where λ_ν and $|\nu\rangle$ are the eigenvalues and eigenvectors of $\hat{D}$. The eigenvectors are normalized so that the sum of the squares of the components is unity. More concretely;

$$D_{ij} = \sum_{\nu} \lambda_\nu v_{\nu i} v_{\nu j} \tag{A-10}$$

To find the response of the material to the applied forces, we note that,

$$\vec{u} = -\hat{D}^{-1}\vec{F}_{int} = \hat{D}^{-1}\vec{F}_{myo} \tag{A-11}$$

where $\hat{D}^{-1}$ is the Greens function. Now,

$$\hat{D}^{-1} = \sum_{\nu} \lambda_\nu^{-1} |\nu\rangle\langle\nu| \tag{A-12}$$

so that

$$[\hat{D}^{-1}]_{ij} = \sum_{\nu} \lambda_\nu^{-1} v_{\nu i} v_{\nu j} \tag{A-13}$$

Then the response to the myosin force is given by

$$u_i = \sum_{\nu,j} \lambda_\nu^{-1} v_{\nu i} v_{\nu j} F_j^{myo} \tag{A-14}$$

The result shows that a large response to an applied force corresponds to small eigenvalues of $\hat{D}$, and that a long-ranged response corresponds to extended eigenvectors of $\hat{D}$. In a periodic system, the eigenvectors are plane waves of displacement, the index ν becomes $\vec{k}$, and the sum determining u_i becomes a Fourier transform.

Fig. A5 is a sample of eigenvalues obtained for the dynamical matrix of different network structures. They span from 0 up to about 15000 in value. Each line in Fig. A5(a) represents a sorted set of eigenvalues belonging to a particular structure. Fig. A5(b) is the distribution of states over the range for all data sets shown in Fig. A5(a).

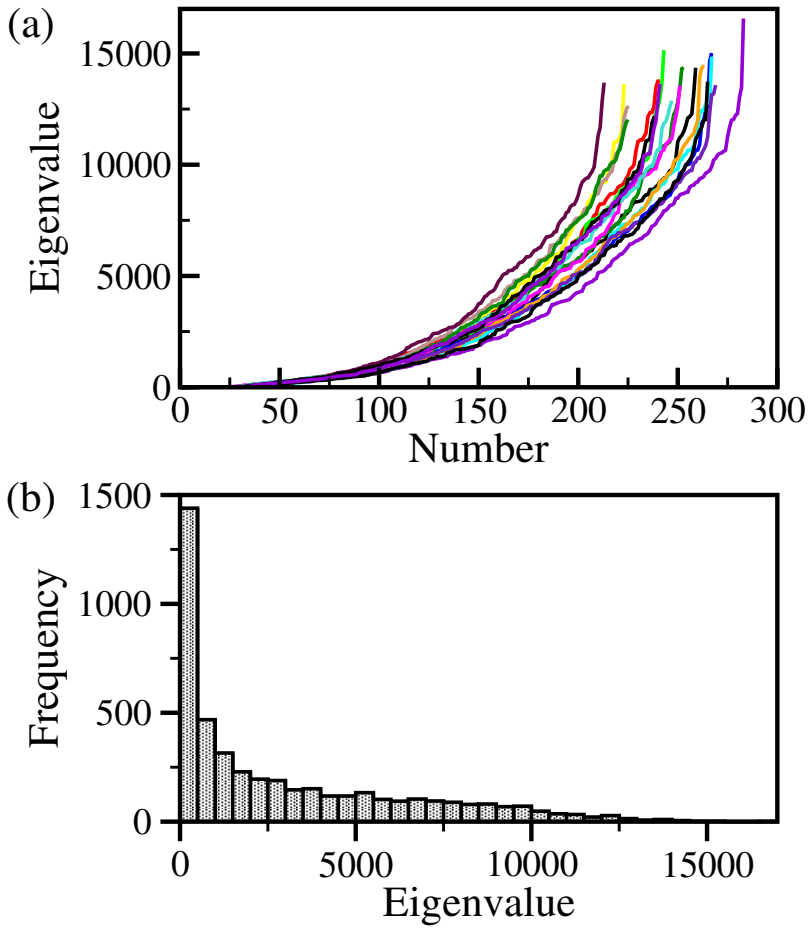

Figure A5: Eigenvalues of dynamical matrix for different networks. (a) Distribution of eigenvalues. Each line corresponds to a set of eigenvalues of a particular network structure. (b) The density of states for all the data sets shown in (a).

It is evident that in the networks that were generated, there are an abundance of soft modes that allow crosslinks to displace without much resistance from the rest of the structure. These modes have eigenvalues that are roughly within the lowest 3% in the set $(0, 15000]$. We find that these occur more when the density of filaments in the network is low or when there is a cluster of rods that is not well connected with the network and when the crosslinks in such a cluster move collectively in the same direction.

Also it is evident that in soft modes, the required displacements can be achieved by bending of filaments. An example of a soft mode is shown in Fig. A6(a). Modes with higher eigenvalues are the ones that produces very small displacements. These occur when there is tight crosslinking of rods and the crosslinks try to move independently. Here even a slight displacement of a crosslink can only occur by stretching the rods that are connected. Hence we find that the requirement to stretch filaments for displacement gives rise to high frequency modes. Fig. A6(b) represents such a high frequency mode.

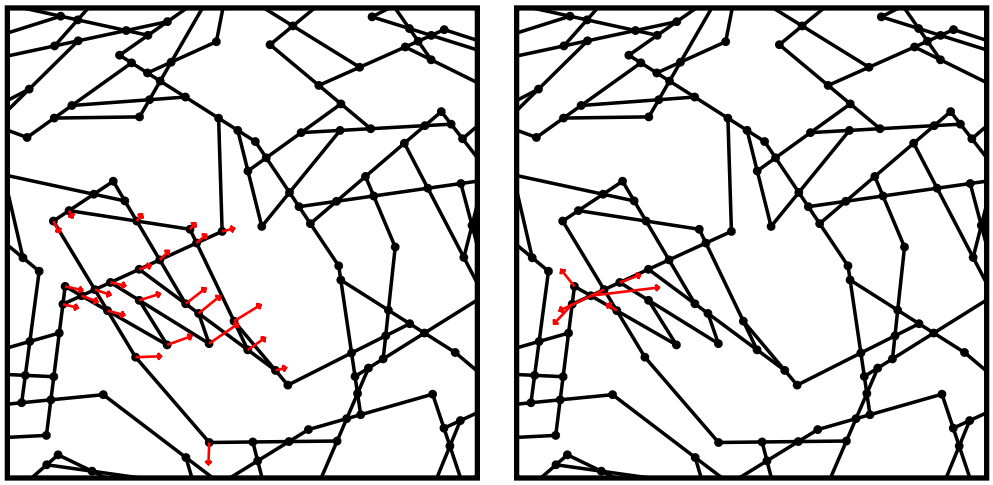

(a) Low frequency mode (b) High frequency mode

Figure A6: A $5\mu m \times 5\mu m$ network having a total of 244 different frequency modes calculated considering displacements of 122 crosslinks in x and z directions. Red arrows show the direction the crosslinks move in a particular mode. Eigenvectors are normalized and only crosslinks with eigenvector magnitude 5×10^{-2} and higher displacement values are associated with an arrow. (a) A low frequency mode which results in large displacements. This mode represents prominently a collection of crosslinks which are in a cluster of rods that are relatively loosely connected to the rest of the network moving collectively in one direction. (b) A high frequency mode that results in small displacements. Crosslinks belonging to a tightly bound rods that forms triangular shapes moving in opposing directions to each other. This is energetically very expensive as a slightest displacement of a single crosslink requires adjacent rods being stretched.

Chapter 3

Contractility in Bundles

3.1 Introduction

As discussed in Chapter 2, force generation due to non-muscle myosin II and actin is essential for key cellular processes, including retraction of the trailing edge during migration, generation of retrograde flow at the leading edge, and the exertion of force on the cell's environment. Myosin in cells is generally found in polymeric units known as mini-filaments, which contain tens of myosin heads at either end, and have length on the order of 0.5 μm. The force generation process often involves the action of myosin mini-filaments on parallel or nearly-parallel actin filament arrays. For example, trailing edge retraction relies on non-muscle myosin II in the middle and rear of the cell [15], where filaments are longer than at the leading edge and are biased toward parallel orientation. Stress fibers, which exert forces on the cell's

environment that may aid mechanosensing, consist of nearly parallel bundles of actin filaments. Traction studies of cells have demonstrated strong correlations between myosin distribution and contraction [16, 17]. These findings have motivated *in vitro* studies of the combination of mini-filaments with actin bundles and ATP. It has been found that this combination produces contraction with [54, 55, 10, 56] or without [9] extra passive cross-linkers. When extra cross-linkers are absent, the mini-filaments themselves, if present at sufficiently high concentration, act as cross-linkers, and this is crucial for maintaining the bundle geometry and generating effective contraction. In recent studies [57], bundles with parallel and antiparallel actin filaments were grown from bars coated with actin nucleation factors. These studies found that antiparallel actin filament arrays generate much more contraction than parallel ones.

Obtaining a quantitative understanding of the origins of the contractile stress, and the relationship of the molecular-level forces to the macroscopic stresses, is important because it is a prerequisite for a detailed understanding of cell migration and mechanosensing. Several studies have addressed the origin of the contractile stress in bundled structures. Application of hydrodynamic theory to linear actin bundles suggested that contraction occurs only if mini-filaments reaching the barbed end stay there [8, 33], and this result is supported by later calculations of myosin patterning in bundles [44]. Other calculations treating one dimensional bundles found that non-linearities such as buckling are required for contractility [9, 34, 10]. Refs. [9, 34] also suggested that having linkers with non-identical unloaded velocities is important

for generating these nonlinearities. However, there have been no studies treating the origin of the contractile stress taking into account the actin network structure in a detailed fashion, in particular the effects of forces and displacements perpendicular to the bundle. The effect of the actin network structure in bundles on the macroscopic stress has also not been addressed to our knowledge, except for a generic study indicating the effect of the filament length [35].

Previously [58] we analyzed stress generation by a myosin mini-filament in a two-dimensional isotropic actin network with bending and stretching degrees of freedom. We found that the forces exerted by myosin mini-filaments are mainly contractile because they rotate from unstable extensile equilibria to stable contractile equilibria as they move toward actin filament barbed ends. We also found that the macroscopic stress often exceeds an estimate based on continuum elasticity, because of force chains leading from the mini-filaments to the walls. In the present work, we extend these calculations to treat a bundle structure obtained by restricting the orientations of the actin filaments so that they are nearly parallel. In multiple stochastic realizations of actin bundles and myosin minifilaments in the bundles, we evaluate the tension on the myosin minifilament, and the force transmitted by the actin network to the walls. We also evaluate the additivity of the transmitted forces, and the extent of strain stiffening caused by the myosins. The goal of this work is to see to what extent actomyosin contraction in bundles can be understood by making only a very economical and well-justified set of assumptions: i) that myosin heads move toward

actin filament barbed ends, ii) that actin filaments are semiflexible polymers with a large stretching modulus, and iii) that the actin filaments form crosslinked bundled structures.

We find that, as in the isotropic networks, rotation of myosin minifilaments to their final configuration leads to contraction. This process does not require nonlinear actin network effects. However, we find an additional contribution resulting from the nonlinear bending of the portions of actin filaments beyond their last crosslink. This bending reduces extensile forces, and is analogous to the nonlinear buckling forces that have been discussed in previous models [9, 34, 10]. This contribution is greater in bundles than in networks, because in bundles myosins are more likely to move to the ends of actin filaments, and because the "dangling ends" of filaments in bundles are longer. We also find that bundles contract more strongly than networks, and that antiparallel actin filaments give stronger contraction than parallel filaments. Surprisingly, the contractile forces transmitted to the walls by the actin filaments can exceed the tension in the myosin minifilament itself. By performing calculations with multiple minifilaments we show that the wall forces are nearly additive. Finally, we find that myosin-based contraction causes large strain stiffening effects.

This chapter is based on, and extends, a manuscript "Stress Generation by Myosin Mini-filaments in Actin Bundles", by N. L. Dasanayake and A. E. Carlsson. This manuscript has received one round of favorable review at Physical Biology, and is currently being revised.

3.2 Methods

Two-dimensional bundles were generated following a modification to the method we used to generate isotropic networks [58], based on Ref. [46]. We first placed filaments with random positions in a two dimensional geometry (see Figs. 3.1a-b). The orientations of the filaments were restricted to be within a cutoff angle θ_c from the x-axis, but taken random within this window. Filaments extending outside the simulation cell were cropped. Passive crosslinks were placed at filament intersections, and their positions along the filaments were fixed. We will refer to a filament segment between two crosslinks, or a segment between a crosslink and a free end, as a "rod". Filaments generating extremely short rods were eliminated for computational convenience. Because our actin structure is two-dimensional, it cannot be directly compared to three-dimensional structures of bundles in cells obtained, for example, via electron microscopy. It is also not clear how to relate the width in our calculations to the width of a three-dimensional bundle, since the number of filaments in a cross-section for a given width will be different between two and three dimensions. For this reason, we perform calculations for two different bundle geometries. The first one we call a "thin bundle". Its width is about 1 μm, and the length is 10 μm. This geometry is designed to mimic as best we can the types of bundles that have been studied *in vitro*. The second one we call a "thick bundle". Its thickness is 2.5 μm and the length is $5\mu m$.

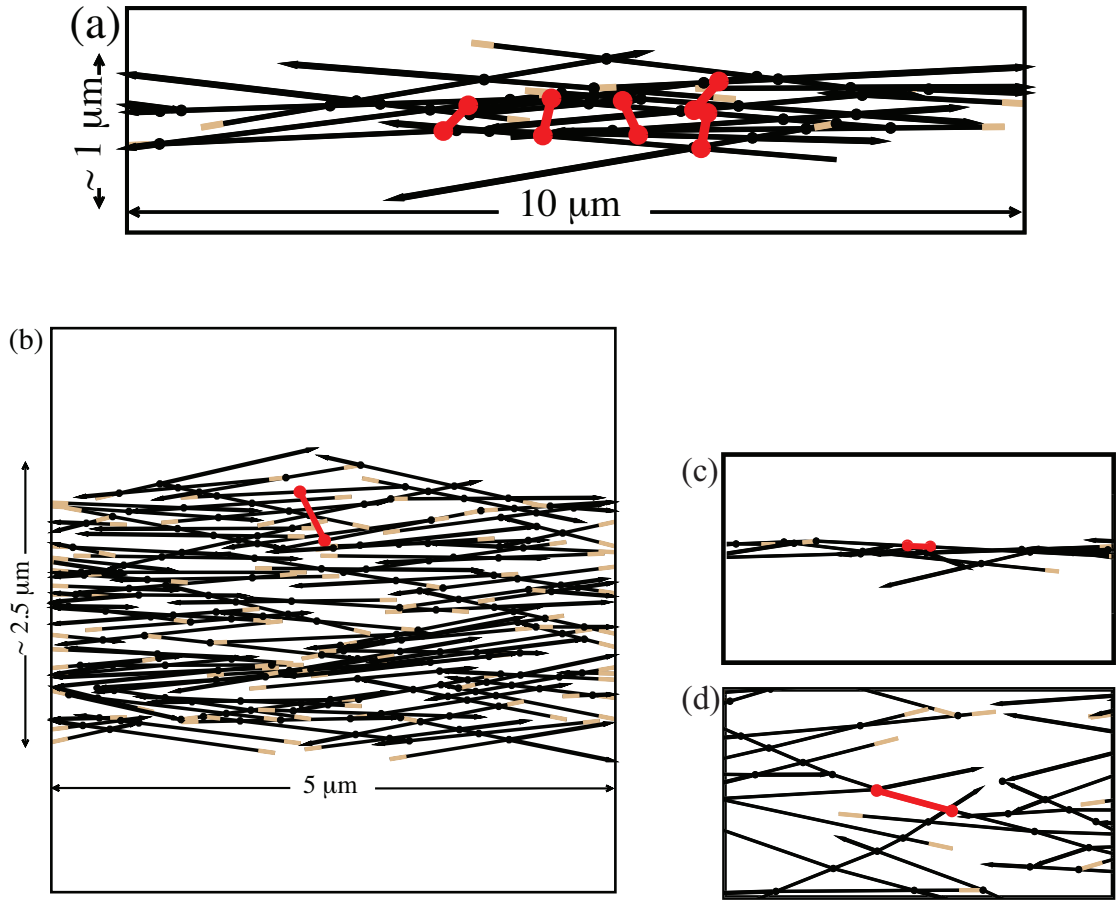

Figure 3.1: An actin bundle (black lines) with a myosin minifilament (red dumbbell). Barbed end is colored in brown and the pointed end is drawn as an arrowhead. a) Initial configuration of the mini-filaments before relaxation for a thin bundle. b) Initial configuration of the mini-filament before relaxation for a thick bundle. c) Final configuration of a mini-filament in a thin bundle. d) Final of a mini-filament in a thick bundle.

This geometry is designed to give the clearest comparison with our previous results for isotropic networks, so that we can focus on the effects of filament orientation on

stress generation. Although our structures are different from true actin bundles, we term them bundles for simplicity.

Next the network was randomly scanned for pairs of points on different filaments that could be linked by myosin minifilaments. The two ends of a minifilament were placed at a pair of points having distance within 10% of the average equilibrium minifilament length $\overline{L}_m$. New, mobile crosslinks were created at these points. This process was repeated for each myosin that was added. The positions of the myosin minifilament ends relative to the respective barbed ends of the actin filaments were defined by variables M_j, the distance to the barbed end measured in units of the size of a single actin subunit. For thin bundles, we typically treated five myosins to have the same number of mini-filaments per unit length as in [9]. For thick bundles, we treated a single myosin for comparison with our previous results for isotropic networks. This is the equilibrium state of the network in the absence of ATP-induced myosin motion.

As in Ref. [58], the myosin heads at the minifilament ends were then moved, and the actin network relaxed, according to forces from the stretching ($E_{stretch}$) and bending (E_{bend}) energies of actin filaments, the myosin minifilament stretching energy E_m, and an ATP-based motor energy E_{motor} driving myosin heads toward barbed ends. We do not consider energies due to rotation of crosslinking points, and thus allow the rods to rotate freely at these points. We assume that the stretching energy is quadratic in the length changes ΔL_i of the rods. We assume that the bending energy is quadratic in the angle changes $\Delta\theta_j$ between rods on the same filament, and that

it is inversely proportional to the average length $\overline{L}_j$ of the two rods on either side of a crosslink. For the mini-filament stretching energy, we assumed, for computational convenience, a form that is quadratic for small changes of the mini-filament length L_m, but has a somewhat different form for larger changes. We described the myosin motion by a motor energy proportional to the number of subunits M_j from an end of the mini-filament to the barbed end of an actin filament. Thus the total energy of the system is:

$$E_{tot} = E_{stretch} + E_{bend} + E_m + E_{motor} \tag{3.1}$$

$$= \frac{\mu}{2}\sum_{i=0}^{N_r}\frac{(\Delta L_i)^2}{L_i^0} + \frac{\kappa}{2}\sum_{j=0}^{N_c}\frac{(\Delta\theta_j)^2}{\overline{L}_j} + \frac{\gamma}{2}[(L_m)^2 - (L_m^0)^2]^2 + (M_1 + M_2)\delta F_{ATP} \tag{3.2}$$

where L_i^0 is the initial length of a rod, N_r is the total number of rods, and L_m^0 is the initial mini-filament length. The parameters are as follows: μ is the stretching modulus, κ is the bending modulus, γ is the minifilament stretching energy constant, δ is the size of an actin subunit, and F_{ATP} is the stall force of the myosin heads at one end of the minifilament.

For each bundle thus generated we evolved the system to a stable steady state minimizing the total energy E_{tot}. Myosin motion along filaments, described by the variables M_j, was treated separately from elastic relaxation of the actin filaments, because the latter process is much faster. For each set of values of M_j, a complete elastic relaxation of the crosslink positions was performed using a nonlinear conjugate-gradient method [59], so that the actin network equilibrated. The elastic energy, and

the derivatives of this elastic energy with respect to the M_j (generalized forces), were calculated. The myosin heads then followed a steepest-descent algorithm driven by the generalized forces and E_{motor}, until the sum of the squares of forces became less than $10^{-12}pN^2$. Mini-filaments were allowed to jump over crosslinking points without slowing their motion. We assumed that mini-filaments reaching the barbed ends of actin filaments stay there and act as passive crosslinkers. We also discuss the effects of making the opposite assumption, that mini-filaments reaching the barbed ends leave the simulation box.

In this final configuration, we evaluated the tension T_m in the minifilament and the macroscopic stress on the walls. We evaluated the stress in two ways. First we calculated the stress (or linear force density)

$$f_{wall} = -\sum_i (\vec{f_i} \cdot \vec{r_i})/A \tag{3.3}$$

where $\vec{f_i}$ is the force exerted by a rod on the wall, $\vec{r_i}$ is the position of a rod-wall contact point, A is the area of the bundle, and the sum is over all points where actin filaments contact the edges of the simulation cell. The motivation for calculating this quantity is to compare our present results for bundles directly to our previous results for random networks [58]. Second we calculated the x-components F_{wall} of the total force on either side of the bundle. We repeated the simulation run 500 times using different random seeds and choices between possible myosin positions. For comparison, we also present data for networks obtained from 250 simulation runs.

The parameter values were chosen as follows. The bending modulus was given the measured value $\kappa = k_B T l_p$, where $l_p \simeq 15\mu m$ [39]. Because use of the experimental value of μ (45 nN [47]) led to slow convergence of the elastic relaxation, we used a smaller value $\mu = 600\ pN$, which is still large enough that filament stretching is negligible compared to bending. For thin bundles, we used actin filament lengths of 5 μm, commensurate with values used in *in vitro* studies. For thick bundles we used actin filament lengths of 2 μm, typical for regions away from the leading edge of cells. We used an average minifilament size of $\overline{L}_m^0 = 0.4\ \mu m$ [41]. To check the effect of the value used for the unknown myosin stiffness parameter γ, it was doubled from 60 $pN/\mu m^3$ to 120 $pN/\mu m^3$. We varied F_{ATP} over a range on the order of pN, which corresponds to myosin heads with a low duty ratio. We also tried different values for orientation cutoff angle θ_c in the bundles, to evaluate the effect of the bundle structure.

3.3 Results

3.3.1 Distribution of mini-filament tension and wall stress

Fig. 3.2 summarizes our main findings. It compares the distribution of minifilament tension T_m (a-c), force density on walls f_{wall} (d-f), and total force on walls F_{wall} (g-i), in thin and thick bundles, to our previous results for networks [58].

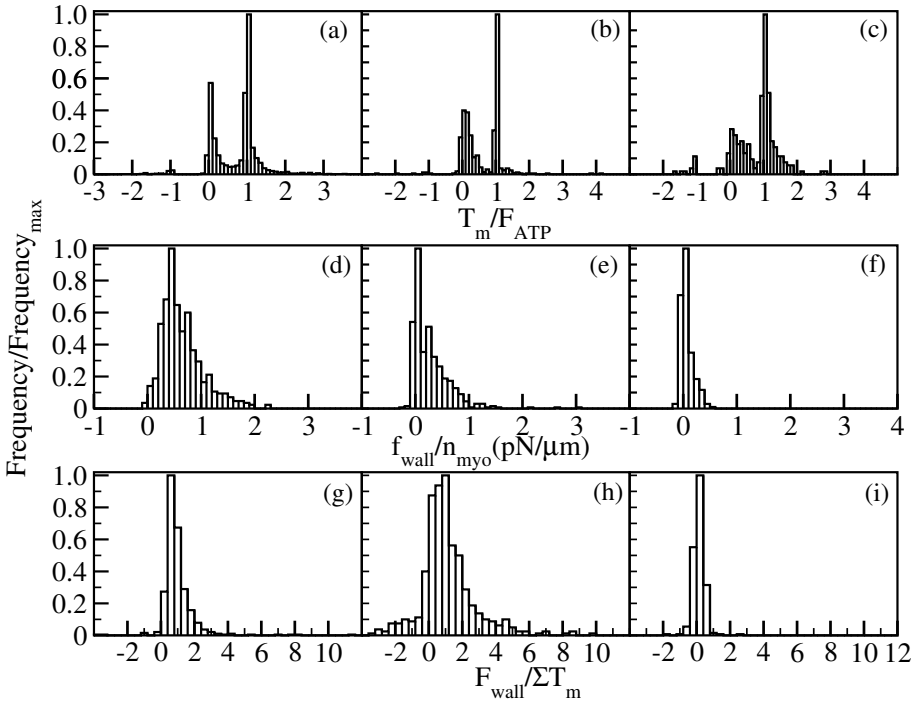

Figure 3.2: Histograms of myosin tension, force density and wall force. Frequency for all histograms is scaled by the maximum frequency. Data is shown for 500 runs for thin bundles (with five mini-filaments), 500 runs for thick bundles (with one mini-filament) and 250 runs for networks (with one mini-filament). Positive tension, force, and force density correspond to contraction. Myosin mini-filament tension scaled by myosin stall force for thin bundles a), thick bundles b), and networks c). Mean values are 0.72, 0.58, and 0.77, respectively. Force density on walls for thin bundles d), thick bundles e) and networks f). Mean values are 3.2 $pN\mu m^{-1}$, 0.28 $pN\mu m^{-1}$, and 0.07 $pN\mu m^{-1}$, respectively. Wall force scaled by sum of myosin tensions for thin bundles g, thick bundles h), and networks i). Mean values are 0.99, 2.58, and 0.35, respectively. About 10 runs in h which gave values greater than 10 were omitted for clarity. These values were exaggerated because they are due to very small T_m values of mini-filaments that moved to dangling ends, rather than from amplification by the network effects.

The following are the key results seen in the Figure, which we explain in more detail below:

- T_m, f_{wall}, and F_{wall} in bundles are overwhelmingly contractile, as in our previous results for isotropic networks. In thin bundles, these quantities are contractile in 99% of the cases. In thick bundles, 85% of the runs had contractile f_{wall} and F_{wall}, while 90% had contractile T_m. For networks these fractions are 70% and 91% respectively.

- The results for bundles differ from networks in that the average T_m is smaller but the average f_{wall} and F_{wall} are larger; furthermore, the distribution of T_m is narrower in bundles and has a pronounced peak at $T_m = 1$.

- The forces exerted on the walls in bundles, particularly thick ones, often exceed the mini-filament tension itself, as shown by the F_{wall}/T_m values in Fig. 3.2g-h

Origin of Contractile Force

In our previous work for isotropic networks [58], we found that mini-filaments starting in extensile configurations rotate into contractile configurations because this process lowers the part of the system energy, that drives myosin heads toward actin filament barbed ends. In the present calculations for bundles, a similar mechanism operates. Consider the simplified model shown in Fig. 3.3a, based on a minifilament moving along two parallel actin filaments. The actin filaments are connected by a

linear spring which tends to keep them at an equilibrium separation. In the initial configuration shown in the picture, the mini-filament has just attached in an orientation perpendicular to the filaments. At this stage the mini-filament moves freely and does not exert forces on the actin filaments, which are at an equilibrium separation determined by the rest of the network. We calculate the properties of the mini-filament motion using an energy function E_{tot} containing E_{motor}, and a quadratic elastic term with spring constant k_{spring} describing the distortion of the actin network. Since the filaments are oppositely directed, E_{tot} is independent of mini-filament position. Therefore, we write it in terms of the mini-filament orientation angle:

$$E_{tot} = -2\left(\frac{L_m}{2}\right)\cos(\theta)F_{ATP} + k_{spring}[L_m - \sin(\theta)L_m]^2/2 \tag{3.4}$$

so that

$$\frac{dE_{tot}}{d\theta} = L_m \sin\theta F_{ATP} - k_{spring}L_m^2 \cos\theta(1-\sin\theta), \tag{3.5}$$

which is positive at the starting point of $\theta = \pi/2$. Therefore θ will initially decrease since this reduces E_{tot}. The final value θ_f of θ (frame b) will be determined by the competition between E_{motor} and the elastic term. To calculate the tension in the minifilament at θ_f, we note that the forces exerted by the actin filaments on the heads are equal and opposite, and (because the torque must vanish) oriented parallel or antiparallel to the mini-filament. The x-direction force on the upper head from the actin filament is $+F_{ATP}$. Because the total force F_{tot}^{act} from the actin filament onto

this head must point parallel to the minifilament, and equals the tension T_m, force balance in the x-direction gives $T_m \cos\theta = F_{ATP}$, so that

$$T_m = F_{ATP}/\cos(\theta_f). \tag{3.6}$$

This force tends to extend the mini-filament, so the mini-filament exerts a contractile force on the network. Note that if θ_f is large, T_m can exceed F_{ATP}.

A similar mechanism also operates if the initial minifilament orientation is parallel to the actin filaments (Fig. 3.3c) so that $\theta \simeq \pi$, and the equilibrium spacing between the filaments is small (we approximate it as zero). Then the energetics of θ dropping from π are described by

$$\begin{aligned} E_{tot} &= -2\left(\frac{L_m}{2}\right)\cos(\theta)F_{ATP} + k_{spring}[\sin(\theta)L_m]^2/2 \\ &\simeq -\frac{L_m(\theta-\pi)^2}{2}(F_{ATP} - k_{spring}L_m) \qquad \text{if } \pi-\theta << 1 \end{aligned} \tag{3.7}$$

The initial configuration will be unstable if E_{tot} is reduced by small changes in θ. According to Eq. (3.7), this will occur if

$$F_{ATP} > k_{spring}L_m. \tag{3.8}$$

In the initial drop of θ from π, the forces driving the minifilament heads compress it, leading to extensile stress on the network. However, as θ increases, one readily shows that $dE/d\theta$ remains negative, so that θ will drop to 0. At this point, the stress is contractile.

These two mechanisms have assumed that the mini-filament comes to equilibrium away from the barbed end of either of the two actin filaments. In our simulations, this happens almost only for antiparallel filaments. For parallel filaments, another mechanism can operate if myosin heads reaching a barbed end remain attached. In this mechanism [8], illustrated in Fig. 3.3d, a mini-filament moves toward the barbed ends of the filaments, and one of the heads (chosen to be the bottom head here) reaches a barbed end and stops. If the top myosin head is ahead of the bottom head, it will be pulled forward and thus in turn pull on the bottom head, giving a contractile T_m. If the bottom myosin head is ahead of the top head (dashed line), then, if the spring constant is small enough, the minifilament will rotate into a contractile configuration and continue to move toward the end. Although myosin heads stopping at barbed ends can generate extensile stress, the above argument suggests that the average contribution should be contractile, and the analysis of the next subsection confirms this.

Under what circumstances will these rotation mechanisms operate? The first will always operate because the mini-filament begins with a nonzero torque. The second mechanism (and the variant of the third mechanism in which the minifilament is intially extensile) will operate if the spring constant k_{spring} describing the resistance of actin rods between crosslinks to bending, is small enough. This resistance will decrease with increasing rod length L_i. Standard mechanics analysis [60] predicts

that $k_{spring} \simeq \kappa/L_i^3 = k_B T l_p/L_i^3$, giving an instability criterion of

$$F_{ATP} > F_{ATP}^{crit} = k_B T l_p L_m/L_i^3. \tag{3.9}$$

In our simulations, $l_p = 15\mu m$, $L_m = 0.4\mu m$, and $L_i \simeq 1\mu m$, which gives $F_{ATP}^{crit} \simeq 0.02pN$. Thus even values of F_{ATP} much less than 1 pN can induce this mini-filament rotation instability.

A more general way of viewing this result is via the force dipole moment

$$P = -\vec{F}_1 \cdot \vec{r}_1 - \vec{F}_2 \cdot \vec{r}_2, \tag{3.10}$$

where $\vec{F}_{1,2}$ are the forces exerted by the network on the two ends of the mini-filament (the opposites of the forces exerted by the mini-filament on the network). Since $\vec{F}_1$ and $\vec{F}_2$ must be parallel or antiparallel to $\vec{r}_1 - \vec{r}_2$ to avoid having nonzero torque on the mini-filament, consideration of the direction of the forces shows that

$$\begin{aligned} P > 0 \quad &\rightarrow \quad \text{extensile stress} \\ P < 0 \quad &\rightarrow \quad \text{contractile stress} \end{aligned} \tag{3.11}$$

But P also equals the energy of a minifilament in the presence of the forces $\vec{F}_{1,2}$ acting on its two heads. Therefore, if the forces do not change too much, rotation of the minifilament to reduce its energy will also result in making P more negative, enhancing contractile stress. This contraction mechanism requires only oppositely directed forces on the two ends of the minifilament, and freedom for the minifilament to rotate in the presence of these forces.

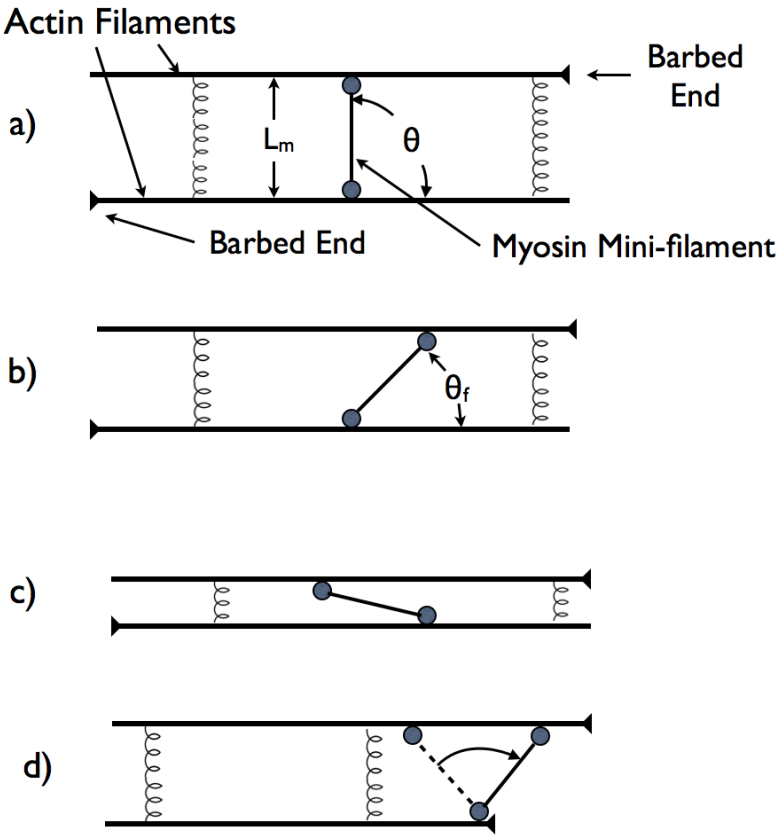

Figure 3.3: Schematic of mini-filament rotation mechanism leading to contractile stress. a) Initial configuration with mini-filament perpendicular to two antiparallel filaments. b) Final configuration where mini-filament has rotated. c) Initial configuration where mini-filament is nearly parallel to actin filaments. d) Rotation mechanism when one mini-filament head stops at an actin filament barbed end.

Origins of smaller average T_m, two-peaked shape of T_m distribution, and larger f_{wall} and F_{wall} in bundles.

These effects stem mainly from three factors: the orientation of the mini-filament at the end of the run, its position relative to the tips of actin filaments, and the differing wall contact areas between the bundles and the networks.

Mini-filament and Actin Filament Orientation. In most of the runs for bundles, the final orientation of the minifilament is parallel to the bundle. As seen in Fig. 3.4(a) the initial mini-filament orientations are mainly perpendicular to the bundle, due to the increased probability of finding two rods which are at a distance matching the mini-filament size. But Fig. 3.4(b) shows that during relaxation, mini-filaments tend to rotate to reach a final configuration nearly parallel to the bundle, so that $\theta \simeq 0$ or $\theta \simeq \pi$ For such orientations, we find that the tension is generally close to the myosin stall force F_{ATP}, as expected from Eq. (3.6). By contrast, in networks, the final distribution of mini-filament orientations relative to the actin filaments is isotropic. As shown in our previous work [58] mini-filaments in networks can reach equilibria on non parallel actin filaments where T_m greatly exceeds F_{ATP}. This occurs much less in bundles. This causes them to have i) a smaller average T_m and ii) a peak at F_{ATP} in the T_m distribution, as seen in Fig. 3.2a-c.

The fact that the actin filaments are nearly parallel in bundles also enhances their ability to transmit force to the walls. Force can be transmitted directly along chains

of filaments to the walls, without large counterbalancing elastic forces as would be present in isotropic networks. This mechanism increases f_{wall} and F_{wall} relative to their values in networks.

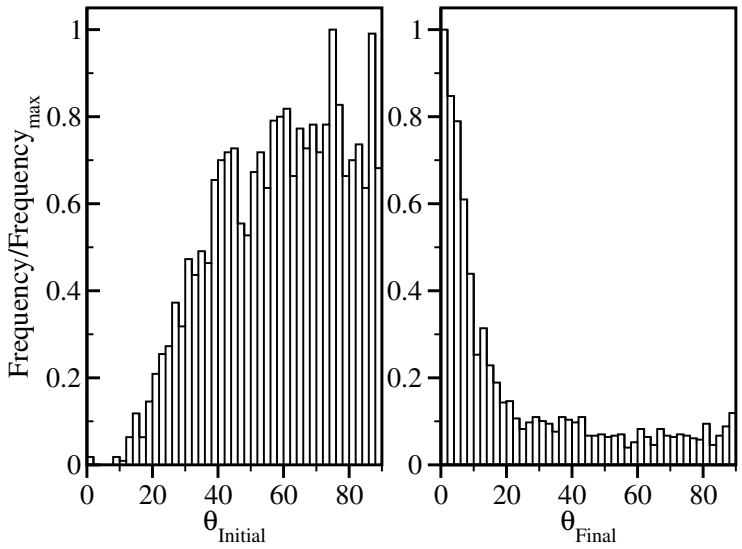

Figure 3.4: a) Angle of the mini-filament from horizontal before relaxation. Mean angle is 59 °. b) Same, after relaxation. Mean angle is 23 °.

Position of Mini-filaments Relative to Actin Filament Tips. The final positions of the mini-filaments relative to the actin filament tips impact force generation strongly, because myosin heads at the filament tips have reduced force generation capacity. Statistics describing this behavior are shown in Tables 3.1a-c. where "ends" refers to the ends of the mini-filament and not actin filaments (see Fig. 3.5). Category

A, "Both ends went to equilibrium" includes the cases where both ends of the mini-filament reached equilibrium points, away from the tips of the actin filaments to which they are attached. This occurs mainly for antiparallel filaments. The fraction in category A is greater in thin bundles than thick bundles because the filaments are longer. This occurred in less than a third of the runs for all three types of structures. Because this category has a large mean T_m, its fractional contribution to the average T_m in thin bundles and networks is about 30%.

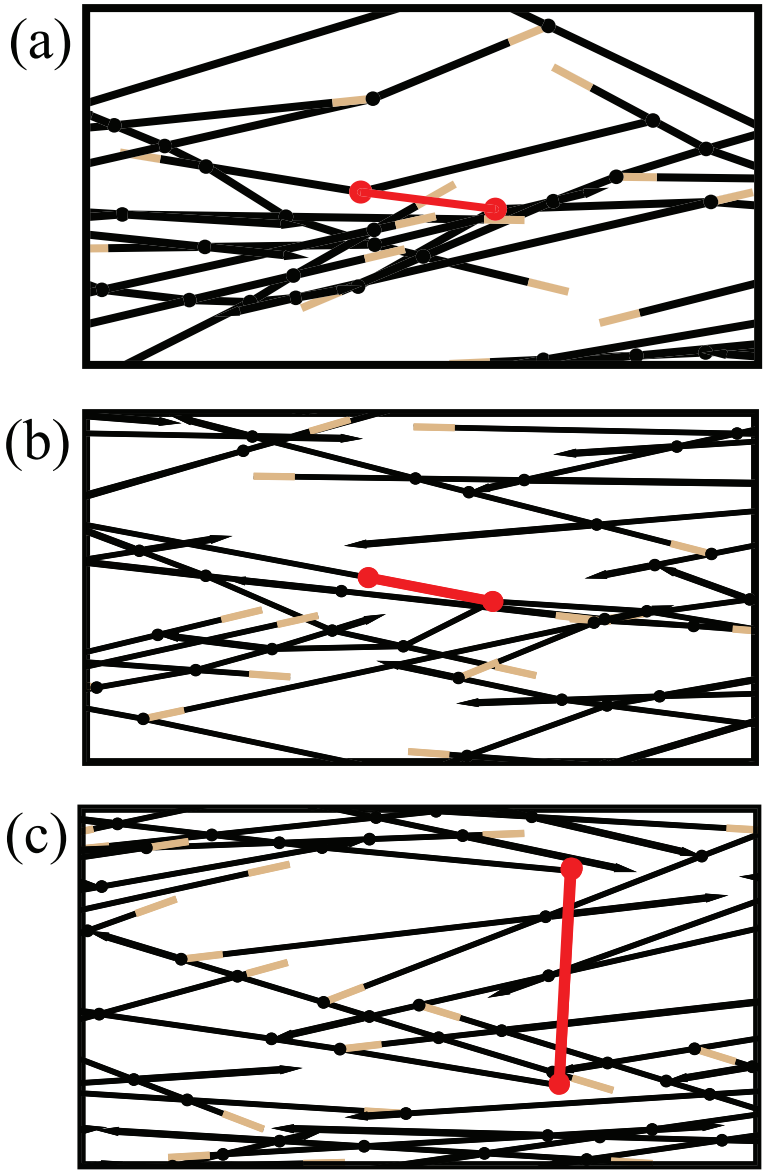

Figure 3.5: Simulation snap shots for different final mini-filament configurations. a) Both ends went to equilibrium. b) One end went to equilibrium. c) Both ends got stuck.

Table 3.1: Statistics for different categories of final mini-filament configurations for bundles and networks. A-Both ends went to equilibrium B- One end went to equilibrium C-Both ends got stuck

(a) Thin bundles.

Category	**Percentage**	**Mean T_m**	**Weighted T_m**
A	28%	1.11	0.31
B	39%	0.94	0.36
C	33%	0.14	0.05

(b) Thick bundles.

Category	**Percentage**	**Mean T_m**	**Weighted T_m**
A	7%	1.19	0.08
B	37%	0.95	0.35
C	56%	0.25	0.14

(c) Networks.

Category	**Percentage**	**Mean T_m**	**Weighted T_m**
A	25%	1.25	0.31
B	36%	0.90	0.33
C	39%	0.33	0.13

The mini-filaments in Category B have one end stuck at the barbed end of actin filament while the other end reaches an equilibrium position away from the end. This can occur with either parallel or antiparallel actin filaments. In the antiparallel case it happens most often when one of the mini-filament ends begins close to the barbed end. In such situations, that mini-filament end reaches the barbed end and stays attached, while the other end keeps moving until it reaches equilibrium. The fraction of such mini-filaments is comparable in all three geometries, and the mean T_m values are also similar, about 20-30% smaller than in Category A.

Category C, where both ends of the mini-filament got stuck at filament tips, is substantial in all three geometries. This category has the smallest mean tension because the dangling ends to which the minifilament is attached can bend easily, relieving the elastic stress built up by the motion of the myosin. The mini-filaments in this category are responsible for the peak in the T_m distribution near 0 see Fig. 3.2a-b.

The results for Categories B and C depend on the assumption that mini-filaments reaching the barbed ends of actin filaments stay there as passive crosslinkers. If we instead assume that mini-filaments reaching the barbed ends leave the simulation box, then only Category A is present. In this case, as seen in Tables 3.1a-c, the averaged T_m is increased, by an amount ranging from about 50% to 100%. For the bundles the fraction of contractile T_m increases to 99%

Contact Area. The contact area with the simulation walls is smaller in the bundles than in the isotropic networks. This results in larger forces on the horizontal walls (Fig. 3.2g-i), because the contractile force from a minifilament is spread out over two walls rather than four. In addition, the smaller area results in a larger stress (see Fig. 3.2d-f), particularly for the thin bundles.

Large magnitude of wall forces compared to T_m.

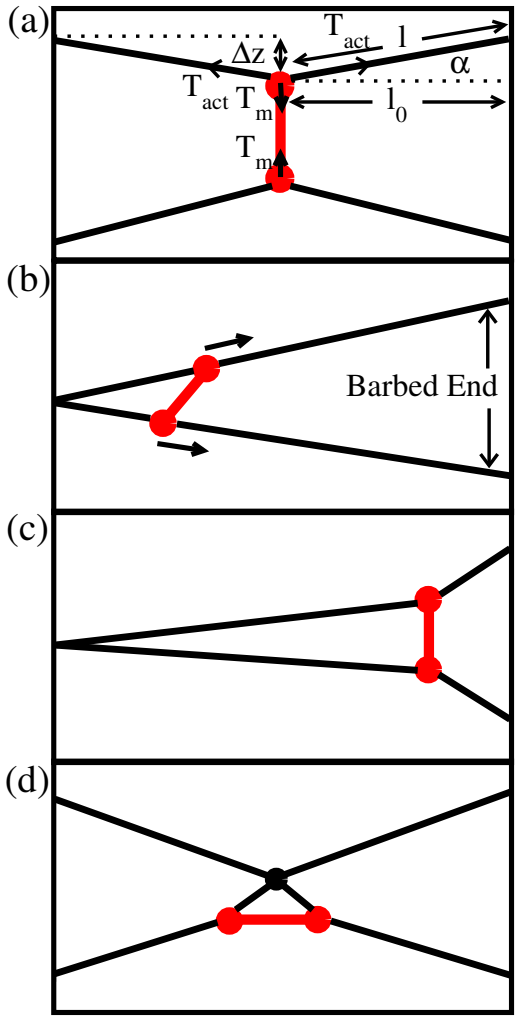

Figure 3.6: Force amplification by bundled crosslinking geometry. a) Schematic diagram of a force dipole acting in the middle of two parallel actin filaments. b) Initial orientation of the miniflament for the simulation. c) Final orientation of the miniflament for the simulation. d) Minifilament with a horizontal orientation.

The wall forces F_{wall} in bundles, particularly thick bundles (Fig. 3.2h), are often much larger than the minifilament tension T_m. This occurs because of a coupling between mini-filament forces transverse to the actin filaments, to stresses along the actin filaments. To understand this effect, we treat a model of a mini-filament as a force dipole exerting transverse forces on two parallel actin filaments, as shown in Fig. 3.6a. The model treats forces due to both bending and stretching of the filaments, and is analytically solvable if the deformations are small.

We calculate the z-direction (up/down) force balance on the upper crosslink in Fig. 3.6a. This has contributions from the bending energy at the crosslink, the stretching energy of the actin filaments, and the minifilament tension. The bending energy is $E_{bend} = \kappa(2\alpha)^2/2l$. Assuming small deformations we take α to be small, so that $\sin\alpha \approx \alpha = \Delta z/l_0$, and

$$E_{bend} \simeq 2\kappa \left[\frac{(\Delta z)^2}{l_0^3}\right]. \tag{3.12}$$

Thus the z-direction force on the crosslink due to bending is

$$F_{bend} = -\frac{\partial E}{\partial(\Delta z)} = \frac{4\kappa\Delta z}{l_0^3} \tag{3.13}$$

The z-direction force due to stretching of the actin filament is

$$F_{stretch} = 2T_{act}\alpha, \tag{3.14}$$

where T_{act} is the tension in the actin filament. To obtain T_{act} in terms of Δz, we note that since $E_{stretch} = \mu(l - l_0)^2/l_0$, $T_{act} = -\partial E_{stretch}/\partial l = -2\mu(1 - l/l_0)$. Further-

more, simple trigonometry shows that $(1 - l/l_0) \simeq \alpha^2/2$. Thus $2T_{act} \sin\alpha \simeq 2\mu\alpha^3 \simeq 2\mu(\Delta z/l_0)^3$, so that the force belance equation becomes

$$\frac{2\mu(\Delta z)^3}{l_0^3} + \frac{4\kappa\Delta z}{l_0^3} - T_m = 0 \tag{3.15}$$

Solution of Eq. (3.15) for Δz can be used to obtain F_{wall}, according to

$$F_{wall} = 2T_{act}\cos\alpha \approx 2T_{act} \approx \frac{2\mu(\Delta z)^2}{l_0^2}, \tag{3.16}$$

Eq. (3.15) has simple solutions in the limits of large and small T_m. When T_m is small, so that the Δz term in Eq. (3.15) exceeds the Δz^3 term, $\Delta z \approx l_0^3 T_m/4\kappa$. Then

$$\frac{F_{wall}}{T_m} = \frac{\mu l_0^4}{8\kappa^2} T_m. \tag{3.17}$$

When T_m is large, the Δz^3 term dominates, so $\Delta z/l_0 \approx (T_m/2\mu)^{1/3}$ and

$$\frac{F_{wall}}{T_m} = \frac{(2\mu)^{1/3}}{T_m^{1/3}}. \tag{3.18}$$

Eqs. (3.17) and (3.18) show that at small T_m values, bending forces exceed the restoring force opposing bending, and F_{wall}/T_m increases linearly with T_m. As T_m increases, stretching forces take over and the ratio F_{wall}/T_m decreases as $T_m^{-1/3}$. This behavior is illustrated in inset of Fig. 3.7a We have also treated numerically a less symmetric configuration (Fig. 3.6b and c), and one with a minifilament parallel to the bundle (Fig. 3.6d). Fig. 3.7a shows that F_{wall}/T_m has a similar dependence on T_m for all of these configurations, and in all cases reaches values much larger than T_m.

To evaluate the crossover tension T_m^c between the limits of large and small T_m, we choose T_m^c to be the value of T_m where the estimates of Eq. (3.17) and Eq. (3.18) are equal. This gives

$$\frac{T_m^c}{\mu} = 2^{5/2} \left(\frac{\kappa}{\mu l_0^2} \right)^{3/2}. \tag{3.19}$$

For our parameters, T_m^c is only about $4 \times 10^{-3} pN$. We conjecture that mini-filaments will be in the large T_m limit (Eq. (3.18)) when the transverse component of the mini-filament tension exerted on the actin filament exceeds T_m^c. Because T_m^c is so small, this will occur for a large fraction of the mini-filaments. The forces generated by these mini-filaments are given by Eq. (3.18), and since $\mu >> T_m$, they will generate F_{wall} values significantly greater than T_m. The analytic theory also suggests that F_{wall}, for small T_m, is proportional to the stretching modulus μ of the actin filaments and inversely proportional to the bending modulus κ. The red and green curves in Fig. 3.7a, which correspond to doubling the stretching modulus and bending modulus respectively, confirm this expectation.

To assess the relevance of this simple model to our simulations, we varied the minifilament tension artificially by changing the initial mini-filament length L_m^0. The results, shown Fig. 3.7b, are generally consistent with the theoretical predictions. At small T_m values, F_{wall} increases with T_m as in the simpler model results shown in Fig. 3.7a. As T_m increases, F_{wall}/T_m turns over. But the enhancement of F_{wall} is not as large as in the model calculations. We believe that this occurs because we do

not have single filaments reaching wall to wall, but rather chains of filaments whose effective stretching modulus is lower than that of single filament; this would reduce the stress amplification.

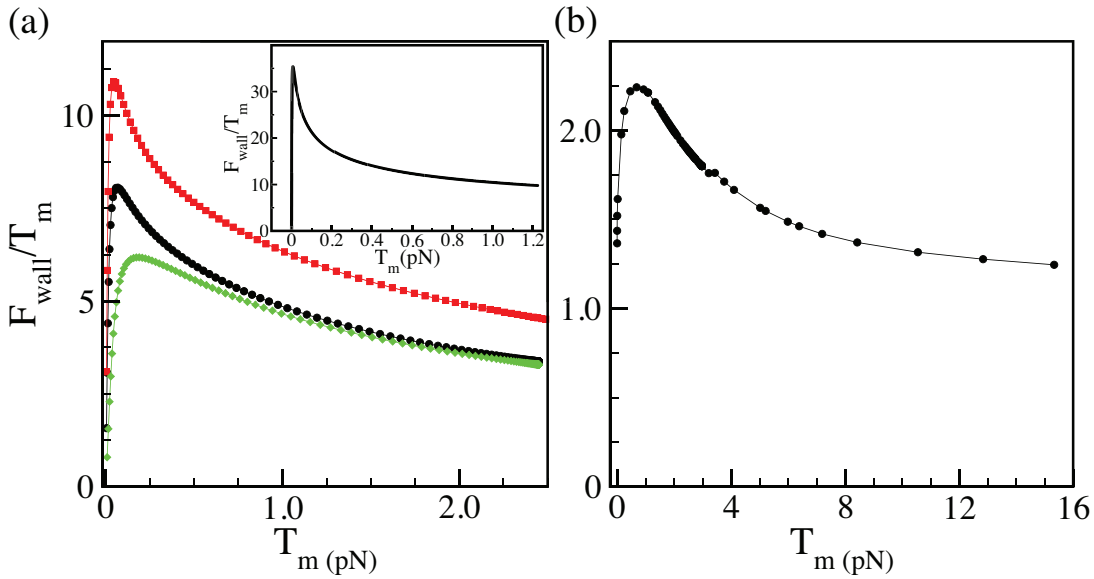

Figure 3.7: a) Variation of F_{wall}/T_m with T_m for geometry of Fig. 3.6 b). Black curve (dots): $\kappa = 0.06\ pN\mu m^2$ and $\mu = 600\ pN$. Red curve (squares): $\kappa = 0.06\ pN\mu m^2$ and $\mu = 1200\ pN$. Green curve (diamonds): $\kappa = 0.12\ pN\mu m^2$ and $\mu = 600\ pN$. Inset shows the theoretical prediction for variation of F_{wall}/T_m with T_m as given in Eq. 3.15 b) Variation of F_{wall}/T_m with T_m for a sample thick bundle with a single mini-filament.

The amplification is also seen in some of our simulation runs for networks, but the effect is much smaller than in thick bundles. The effect is also much smaller in

thin bundles than in thick bundles. We believe that this is because the mechanism, as illustrated in Fig. 3.6, requires resistance to vertical deformation of bundle. If the wall attachment points in the figure could move freely, there would be no amplification. We find that the thin bundles often collapse as a result of the myosin forces, suggesting that their resistance to vertical deformation is reudced, which might explain why they have less force amplification.

3.3.2 Addivity of stress contributions from different minifilaments

To evaluate the extent to which mini-filaments act independently in generating stress, we first calculated the stresses in thin bundles, with a single-minifilament in various locations. The sum of these stresses was then compared to the stress resulting from five mini-filaments acting on the same bundle simultaneously. Figure 3.8 summarizes the runs for 100 collections of five myosins in a bundle. The ratio of the stresses plotted here would be 1 for perfect additivity. The mean value is 0.90, indicating that the behavior is close to additive but somewhat subadditive. Similar results hold for thick bundles.

Figure 3.8: Ratio between stress generated in thin bundles by five mini-filaments to sum of stresses generated by the five mini-filaments acting individually. Data shown for 100 different runs.

3.3.3 Strain stiffening

Strain stiffening in actin networks due to myosin activity has been observed in several types of *in vitro* experiments [39, 38]. We evaluated this effect for our thin model bundles each containing five mini-filaments. We calculated the stiffening as follows. We first calculated the Young's modulus of the bundle without myosin, by applying a 0.2% strain in the x-direction, relaxing the bundle, and then evaluating

the wall forces. We then repeated the procedure with bundles containing five mini-filaments, equilibrated before and after the application of the strain, calculating the difference in the force induced by the strain.

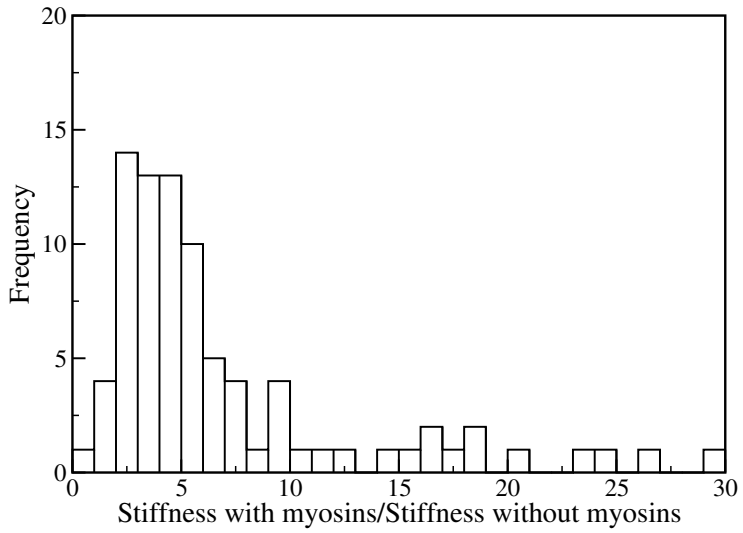

Figure 3.9: Ratio between stiffness of bundles containing five myosin minifilaments to bundles without myosin. Data shown for 85 thin bundles.

Fig. 3.9 shows our data for 85 different bundles. The magnitude of stiffening varies from about 1 to 30, but the average strain stiffening about 7 is very substantial. We believe the origin of this effect lies in the transverse contraction of the bundles induced by the myosins. The width of the bundles typically drops by about 50% as a result of the myosin contraction. This results in the chains of filaments connecting the myosins

to the walls being straighter, and thus more difficult to extend.

3.4 Robustness of results to assumptions made

We have evaluated the robustness of our results by varying a broad range of input parameters and assumptions.

Input parameters

With increasing F_{ATP}, the force density on the walls f_{wall} increased sub-linearly, maintaining contractility. For thin bundles, T_m/F_{ATP} decreased by about 5% when F_{ATP} was doubled; for thick bundles T_m/F_{ATP} decreased by about 20%. These decreases occur because with increasing F_{ATP}, more mini-filaments reach filament ends where their force generation capacity is reduced. This effect is smaller in thin bundles because their filaments are longer. Doubling γ changed f_{wall} and T_m by less than 1%. Doubling the length of thin bundles by 100%, while doubling the number of myosins, did not change the mean T_m or F_{wall} significantly. This is because when the length of the thin bundle is doubled, it acts as two "contractile units" [9, 34] in series, each generating the same stress. Increasing the length of a thick bundle by 40% decreased both the stress and T_m by about 15%. This reduction was due a larger fraction of mini-filaments reaching filament ends in longer bundles. Changing the maximum angle of span, θ_c for the actin filaments in the bundle had a substantial effect. As seen in Fig. 3.10, Smaller θ led to higher wall forces. When θ_c was decreased by 50%,

f_{wall} increased by 10% and when it was increased by 50%, f_{wall} decreased by 5%. But, surprisingly, it causes a decrease in T_m. When θ_c was decreased by 50%, T_m decreased by 10% and when it was increased by 50%, T_m increased by 20%. This is because small values of θ_c allow many mini-filaments to end up at actin filament ends, reducing their T_m values.

Mini-filament behavior at barbed ends and crosslinks

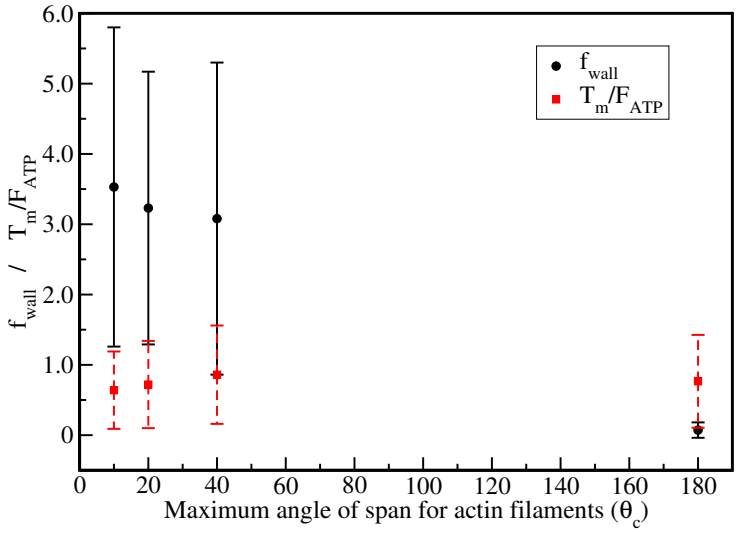

Figure 3.10: Variation of f_{wall} and T_m/F_{ATP} with varying angle of maximum span. Error bars represent the standard deviation in f_{wall} and T_m/F_{ATP} for each case. Values at 180 ° correspond to the random networks.

The effect of varying the assumption that mini-filaments always stay at actin filament barbed ends was discussed above in connection with Tables 3.1 a-c.

The effects of allowing the mini-filament to jump over a crosslink vs not allowing it are summarized in Table 3.2 for thick bundles and Table 3.3 for thin bundles.

Table 3.2: Statistics for different categories of final mini-filament configurations for thick bundles when mini-filament is allowed to jump over a crosslink and when it is stopped at a crosslink.

Category	Allowed to jump			Stuck at crosslink		
	Percentage	mean f_{wall}	mean T_m/F_{ATP}	Percentage	mean f_{wall}	mean T_m/F_{ATP}
All runs	100%	0.28	0.58	100%	0.19	0.44
Both ends eq	7%	0.42	1.19	4%	0.36	1.02
One end eq	38%	0.42	0.95	31%	0.43	1.00
Both ends stuck	55%	0.17	0.25	65%	0.07	0.13

Explanation of results for thick bundles:

- **All runs :** Both mean f_{wall} and mean T_m/F_{ATP} decrease when the mini-filaments are not allowed to jump. This we believe is because when the mini filament is allowed to jump, it travels for a longer time hence a longer distance along the filament it is attached to, deforming the network more compared to when it is stopped at the first crosslink, resulting in higher mean f_{wall} and T_m.

- **Both ends went to equilibrium :** Here again the mean f_{wall} and mean T_m/F_{ATP} are lower in the category that the mini-filament is stuck at the crosslink.

However, for this sample of runs, the behavior of the mini-filament at the crosslink does not matter for those cases where the mini-filament goes to equilibrium on the initial two rods they were attached to, before they reach the crosslink. Hence the difference arises because the remaining 3% of the runs, that reach equilibrium only when allowed to jump over the crosslink, have higher tension as these deform the network more while moving toward the equilibrium.

- **One end went to equilibrium :** In this category, the mean values are almost similar, but there is a slight increase in the values when the mini-filaments are not allowed to jump over the crosslinks. This difference however is within the error bars of the simulations (error = 4.5%).

- **Both ends got stuck :** Here the mini-filaments that were not allowed to jump over crosslinks have significantly lower mean values. These are the mini-flimants which have travelled the least amount of distances . In other words, they must have started closer to a croslslink initially, and hence did not produce much deformation of the network, resulting in lower mean f_{wall} and mean T_m/F_{ATP}.

Overall we observe the mini-filament tension increases with the distance it travels along the actin filament is proportional to and stress produced.

Table 3.3: Statistics for different categories of final mini-filament configurations for thin bundles when mini-filament is allowed to jump over at a crosslink and when it is stopped when reach a crosslink.

Category	Allowed to jump		Stuck at crosslink	
	Percentage	mean T_m/F_{ATP}	Percentage	mean T_m/F_{ATP}
All runs	100%	0.72	100%	0.68
Both ends eq	28%	1.11	21%	1.04
One end eq	39%	0.94	39%	0.99
Both ends stuck	33%	0.14	40%	0.18

Explanation of results for thin bundles:

- Here when the mini-filaments are not allowed to jump over the crosslinks, the changes in the mini-filament tension are much smaller than in thick bundles. We believe this difference in thin bundles compared to the 24% decrease in the thick bundles occurs because the mean rod length is higher in the thin bundles, and because of the thickness itself. For thick bundles the mean rod length is $0.45\mu m$ where as in thin bundles it is $0.91\mu m$. The thickness is $\sim 2.5\mu m$ and $\sim 1\mu m$ for thick and thin bundles respectively. Hence, in the case of thin bundles, the mini-filament has in many cases a considerable distance to travel on the same rod and can thus reach higher tensions, especially when it is attached to anti-parallel filaments. Also due to the smaller thickness of the thin bundle, when the mini-filament is allowed to jump over the crosslinks, it most likely jumps to dangling ends easily (as the filaments are more parallel here),

releasing the tension. This may be the cause for the reduction in tension when the mini-filament is not allowed to jump for the categories "one end going to equilibrium" and "both ends getting stuck".

- As a result, change in the force density (f_{wall}) per mini-filament is also insignificant for thin bundles. The mean values are $0.64pN\mu m^{-1}$ and $0.63pN\mu m^{-1}$ when allowed to jump over crosslinks and not allowed respectively.

Effects of actin filament treadmilling

Below we compare the effect of treadmilling on the mini-filament tension and the stress generated by the bundle to those of a static bundle. Motivation for this comparison comes from the expectation that due to treadmilling, the mini-filaments that reach barbed ends in a static bundle can move further along the filament because the barbed end is extended. Our results for the static bundle implied that the stress generated in the bundle and the tension on the mini-filament increases with the distance it traveled. This effect was especially prominent in the case where the mini-filament is attached to two anti-parallel filaments. Hence here, 10 μm long thin bundles with one mini-filament each, which have nearly anti-parallel filaments, were used to investigate the effect. According to experimentally observed rates, treadmilling occurs only about once every ten mini-filament steps. However in these simulations, we have allowed the treadmilling to occur after every mini-filament step in order to enhance the effect, if there is any. In first set of runs, the bundle is static and no treadmilling

occurs. In the second set of runs, treadmilling occurs in parallel with every mini-filament step. In each case, the mini-filament is allowed to take 250 steps (about 25 % of the filament length). In order to keep the bundle from breaking apart in the dynamic case, we did not allow: 1) Treadmilling to occur in a small band right next to the wall as shown in Fig. 3.11 or 2) Depolymerization beyond crosslinking points, as shown in point A of Fig. 3.11. In the static bundle, the mini-filament was allowed to stay attached to the barbed end. At the end mini-filament tension and force on the wall were compared for two cases.

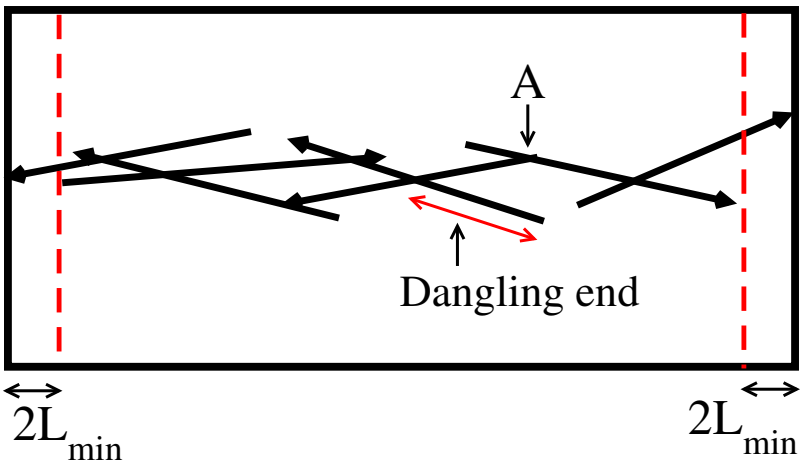

Figure 3.11: Schematic diagram of a thin bundle used for treadmilling. The diagram is not drawn to scale, to make it more clear. In the real bundle, the filaments are more parallel and the bundle is thinner compared to its length. Red dashed lines show the limits beyond which the treadmilling is not allowed near the walls. Point A is a crosslinking point and depolymerization is not allowed beyond that crosslink.

Simulations were terminated before 250 mini-filament steps if any of the following occurred:

- Both ends of the mini-filament went to equilibrium - for both static and dynamic bundles.
- Both ends of the mini-filament went to filament barbed ends - for static bundles.
- One or both ends of the mini-filament went to filament barbed ends and the polymerization was slower than the mini-filament motion- for dynamic bundles.
- One or both ends of the mini-filament were slower than the treadmilling, so the pointed end depolymerized passed the mini-filament - for dynamic bundles.

Fig. 3.12 compares the distributions of mini-filament tension T_m, when treadmilling is turned off and on respectively. Both histograms look similar qualitatively. As we observed earlier, the mini-filament tension has two prominent peaks near values zero and stall force. The peak near zero arises due to the mini-filaments that end up at dangling ends. The mini-filament tension built up during the movement releases as soon as one end of the mini-filaments jump to a dangling end, as these rods can freely rotate around the crosslink. The peak near the stall force arises due to mini-filaments with at least one end reaching an equilibrium position. Compared to the static bundle, the dynamic bundle has more mini-filaments with near zero tension.

This effect is clearly evident in the mean values for the two cases. When treadmilling is turned on, the mean T_m drops by 27%, to 0.46 pN compared to 0.64 pN in the static bundle. This occurs as more and more mini-filaments reach the dangling ends when the filaments are allowed to grow.

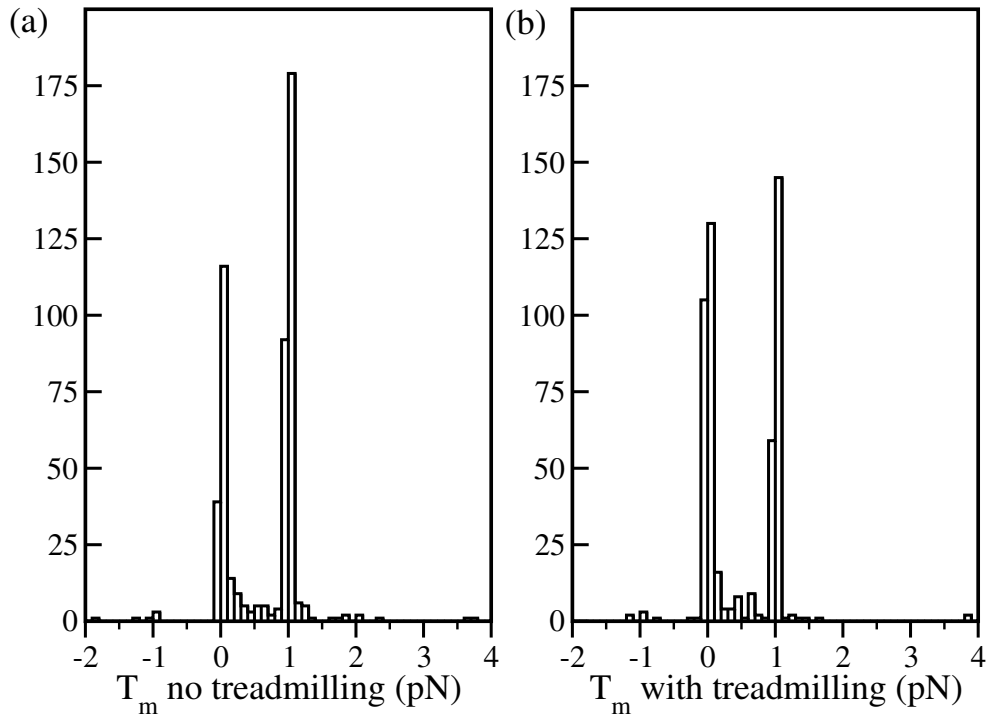

Figure 3.12: Mini-filament tension after iterations for 500 total runs. (a) Static bundle, no treadmilling occurs. The mean value for T_m is 0.64 pN. (b) Dynamic bundle. Treadmilling occurs after each mini-filament step along the actin filament. The mean value for T_m is 0.47 pN. Due to treadmilling, overall the mini-filament tension has decreased by 27%.

The wall force also decreases by 36% as the mean value drops from 0.67 pN to 0.43 pN going from static bundles to dynamic bundles. Fig. 3.13 shows the

histograms of f_{wall} for static and dynamic bundles. Thus the overall results do not confirm our initial expectation that treadmilling would increase T_m and f_{wall}. To understand this result, we categorized runs according to the final state and position of the mini-filament. This gave us useful insights for effects due to treadmilling in a much simpler situation than treadmilling in a real actin bundle.

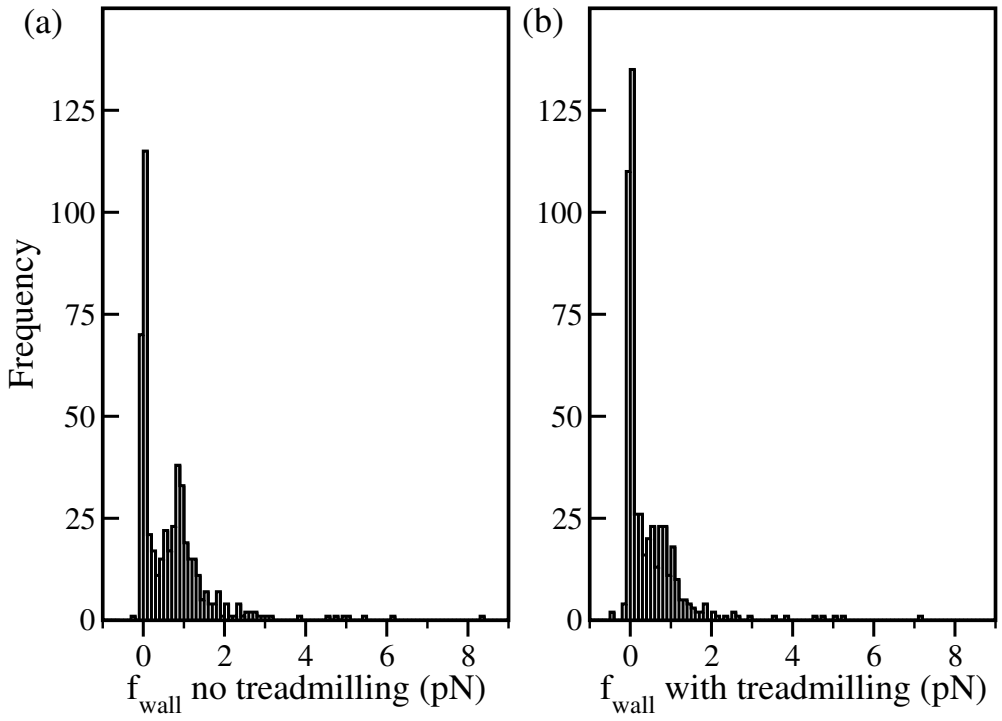

Figure 3.13: Distribution of x-component of the force on left wall at the end of each run for 500 total runs. (a) Force on wall for static thin bundle. The mean value for f_{wall} is 0.669 pN. (b) Force on wall for dynamic thin bundle. The mean value for f_{wall} is 0.43 pN. Due to treadmilling, overall the wall force has decreased by 36%.

Table 3.4 summarizes the results in categories describing the final mini-filament

configuration, and compares T_m and f_{wall} values for static and dynamic bundles[1].

Table 3.4: Statistics for different categories of final mini-filament configuration transitions between static and dynamic thin bundles. Transitions are defined going from static bundles to dynamic bundles.

Category		Static Bundles		Dynamic Bundles	
	Percentage	mean f_{wall}	mean T_m/F_{ATP}	mean f_{wall}	mean T_m/F_{ATP}
eq to eq	5%	0.87	1.00	0.74	1.00
oneend to eq	1%	0.27	0.75	0.46	1.00
oneend to oneend	12%	1.01	0.88	0.88	0.88
bothstuck to eq	7%	0.89	0.80	0.75	1.00
bothstuck to oneend	3%	0.54	0.60	0.61	0.63
bothstuck to bothstuck	72%	0.52	0.43	0.36	0.38

In Table 3.4, the first column indicates the transitions that occurred between static and the dynamic bundles. For example, the first row indicates that 4% of the runs had both ends of the mini-filament going to equilibrium in the static bundles, and both ends of the mini-filament going to equilibrium when the treadmilling was turned on as well. Again, overall we do not see a drastic increase in forces due the treadmilling. However, in the transitions that go from both ends initially stuck to both ends going to equilibrium or one end of the mini-filament going to equilibrium, T_m increases, as we expected.

[1]The definitions of the notation used: **eq** - both ends of the mini-filament went to equilibrium, **oneend** - one end of the mini-filament went to equilibrium, **bothstuck** - neither of the mini-filament ends went to equilibrium

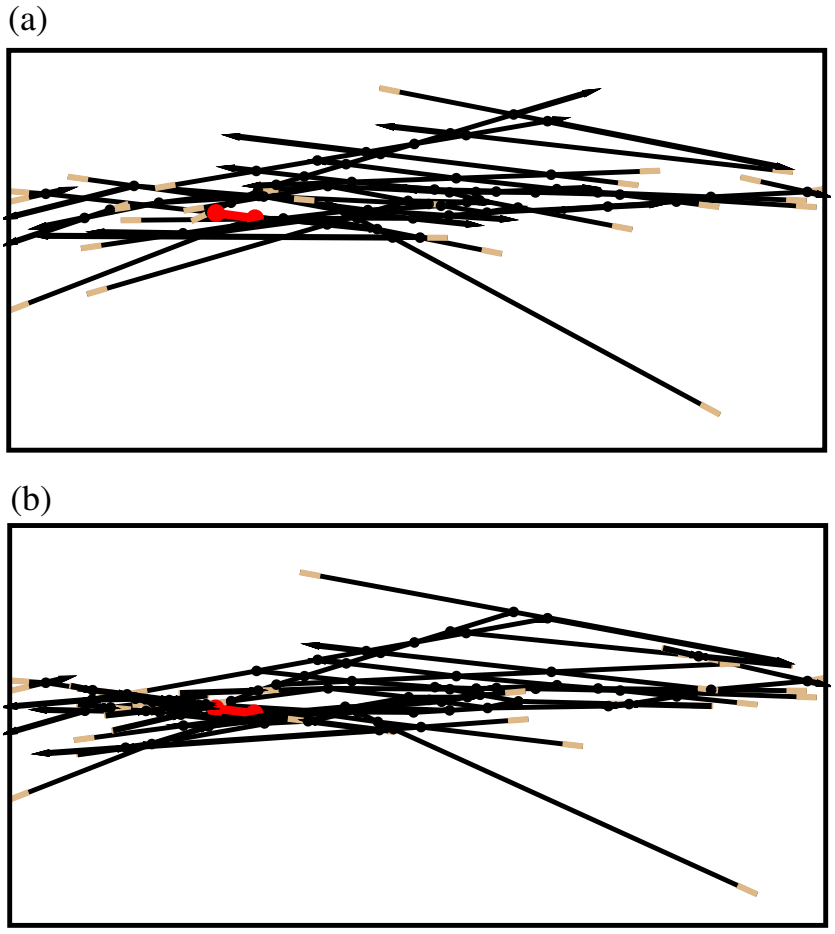

Figure 3.14: Thin bundle after the mini-filament movement has stopped for the static case (a) and dynamic case (b). Actin filaments are represented in black and the mini-filaments in red. The pointed end of actin is drawn as an arrowhead while a segment at the barbed end is colored in brown. In the dynamic bundle, towards the left end, a thick segment consisting of tightly crosslinked filaments is formed in the vicinity of the mini-filament. Compared to that, the corresponding area in the static bundle has fewer crosslinks. Both diagrams have been stretched along z direction for clarity. Also note that in the dynamic bundles, the barbed ends have grown significantly compared to those in the static bundles.

However, the major effect that we observe here, and did not expect initially, is that f_{wall} has smaller values in the dynamic bundle even when T_m increases at least slightly. This we believe occurs because in the dynamic bundles, the rods make new crosslinks with the rest of the bundle as they grow. This can produce locally stiff regions that seems to absorb the stress generated by the filament within that structure as if it were a separate entity from the original bundle. Fig. 3.14 shows such a case. Fig. 3.14(a), shows the static bundle, which does not make new crosslinks when the rods overlap. Fig. 3.14(b) shows the bundle when the treadmilling is turned on. Towards the left end of the bundle a tightly crosslinked region is clearly visible. In the example shown, f_{wall} decreased by 60% when transitioning from a static to dynamic network where only one end went to equilibrium in the static network but both ends went equilibrium in the dynamic case. This suggests that the stiffer region was not able to transmit stress as much effectively as a relatively compliant region.

Following is a list of other reasons that might have reduced the force enhancement due to treadmilling:

- In the static bundles, the mini-filament was allowed to stay attached to the barbed end if the other end on the mini-filament is still moving. This might result in both larger T_m and f_{wall}. In the dynamic case this is not possible, because if the mini-filament stepping is faster than the barbed end growth rate, then it will detach from the rod immediately. Hence in the dynamic network, the mini-

filament does not have the opportunity to move further at one end while the other end is attached to the filament unless the other end reach an equilibrium position (In dynamic bundles this can only happen when the mini-filament attaches to two antiparallel actin filaments, but for static bundles this can occur in any filament orientation giving them a statistical advantage as well.)

- When the filaments are allowed to grow, the probability that at least one end of the mini-filament jumps to a dangling end releasing tension becomes higher. Hense the probability for these mini-filaments to release the built up tension is higher. However if the code allowed the "mrods" [2] to make new crosslinks with the bundle, this effect could have been reduced. Also in the cell, it might be possible that any growing rod make new crosslinks with the network.

- The probability for the mini-filament to release tension when it jumps to a dangling end is enhanced as the code does not impose any energy cost for the rotation of these filament ends around the crosslink. We observe in the case of anti-parallel filaments, when the mini-filament jumps to a dangling end while the other end still moves, that the dangling end rotates 180° very easily to facilitate cooperative movement at both ends (this kind of rotation makes the two ends of the filaments look parallel).

- Also here the treadmilling is set to a fast rate. This might have caused mini-

[2] rods to which mini-filaments are attached

filaments starting closer to the pointed end to detach quickly. Such mini-filaments might not had enough time to generate significant forces before leaving the bundle.

- Finally the simulation is done in two dimensions. The rods might not be able to move and rotate as freely if they were in a thee dimensional environment. Our results can be taken as a validation for the assumption made in our main results, that in two dimensions the treadmilling is not that important. However this also implies that if one needs to investigate the effect of treadmilling, having a three dimensional bundle (or network) is a minimum requirement.

Hence further improvements to the current work can be done along the above mentioned directions and also imposing crosslink dynamics, which is important in the cellular environment.

3.5 Discussion

The calculations described above have shown that a minimal model, whose key ingredients are the motion of myosin heads toward barbed ends of actin filaments and actin filament flexibility, leads to contractile behavior in bundle-like structures. Our finding that contraction is practically universal is consistent with a multitude of *in vitro* studies which have found contractile stress. Unlike the mechanism of Refs. [9, 34], the present model does not require nonidentical motors. We believe that

this mechanism required nonidentical motors because mini-filament rotation was not taken into account. The mechanism seen here is also different from that of Refs. [8, 33], which was based on interactions between parallel filaments caused by binding of myosins to barbed ends. In the present mechanism, contraction results more from myosin motion on antiparallel filaments than on parallel filaments. We find that the average T_m value for parallel filaments is only about 70% of that for antiparallel filaments. Furthermore, generation of contraction by parallel filaments will be greatly reduced if myosin heads leave barbed ends.

We found that myosin generates higher stresses in actin bundles compared to networks, and between antiparallel filaments compared to parallel filaments. In recent *in vitro* studies [57] actin filaments were grown off rods coated with actin-polymerization nucleators. Three distinct structures were formed in different regions: branched networks, parallel bundles, and antiparallel bundles. It was found that antiparallel bundles generated the strongest contraction, while branched networks had weaker contraction, and parallel bundles were comparatively unaffected by myosin. These findings are consistent with our predictions that antiparallel filament arrangements contract more strongly than networks or parallel arrangements. However, myosin does contract parallel actin filaments in our simulations if it remains attached at barbed ends (Fig. 3.3d). Therefore, the experimental results suggest that myosin leaves barbed ends when it reaches them. We also note recent studies [61] showing that Arp2/3 complex, which generates branched networks, inhibits myosin-dependent

retrograde flow. This may be because networks contract less efficiently than bundles.

The present model also predicts that a longer distance between crosslinks will enhance the mini-filament rotation instability and thus favor contraction (see Eq. (3.9). This is consistent with experimental observations [10] that, although crosslinkers are required for contractility, a very large density of crosslinkers prevents contraction.

Another prediction of the model is that bundles can amplify the stress generated by actin filaments (Fig. 3.2g-h). This prediction is not very general since, of the three cases we considered, large amplification occurred only in the thick bundles. Nevertheless, we note that in the experiments of Ref. [39], forces of about 1 piconewton per myosin head were measured. If the duty ratio of myosin is low, as is generally believed, then T_m values of tens of piconewtons would be unlikely. The amplification mechanism discussed here may be relevant to these results.

Our observation of network stiffening by myosins is consistent with recent *in vitro* studies [38, 39] in which myosin activity was found to increase the elastic modulus of actin networks. Although the mechanism in these experiments was not clear, it could be due to the stretching out of actin filaments so that their wiggles disappear [62]. The present mechanism appears to be similar to this one, except that chains of filaments connecting myosin to the walls stretch, rather than individual filaments stretching. Our mechanism differs from a recently proposed one, which suggested that the stiffening occurs due to the network deformations resulting from compliant crosslinkers [43]. In this mechanism, when the crosslinkers are more compliant, the

final stiffness will be higher. However, the present model has completely incompliant crosslinkers and substantial strain stiffening is still seen.

This work was supported by the National Institutes of Health under Grant Number R01 GM086882.

Appendix

A Effect of varying stretching modulus (μ)

Here we consider variations of μ that are out of the physical range. These results may be relevant where the actin filaments are very wiggly, including the case their effective modulus is determined by the bending energy. To evaluate the sensitivity of the results to μ, we decreased it from $600pN$ to $10pN$ so that the stretching of actin filaments on the order of 10%. (The force on an actin filament due to stretching is roughly equal to μ $(\Delta L/L_0)$, where ΔL is the change in length due to stretching and L_0 is the initial length. For an applied force equal to the stall force, 1 pN, to achieve $\Delta L/L_0 = 0.1$, (10%), the stretching modulus should be $10pN$.) The effect of this change was evaluated for the mini-filament tension scaled by the stall force (T_m/F_{ATP}), the wall force density per mini-filament(f_{wall}/n_{myo}) and the wall force scaled by the sum of mini-filament tensions$(F_{wall}/\Sigma T_m)$. We performed these tests for thin bundles.

When the stretching modulus was decreased, the mini-filament tension decreased

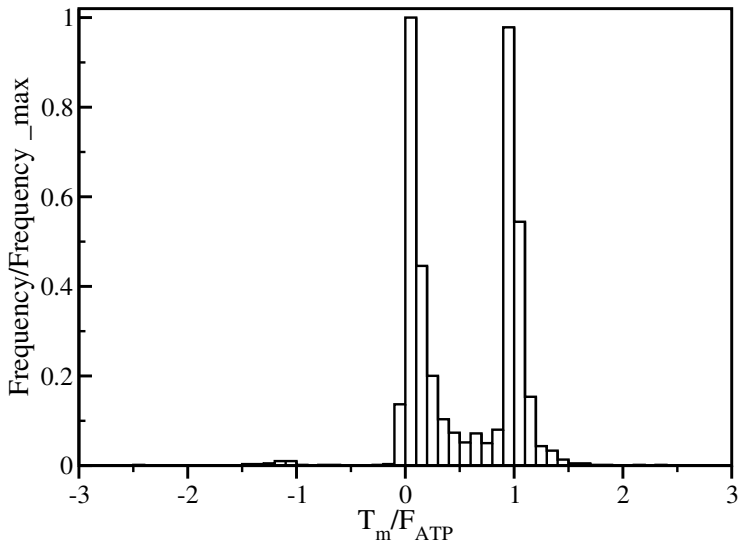

Figure A1: Distribution of T_m/F_{ATP} for thinbundles with stretching modulus reduced to $10pN$. Mean value is $0.54pN$

by 25%, Fig. A1. We believe this was because more mini-filaments ended up at filament ends as the actin is more compliant. The mean value for the wall force density per mini-filament decreased by 56% (Fig. A2), as the opposing force from the bundle decreased due to the decreased mini-filament tension. The overall result is that the wall force scaled by mini-filament tension was reduced by 50%, Fig. A3. The sign of the change is also in agreement with our calculation which shows that $F_{wall}/\Sigma T_m$ is proportional to μ in subsection 3.3.1, Eqs. 3.17 and 3.18. Furthermore, we used $\mu = 600\ pN$, a value smaller than the experimental value ($45nN$) to make the convergence criteria at energy minimization faster. Hence if the actual value has been used, we would expect slightly larger wall stresses and mini-filament tensions.

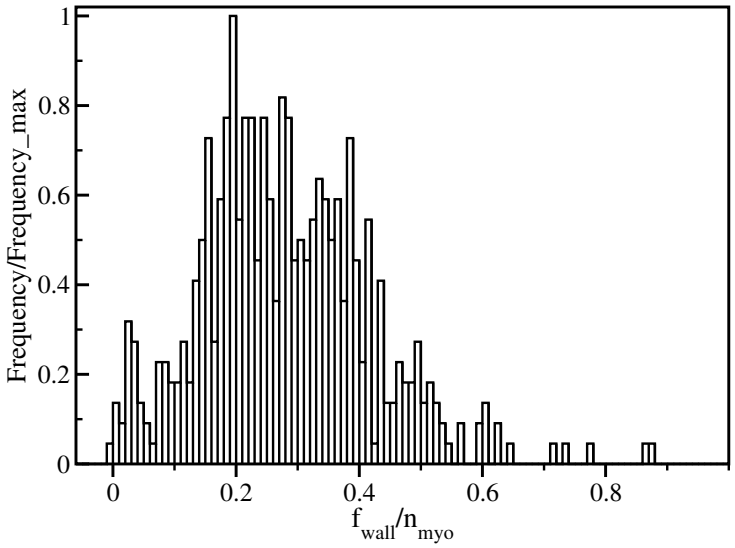

Figure A2: Distribution of f_{wall}/n_{myo} for thin bundles with stretching modulus reduced to $10pN$. Mean value is $0.28pN\mu m^{-1}$

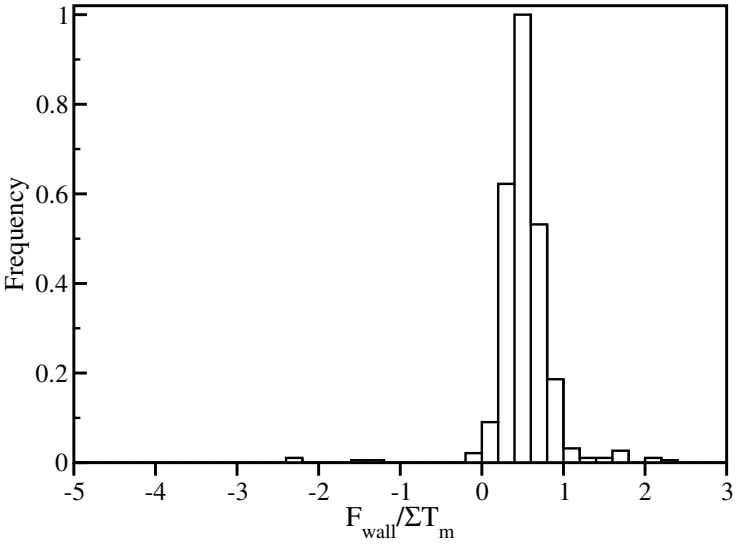

Figure A3: Distribution of $F_{wall}/\Sigma T_m$ for thin bundles with stretching modulus reduced to $10pN$. One column at -11 was omitted for clarity of the graph. Mean value is 0.5.

Chapter 4

Simulation Method

4.1 Introduction

In this chapter the functions of the subroutines in the simulation code used for all the simulations are explained. The code is written in C. When switching between random networks and bundles, only the parameter values are changed. The way the network was generated and all the subroutines used are almost similar. The subroutines used in the simulations with treadmilling are also explained. At the initial stage of the code arrays are used to store data for filaments laid in the simulation box. Then after filaments that do not make any crosslinks with the rest of the network, and ones that make just one connection, are removed, the data are written into structures. We first briefly discuss the structures and variables used.

4.1.1 Structures

The C command used to create structure is "struct" and it aggregates different objects or properties with different data types into one object. This made data easier to handle, and data manipulation was less complicated compared to using arrays. Separate objects are created to save properties of rods to which no mini-filaments are connected (rod structure), rods to which mini-filaments are connected (mrod structure), crosslinks (link structure), made by mini-filaments on rods (mlink structure) and finally for mini-filaments (myo structure). Table A1 summarizes the data type of each field, the name of the field used and gives a description of each field for all the objects used in the code.

4.1.2 Global variables used

Table 4.1 defines all the global variables used in the simulations. [1]

[1]Values on the table are for thin bundles. For thick bundles and random networks $\ell = 2\ \mu m$ limit1=4.97 μm, frame1 = 5 μm

Table 4.1: Global variables used

ℓ	Length of a filament laid down (=5 μm)
L0	Minimum allowed length of a rod(=0.15 μm)
lmin	Minimum allowed length of a filament initially laid down(=0.4 μm)
Mu	Stretching modulus of actin (= 600 pN)
K	Bending modulus of actin (= 0.06 $pN\mu m^2$)
lmyo	Length of a mini-filament laid down (= 0.5 μm)
d_a	step size (= 0.0054 μm)
myoE0	A constant used in calculating mini-filament stretching energy (= 60.0 $pN\mu m^{-3}$)
E_{barb0}	Energy of an ATP (=0.0054 $pN\mu m$)
eps	A constant used when a mini-filament takes a step (= 500.0)
jnum	Minimum distance allowed between mini-filament and a crosslink before it jumps to the next rod (=6.0)
limit0	Defines the limit a rod is considered as fixed to the left wall (=0.03 μm)
limit1	Defines the limit a rod is considered as fixed to the left wall
frame0	Left wall position (placed at origin)
frame1	Right wall position (=10 μm)
frame2	Thickness of a bundle. Only used when a bundle is generated (=0.5 μm)

4.2 Description of subroutines used

void makeactin(void)

This subroutine is called in the main program and generates a network with the specified number of filaments and the filament angles. Number of filaments to generate is stored in the global variable "n" and the maximum angle of span for filaments is specified inside makeactin();

Table 4.2: Arrays generated in makeactin(). All these arrays are saved as global arrays.

$x[i], x0[i]$	Initial and final x position of the i^{th} filament respectively.
$z[i], z0[i]$	Initial and final z position of the i^{th} filament respectively.
$a[i], ar[i]$	Angle of the i^{th} filament measured from the upward direction (Z direction), angle in degrees and radians respectively.
$L[i]$	Length of the i^{th} filament.
$edge[i]$	polarity of the i^{th} filament. Stores 1 if the starting point is pointed and 0 if the stating point is barbed.

Procedure

A "for" loop was used to generate the required number of filaments. Three random integer variables ran1, ran2, ran3 are generated and scaled to required ranges to create the starting x position, z position and angle of a filament respectively. ran3 was used to determine the polarity of the filament as well. If it was a even number, the starting point was chosen as the barbed end and else the starting point was chosen to be the pointed end. If a filament extended beyond the simulation box, it was cropped, and the end that touched the frame was taken as the starting point of the filament. Before the next for loop iteration, the subroutine "CheckCrossLinks()" was called to check if this filament was a legitimate filament or not. If the filament was not acceptable, CheckCrossLinks() decreased the filament count by one and returned the new filament count back to makeactin(). This procedure was repeated until the simulation box was filled with n filaments.

intCheckCrossLinks(int q)

This subroutine was called by the makeactin() subroutine to check if a given filament was acceptable or not. Input parameter "q" specifies the filament that needs to be checked. The subroutine checks the crosslinks the new filament make with existing filaments. If the distance between two crosslinks on the new rod due to existing filaments or on an existing filament due to the new filament is smaller than $\ell_0 = 0.15\ \mu m$, the new filament was not acceptable. The reason to have this condition is that later in the code a filament section between two crosslinks was named a rod and too short rods made the minimization procedure difficult to handle.

Procedure

Coordinates of the middle of the new filament are calculated and a virtual box of size $2\ell \times 2\ell$ is created. In order to make the subroutine efficient, only the filaments with their starting or the ending points within this box are checked for possible crosslinks with the new filament. The center of the virtual box is placed at the mid point of the new filament. If the limits of the virtual box go beyond the frame of the network, the virtual box is cropped and the frame limit is set as the new box limit as shown in Fig. 4.1. A for loop goes through all the existing filaments and checks if the starting point or the ending point of any of the existing filaments falls inside the virtual box. If so, a possible crosslinking point between that filament and the new filament is calculated using the gradients.

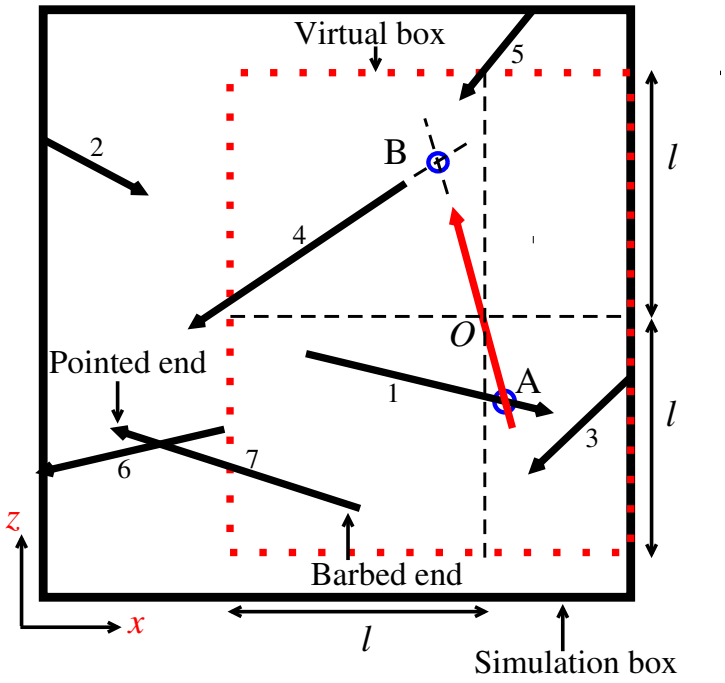

Figure 4.1: Simulation box after 7 filaments (black) have been successfully laid down. The virtual box of size $2\ell \times 2\ell$ for the new filament (red) is shown in red dotted box. The center of the box is at the point O which is also the center of the new filament. The virtual box has been cropped at the right side.

The distances from the crosslinking point to the starting and ending points of the two filaments are calculated to determine if the filaments actually cross each other. As shown in Fig. 4.1, the subroutine will check existing filaments 1,3,4,5, and 7 for possible crosslinks. Point A and B are two examples of such points the code will recognize as crosslinking points. Then point A will be accepted as a proper crosslink while point B will be eliminated after calculating the distances as described above.

First all the crosslinking points for the new filament are checked for the distance between them, and next the existing filament is checked for the same. If the new filament makes a too small rod, the rod count q is decreased by one and makeactin() is called to replace it. Else q is returned to generate the next filament.

void crosslinks(void)

This is the subroutine that calculates all the crosslinking points after all n filaments have been laid down successfully by subroutine makeactin(). Here global arrays save the positions of each crosslink, the distance to it from the starting point of the filament, the index of the filament that crosslinks with it, and the number of crosslinks for each filament. At the end of the subroutine, the global variable *nlinks* that holds the total number of crosslinks is specified. Following are the arrays used to store new data.

Table 4.3: Arrays generated in crosslinks(). All these arrays are saved as global arrays.

$xca[i],\ zca[i]$	x and the z position of i^{th} crosslink respectively.
$xcl[i][j],\ zcl[i][j]$	x and z position of j^{th} crosslink of i^{th} filament respectively.
$lc[i][j]$	Distance to the j^{th} crosslink from the starting point of i^{th} filament.
$xci[i][j]$	index of the filament that makes j^{th} crosslink with i^{th} filament.
$cc[i]$	number of crosslinks on i^{th} filament.

Procedure

Here the procedure is exactly the same as that in CheckCrossLinks().

void SortCrossLinks(void)

Here the arrays generated in crosslinks() are sorted according to the distance to each crosslink from the starting point of each filament or in the ascending order of the values in $lc[i][j]$. Accordingly, order in $xcl[i][j]$, $zcl[i][j]$ and $xci[i][j]$ are also changed.

void RemoveRods(void)

This subroutine searches for filaments that make less than 2 crosslinks. The filaments that do not make any crosslinks with other filaments do not affect the simulation at all and the filaments that make just one crosslink are considered floppy as they can rotate around the crosslink freely. Also here it checks the distance from first crosslink to the starting point and the last crosslink to the ending point of each filament. If any or both of these distances are again less than L_0, the starting point and/or the ending point is changed to the place of that crosslink. The new rod length of the i^{th} filament is calculated and stored in the global array $la[i]$. Length of all the filaments with zero or just one crosslink are set to zero. Also two new arrays save the index of the first crosslinking filament(array MAX[]) and the last crosslinking filament (array MIN[]) for each rod.

void RR(void)

This subroutine searches for filaments with crosslinking points that are due to

zero length filaments resulting from the RemoveRods() subroutine. These crosslinks are removed and the arrays MAX[], MIN[], and cc[] are updated. This subroutine is called iteratively for 6 times to make sure all the filaments with one crosslink are removed.

void Recalculate(void)

Here, the arrays are copied back to a new set of arrays to remove the filaments that are labeled as zero length. After this point crosslinks, rods and mini-filaments are arranged into structures. At the end of the Recalculate subroutine, it calls the two subroutines CalculateRodLength() and CalculateAngle(). These subroutines calculate the rod lengths and angles from the z direction respectively.

void CalculateRodLength(int Pval)

Calculates lengths of the rods using the starting and ending point coordinates. The input parameter "Pval" specifies the stack index where the calculated lengths need to be saved. For example, if this subroutine is called just after the network is generated and if this is called to calculate the initial lengths of rods, then Pval will be equal to 0. In such a case, the length of i^{th} rod will be saved at rod[i].length[0]. This routine is also called after every minimization step which changes the crosslink positions. In such situations, the data will be saved to a higher stack (1 or 2) as those represent later configurations of the network.

Procedure

A for loop goes through all the rods in the network and calculates the lengths. When this is called after minimization, the filament dangling ends are identified and instead of recalculating their lengths, the saved lengths in stack 0 (initial lengths) will be written to the current stack (specified by Pval). This is because during minimization, these rods do not stretch or compress to change lengths as only one end of these are connected to a crosslink.

void CalculateAngle(int Pval)

Calculates the orientation angle of rods. A for loop iterates over all the rods and identify the rods that does not have a minifilament attached to them and calculates the angle by calling CalculateRodAngle() subroutine. Again the input parameter Pval specifies the stack the data needs to be written to.

double CalculaterodAngle(double X0, double Z0, double X, double Z)

Calculate the orientation angle of a given rod relative to z-axis. Input parameters specifies the x and z position coordinates of the starting and ending position of the rod respectively.

Procedure

The angle of the rod is calculated using the inverse tangent from position coordi-

nates. Then this angle is changed to represent the angle from the z direction. The new calculated value is passed back to the CalculateAngle() subroutine.

void MakeLinkStructure(void)

Here data on crosslinks are organized into a link structure. The position data and the number of rods that intersect are directly copied from the arrays and, to find the exact indices of the rods, Findrod() is called.

Procedure

A for loop goes through the filament array and saves each crosslink on the filament into the link structure. Since every crosslink appears on two filaments, Checklink() is called at the beginning to make sure that a crosslink is not saved twice in the link structure.

intChecklink(double xval, double zval, int qval)

This subroutine is called by MakeLinkStructure() and it checks if a crosslink at coordinates (xval, zval) already exists on the link structure or not. The third input parameter "qval" specifies the number of links saved to the data structure.

Procedure

This function simply compares the position of an existing link to that sent to the subroutine. If the x coordinate and the z coordinate are within a distance 10^{-6}, the

function identifies the crosslink as an existing link. In that case a "1" is sent to the MakeLinkStructure() or else a "0" is sent and that crosslink will be saved on the link structure as a new link.

void Findrod(double xs, double xe, double zs, double ze, int qval, int fval)

Again MakeLinkStructure() calls this subroutine and it finds the indices of the rods that intersect at this crosslink position. The input parameters xs, xe, specify the x-position of the link and the potential starting or ending x position of the rod that the subroutine is looking for, zs and ze are the z components of the same positions respectively. Further, qval is the index of the link in linkstructure and fval is the index of the intersecting rod for that particular link. For example, if the link number 5 is looking for the 1st rod that intersects with it, then the rod number of that rod will be saved at link[5].nbname[0] . The nbname array can have from 2 up to 4 rod names (indices run from 0 - 3).

Procedure

Here a for loop goes through all the rods in the rod structure and compares the starting and ending position coordinates of each rod with the coordinates sent to the subroutine. Again the subroutine checks if all four coordinates are within a distance 10^{-6} with any of the rods. When the matching rod is found, the rod number is saved to the favl position of the nbname array, in link qval (link[qval].nbname[fval] = found

rod number). Since the MakeLinkStucture() expects the rod name to be added each time this subroutine is called, an error massage is produced if no matching rod could be found. This error is an indicator that the saved data on initial arrays are not consistent. Hence successful calls to this function ensure the consistancy in switching from arrays to the link structure.

void FindMyo(int nm, int pos, int num)

This is the subroutine that lays mini-filaments in appropriate places. The input parameter "nm" specifies the number of mini-filaments to lay down on the network, "pos" specifies to which position in the myo structure the mini-filament should be added, and "num" specifies the data stack that should be used to save the data. The parameter pos is important when the treadmilling is turned on. This is because when there is more than one mini-filament, a mini-filament can leave the actin rods to which it is attached when it reaches the barbed end, or when the pointed end depolymerizes past the attachment point of the mini-filament. In that case, this subroutine put the mini-filament is a new place and the pos parameter is required to specify exactly which mini-filament should be reattached.

Procedure

Similar to laying down actin filaments in makeactin(), three random variables are generated to specify the x , z coordinates and the angle of orientation. Then these coordinates are sent to Checkmyo() to check if it is an acceptable mini-filament or

not. A flag (with value 1) is returned from the Checkmyo() if the mini-filament is accepted. If the flag is 0, a while loop keeps generating new positions for the mini-filament. Each time a mini-filament is laid down successfully, the minifilament count is increased and a do loop iterates the whole process untill the specified mini-filament number (nm) is achieved.

intCheckmyo(double X, double Z, double X0, double Z0, double a, int q, int num)

Here the potential coordinates and orientation for a mini-filament generated by Findmyo() are checked for validity. First four input parameters specify the starting coordinates ((x,z)) and the ending coordinates respectively, "a" specifies the angle, "q" specifies the number of mini-filaments that already exist and "num" is the stack index to save data. This subroutine returns 1 if the mini-filament coordinates are accepted and 0 if not.

Procedure

The main function of this subroutine is to check if the mini-filament just laid down makes connections with the network and if so, to check whether the distance between the first and the last crosslink (this distance is taken as the length of the mini-filament) falls within a specified range. The procedure for checking the crosslinking with the network is same as that in the subroutine CheckCrossLinks(). Following is a list of exact conditions checked here.

- The mini-filament makes at least two crosslinks with the network.
- The distance between the first and the last crosslinking point is within $\pm 10\%$ of $0.4\ \mu m$.
- That neither of the filaments to which the rods that make crosslinks with this mini-filament belongs to, has a mini-filament attached already.

Finally, if the mini-filament is accepted, data is written into myo, mlink and mrod structures. When Findmyo() is called during treadmilling, CopyMyoPositions() is called after finding a successful mini-filament. This copies the new position data of the mini-filament into the 0 stack or the stack that saves initial orientation.

void CopyMyoPositions(int num1, int num2, int q)

This copies mini-filament data from one stack index to another. Input parameters "num1" and "num2" specifies the stack index the data should be copied to and the stack index the data should be copied from respectively, and "q" specifies the number of the mini-filament in the myo structure for which this copying should be done.

void Minimize(int num)

This is the subroutine that calls the energy minimization functions. A nonlinear conjugate gradient method (included in subroutine conjgrdnt()) is used to find the energy minimum of the system. Depending on the forces on crosslinks and the total

energy of the system, this method calculates a new set of positions for crosslinks that brings the total energy of the system to a minimum.

Procedure

First, the mini-filaments are allowed take a step towards the barbed end. The size of the step is determined by the sum of the elastic energies, the energy of ATP and a constant ϵ (= 500). The flag "barbflag" is set to 1 when there is at least one mini-filament that is mobile. The minimization is done on data at stack index 2 of the data structures and the current positions are saved in stack index 1. Hence before each minimization step, CopyStartingPositions() copies the starting positions from one stack index to another (from 1 to 2 here). Then conjgrdnt() is called. Once the conjgrdnt() moves the crosslinks to achieve the minimum energy configuration, SetPositions() is called to update the data on stack index 1 and to calculate and save new forces on rods and crosslinks. At this point forces on walls are saved to a file (forceonwalls() is a subroutine that saves these wall forces) for later analysis. Next the new elastic energy of the system is calculated, the total energy is checked on each end of the mini-filament and various actions are made depending on their energy and position on the actin filament. The following list summarizes the conditions checked and the decisions made for each case.

- **If a mlink corresponding to a particular mini-filament has total energy less than** 10^{-6} $pN\mu m$ **:**

That mini-filament end is considered as reached an equilibrium position and the corresponding mlink will be marked as stopped by setting mlink[i].stop equal to 1 for the i^{th} mini-filament.

- **If a mini-filament end has reached the barbed end of a rod and if the same filament extends beyond the nearest crosslink:**

  The mini-filament is allowed to jump over the crosslink onto the next rod. jumptonextrod() is the subroutine that updates new positon of that mini-filament end.

- **If a mini-filament makes a jump[2] over a crosslink and if the equilibrium position for that mini-filament end lies at a position between the jump and the initial position:**

  The mini-filament is considered as stuck moving backwards. Again it will be marked as a stopped mlink.

- **If a mini-filament reaches the barbed end :**

  Depending on the requirements, the decision taken here changes. When we make the assumption that the mini-filaments reaching barbed ends stay attached, we just mark the mlink as stopped. But when treadmilling is switched on, the

[2]a jump over a crosslink will be performed when the mini-filament end reaches a distance within 6 subunits to the crosslink and it will jump 6 subunits beyond the crosslink over to the next rod. A minimum number of subunits had to be maintained in order to prevent too small rod segments.

mini-filaments are allowed to detach and reattach at a different location.

In a simulation that does not have treadmilling, we allow the process to continue until all the mini-filament ends have stopped, either by reaching an equilibrium position or by getting stuck at a filament end. When the treadmilling is turned on, after calculating the elastic energy following the minimization, the network is allowed to treadmill at a given rate and the process is carried out for a fixed number of mini-filament steps.

void CopyStartingPositions(int num0, int num1)

This subroutine copies data from stack index num0 to num1. For example, following argument shows the starting x-position of the i^{th} rod being copied onto stack index 1 from stack index 0 where initial positions are stored. rod[i].xspos[1] = rod[i].xspos[0].

void conjgrdnt (void)

This is the subroutine that carries out a nonlinear conjugate gradient method to find the minimum energy configuration in terms of the crosslink positions. A description of the conjugate gradient method is given in section 4.3. The coding for this subroutine was done closely following the algorithms written in [59, 63].

Procedure

First the GetPosition() function saves all the mlink and link positions into the

pos[] array. Then the gradient is calculated by calling the function findgradient(), where it changes the current positions of crosslinks in a certain direction and gradients are saved onto the *currentgrad*[] array. Then the conjugate gradient algorithm is followed as described in section 4.3 where a complete description of the displacements and the directions are included. New crosslink positions assigned by the conjugate gradient method are saved on to the array *currentx*[]. During the minimization, the Evaluatefunct() subroutine is called to calculate all the energies of the network while Evaluategradient() is called to calculate all the forces on the network.

double EvaluateFunc(int num)

This is the subroutine that calls all the energy calculating subroutines, and calculate the total energy due to stretching, bending and myosin movement towards the barbed end. The input parameter "num" specifies which stack is to be used for calculations.

Procedure

Here, first the new positions of the crosslinks are copied back on to the link and mlink structure from the *currentx*[] array. Then the functions ChangeMrodPosition(), ChangeMrodPosition2() and ChangeRodPosition() update the mrods and rods intersect at these crosslinks. After that the subroutine CalculateDimensions() calculates the new lengths and angles of all the mrods and mini-filaments. Finally CalculateRodLength() calculates the new lengths of the normal rods (not mrods).

Then the following functions are called to calculate different energy terms.

- **StretchingEnergy()** - Calculates the energy due to stretching of rods
- **BendingEnergy()** - Calculates the energy due to bending of rods
- **CalculateMenergy()** - Calculates the energy due to stretching of mini-filament
- **MstretchingEnergy()** - Calculates the energy due to stretching of mrods
- **MbendingEnergy()** - Calculates the energy due to bending of mrods
- **BarbendEnergy()** - Calculates the energy due to movement of mini-filament toward the barbed end

All of the above energy-calculating subroutines have an input parameter "num" that specifies data on which stack is to be used for calculations, and they all return the calculated energy. EvaluateFunc() in turn returns the sum of all these energies to the subroutine that calls it.

void Evaluategradient(int num) This subroutine calls all the force-calculating subroutines and the procedure is exactly the same as EvaluateFunc(). The only exception is that it calls CalculateForce() and CalculateMforce() instead of the energy functions in the latter.

void CalculateForce(int num)

This is the subroutine that calls the functions that calculate stretching forces and bending forces for rods that do not have mini-filaments attached to them. This is called by the Minimize() subroutine, after the crosslinks have been displaced.

Procedure

First InitializeForces() is called to set all the forces to zero before calculating forces after crosslink displacements. Then a for loop goes through all the crosslinks and first the stretching force components of all the rods that intersect at each point are calculated by calling SXForce() and SZForce() by looping through all the rod neighbors of that link. Force components acting on the two crosslinks at the two ends of the rod are also updated. For the i^{th} rod, rod[i].flag is set to 1 when the stretching force is calculated on that rod. This prevents recalculating the stretching force on this rod when the loop goes over the crosslink on the other end of the rod. Finally a second loop goes through the remaining rods (rods other than the one that stretching force is calculated immediately) and checks for rods generated from the same original filament (by checking the field rod[i].origin for the i^{th} rod). BendingFx() and BendingFz() calculate and return the forces acting on the crosslink due to the bending of a filament at that crosslink. Stretching forces and bending forces are not calculated for dangling ends as one end of these rods are free to move.

void InitializeForces(int num)

Initializes x and z components of the forces to zero on all rods in the stack specified by "num" and on all the crosslinks.

void InitializeMforces(void)

Initializes x and z components of the forces to zero on all mrods and mlinks.

double SXForce(int Pval, int odr, int num)

This calculates the x-component of the stretching force on a rod at its starting point. Input parameter "Pval" specifies the rod number, "odr", specifies whether the starting or the ending point of the rod is at the crosslink (crosslink on which the forces are calculated in CalculateForces()) "num" specifies the stack on which the data should be saved.

Procedure

X-component of the stretching force at the starting point of the rod is calculated using initial and current length of the rod. Depending on the value specified in variable "odr" the calculated force (if the starting point of the rod is at the crosslink or odr = 0) or the negative value of the calculated force (if the ending point of the rod is at the crosslink or odr = 1) is sent back to CalculateForce() to update the force on the respective crosslink.

double SZForce(int Pval, int odr, int num)

Here the z component of the stretching force is calculated. Procedure and input parameters are exactly the same as those in SXForce().

double BendingFx(int nb1, int nb2, int no1, int no2, int lno, int num)

This subroutine calculates the x-component of the bending force at a given crosslink. The input parameters are as follows:

- **nb and nb2** indices of the rods no1 and no2 in *nbname*[] array of the link lno.
- **no1 and no2** rod numbers of the rods belonging to the same filament.
- **lno** crosslink number
- **num** index of the stack to save data to.

Procedure

X-component of the bending energy is calculated using the mean length and cosine between the two rods considered. lno is the crosslink common to both rods and the force on this crosslink is sent back to CalculateForce(). However there are at least two more crosslinks that are affected by bending of the filament at this crosslink. Those are the crosslinks at the other two ends of the rods. Force on these crosslinks and on

the two rods are updated inside this subroutine.

double BendingFz(int nb1, int nb2, int no1, int no2, int lno, int num)

Here the z component of the bending force is calculated. Procedure and input parameters are exactly the same as those in BendingFx().

void CalculateMforce(int num)

This subroutine calls the following force-calculating functions for mrods after calling InitializeMforces() to set all the forces on mrods and mlinks to zero. Input parameter "num" specifies data on which stack to be used for calculations.

- **MyosinForce()** - Calculates force on the mini-filament due to length changes during its movement and elastic relaxation.
- **MstretchingForce()** - Calculates stretching forces on mrods
- **MbendingForce()** - Calculates bending force on mrods

All these subroutines have only one input parameter, "num" that specifies data on which stack to be used for calculations. In MyosinForce(), a for loop goes through all the mini-filaments in the system and calculates the forces on each of them due to individual length changes. Procedure in MstretchingForce() and MbendingForce() are similar to that in SXForce() and BendingFX() However, in these, the looping over all

the mrods and mlinks respectively happens inside the subroutine itself. None of the above three subroutines return any parameters, since the forces on mrods, neighboring rods, mlinks and links due to calculated forces are updated inside each subroutine.

void SetPositions(int num)

This subroutine is called after each elastic relaxation of the network to update the current positions and orientations of rods and mrods. The argument "num" specifies to which stack these updates will be applied.

Procedure

Similar to subroutines EvaluateFunc() and Evaluategradient(), here the new positions of the crosslinks are copied back onto the link and mlink structure from the *currentx*[] array. Then functions ChangeMrodPosition(), ChangeMrodPosition2() and ChangeRodPosition() update the mrods and rods intersect at these crosslinks. After that following subroutines are called in the given order to compete the update.

- CalculateDimensions()
- CalculateRodLength()
- CalculateAngle()
- ChangeDanglingAngle() - aligns the dangling end with the rod next to it.
- CalculateForce()

- CalculateMforce()

void ChangeDanglingAngle(int num)

This subroutine aligns a dangling end with the rod immediately next to it and that belongs to the same filament.

Procedure

Depending on whether the starting point or the ending point of the dangling end is at the crosslink, the new position of the other end is calculated while assigning the angle taken from the rod adjacent to the dangling end. A for loop goes over all the rods and the procedure is performed on the rods identified as dangling ends.

void jumptonextrod(int mrd, int num)

This subroutine facilitates the jump of a mini-filament over a crosslink. Input parameter "mrd" specifies the corresponding mlink or the mrod number (for a particular mini-filament end, the indeces of the mrod and mlink are the same) and "num" specifies the stack index to write the data onto.

Procedure

First the rod that the mini-filament is originally attached is recovered. After the mini-filament attachment, the rod is saved as a mrod which consists of two rod segments. During elastic relaxation the mrods are updated and since the rod is at a non-active state its coordinates and orientation are not updated. Hence when the

mini-filament leaves, the original rod needs to be recovered by calculating its x, z coordinates, length and angle. This is done using the positions of links at the starting and ending points of the rod. Then new coordinates and the orientation, as well as neighbor rods and crosslinks, are assigned for the mrod that is attached to the new rod. The stack index 0 for the mrod is also updated as this stack should contain the initial positions' orientation data. Finally the properties of the mini-filament are also updated according to the new position.

void treadmill(int num)

This subroutine enables the treadmilling of filaments. Input parameter "num" specifies the stack index of the data that should be updated.

Procedure

A for loop runs through all the rods. First, if it finds a dangling end that contains the barbed end of a filament, a subunit is added at the barbed end of that rod (the dangling end). The rod length is also updated after each addition, and depending on whether it is the starting position or the ending position of the rod, ChangeStarting-Position() or ChangeEndingPosition() updates the new starting or the ending point respectively. Similarly, in the case of a dangling end that includes the pointed end, a subunit is removed from the rod and again above two functions update the starting or the ending position. Polymerizing rods are checked for 1) crosslinking with other rods 2) reaching the wall or the frame of the simulation box. Depolymerizing rods are

checked for 1) rod lengths going to zero and hence resulting in removal of a crosslink and a rod 2) detaching from the wall. In any of the four cases mentioned, the value of the link at corresponding end[3] is updated.

After the growing end of a filament makes a connection with an existing rod (Checkrodforcrosslinking() searches for new crosslinks and if a new crossing point is found, the intersecting rod is divided into two rods), a new rod is generated beyond that new crosslink. CreateNewRod() assigns values to the properties of the new rod and both the variables nrods and nlinks are updated (increased by one). On the other hand, when a rod shrinks or depolymerizes beyond an existing crosslink, a rod and a crosslink should disappear. Since deleting an element in the middle of the structure arrays can complicate the situation, a removal of a rod or crosslink is facilitated by setting the active property to 0 for both. Hence when energy, force or any other property is calculated, the calculations are performed only on active components. Further when a rod at an intersection with three or more rods depolymerizes completely, it can leave two rods that belong to the same filament with a crosslink in the middle. Such crosslinks are also inactivated and the two rods are combined to a single rod by updating the position and dimensions of one rod to include the length of both rods and the other rod is marked as inactive. This combining is performed in the subroutine JoinRods().

[3]A dangling end is denoted by a value -2 and a rod connected to the frame is denoted by a value -1 at rod[i].slink and/or rod[i].elink

All these steps are repeated for mrods. However, since each mrod has a mini-filament attached to it at one end, when an mrod depolymerizes beyond a mini-filament, the remaining section of the mrod is recovered (by calling RecoverRod()) as a normal rod and the mini-filament is allowed to reattach at a new place by calling FindMyo().

void ChangeEndingPosition(int type, int rd, int pol, int num)

This subroutine is called when an ending position of a rod undergoes polymerization or depolymerization. Input parameter "type" denotes whether the change should be done on a rod (if type = 0) or a mrod (if type =1). "rd" specifies the index of the rod/mrod to update, "pol" specifies the polarization of the rod/mrod and "num" specifies which stack index should be updated.

Procedure

The ending position coordinates are recalculated for the given rod/mrod by using its angle, length and starting point coordinates along with the gradient calculated using the tangent of the angle.

void ChangeStartingPosition(int type, int rd, int pol, int num)

Here the input parameters and the procedure are the same as ChangeEndingPosition() and the starting position coordinate are updated.

void CreateNewRod(int type, int rd, int nrd, int num)

This is the subroutine that creates a new rod at an intersection of three rods, when the rod that belongs to the different filament (in a three rod intersection, two rods belong to the same filament and the other to another filament) polymerizes. Input parameter "type" again specifies if the growing rod is originally a rod/mrod, "rd" is the index of the rod/mrod, "nrd" is the current value of nrods, which will become the index of the new rod and "num" is the stack index to update.

Procedure

Here a rod with length equal to that of one subunit is created. All the fields in the rod structure for new rod are assigned values.

void JoinRods(int lnk, int num)

This is the subroutine that combines two rods that belong to the same filament and are left with a crosslink between them that does not have any other rods (belonging to a different filament) intersecting. This situation occur when an intersecting filament depolymerizes beyond the crosslink. Hence this subroutine is called when a crosslink just has two neighboring rods that have the same origin (that belong to the same filament). Input parameter "lnk" specifies the link that needs to be inactivated and "num" the stack index to update.

Procedure

First, the rod with the pointed end at the given link is named rod1 and the other rod2. Then the pointed end of rod1 is assigned the coordinates and the neighboring rod names and link names of rod 2. Angle, length and subunit number are recalculated for rod1 and the stack index 0 is also updated with the new values. The neighbor rod name at the corresponding index of the link at the pointed end of rod2 is also updated with rod1. Finally rod2 and link lnk are marked as inactive (rod[rod2].active =0 and link[lnk].active =0).

void RecoverRod(int mrd, int num)

This subroutine is called when a mini-filament leaves the rods it is attached to and reattaches at a different location. This can occur either when the mini-filament reaches a barbed end of a filament or when the filament depolymerizes past the point of attachment of a mini-filament. In either case two rods (corresponding to the two attachment points of the mini-filament and rods saved as mrods) need to be recovered. The input parameter "mrd" defines the mrod that needs to be recovered and "num" the stack index to update.

Procedure

First it is identified whether the mrod is a dangling end or a one that is in the middle of a filament. Then by using the number of subunits left on the mrod and the positions of the crosslinks at two ends, the x, z coordinates, length and angle are calculated for each case.

void RemoveNbrods(int lnk, int rd, int num)

This subroutine is called when a rod depolymerizes completely or depolymerizes beyond a crosslinking point, to update the link at the intersection. Data on this rod in the *nabname*[] and *nborder*[] arrays in the link structure needs to be removed. Since the maximum length of these arrays is four, each time a rod depolymerizes completely, the data about it on these two arrays are deleted. If the data is written in a index in the middle, then the array elements behind are shifted and the number of neighbors (link[i].nbs) is reduced by one. Input parameter "lnk" specifies the index of the link to update, "rd" is the rod name to be removed and "num" is the stack index to update.

Procedure

First, link[lnk].nbname[] array is searched to find the index which has the matching content to rd. Then, if this is the last element in the array, then the number of neighbors (link[lnk].nbs) is simply reduced by one. But if this is an element in the middle, then the remaining elements in link[lnk].nabname[] and link[lnk].nborder[] arrays are shifted up by one and the number of neighbors is reduced by one. Finally, two checks are done on the number of remaining neighbors. 1) If the number of remaining neighbors is less than 2, the link is marked as inactive and the data on the link on remaining rod is updated. 2) If the number of neighbors is equal to two and if they belong to the same filament, JoinRods() is called.

void Checkrodforcrosslinking(int rd, int num)

This is the subroutine that searches for a possible crosslinking point for a polymerizing rod. Input parameter "rd" specifies the growing rod, "num" is the stack index to update.

Procedure

The procedure here is similar to CheckCrossLinks(). However here, a smaller virtual box is used (size here is $0.5\ell \times 0.5\ell$) to choose rods to calculate possible crosslinks. If a crossing rod is found, then the crossing rod is divided into two at the crosslinking point. Hence the number of rods and the number of crosslinks increase by one in such a case. Finally all the properties in the rod structure are updated for all three rods involved and similarly the new link is update with corresponding rod data and coordinates.

Initially we allowed a growing mrod to make crosslinks when it intersects with other rods in the network. However during the elastic relaxation, such crosslinking events generated unphysical energies as the subunit number changed suddenly. Therefore, mrods are not allowed to make crosslinks when they overlap with rods or mrods.

4.3 Conjugate Gradient Method

Linear Case

The conjugate gradient method is an iterative method used to solve large systems of linear equations of the form

$$\hat{A}\,|x\rangle = |b\rangle\,, \tag{4.1}$$

where $\hat{A}$ is a square, symmetric and positive definite[4] matrix, $|x\rangle$ is an unknown vector, and $|b\rangle$ is a known vector. The solution of a quadratic problem of the type

$$\text{minimize} \quad f(x) = \frac{1}{2}\left\langle x \,\middle|\, \hat{A} \,\middle|\, x \right\rangle - \langle b|\,|x\rangle \tag{4.2}$$

is identical to that of the above linear equation when the matrix $\hat{A}$ is positive definite. Hence solving the quadratic minimization problem is equivalent to solving the linear equation problem. The basic mathematical steps behind developing the conjugate gradient algorithm are described below. A sequence of vectors $\{d_i\}$ are said to be conjugate to each other with respect to $\hat{A}$, if $\left\langle d_i \,\middle|\, \hat{A} \,\middle|\, d_j \right\rangle = 0$ for $i \neq j$. Such a set of vectors are linearly independent given the matrix $\hat{A}$ is positive definite. Therefore a solution $|x^*\rangle$ can be written to the above linear equation using $|d_i\rangle$s as follows:

$$|x^*\rangle = \alpha_0\,|d_0\rangle + \text{.....} + \alpha_{n-1}\,|d_{n-1}\rangle\,, \tag{4.3}$$

where $\hat{A}$ is a $n \times n$ matrix. Now multiplying this by $\hat{A}$ and taking the scalar product

[4]For a positive definite matrix $\hat{A}$, $\left\langle x \,\middle|\, \hat{A} \,\middle|\, x \right\rangle > 0$ for all non zero vectors $|x\rangle \in \mathbb{R}^n$

with $\langle d_i|$ gives

$$\begin{aligned} \left\langle d_i \middle| \hat{A} \middle| x^* \right\rangle &= \alpha_i \left\langle d_i \middle| \hat{A} \middle| d_i \right\rangle \\ \alpha_i = \frac{\left\langle d_i \middle| \hat{A} \middle| x^* \right\rangle}{\left\langle d_i \middle| \hat{A} \middle| d_i \right\rangle} &= \frac{\langle d_i \,|\, b \rangle}{\left\langle d_i \middle| \hat{A} \middle| d_i \right\rangle}. \end{aligned} \tag{4.4}$$

here we have used the summation convention,

$$|x^*\rangle = \alpha_i \sum_{i=0}^{n-1} \frac{\langle d_i \,|\, b \rangle}{\left\langle d_i \middle| \hat{A} \middle| d_i \right\rangle}. \tag{4.5}$$

The above steps show that by having the $|d_i\rangle$s be conjugate rather than orthogonal is important to obtain the α_is in terms of the known vector $|b\rangle$, even when the exact solution to the problem $|x^*\rangle$ is unknown. The solution $|x^*\rangle$ can be obtained iteratively in n steps by adding $\alpha_i |d_i\rangle$ at every i^{th} step by starting at an arbitrary point. When the $|d_i\rangle$ are some arbitrary choice of conjugate directions, this method is called the conjugate direction method. The conjugate gradient algorithm is developed by assigning each $|d_i\rangle$ a direction which is conjugate to all the directions taken before (i.e. for all $j < i$) and determined by the gradient. Hence the direction to move in the i^{th} iteration is determined at that step. At each step, $|d_i\rangle$ is assigned the current negative gradient vector $(|g_i\rangle)$[5] plus a linear combination of the previous direction vectors. At the first step or when $i = 0$, similar to the steepest descent algorithm, the negative gradient is chosen as the direction of the step. The conjugate direction theorem[6] shows that such an iterative process will converge to the exact solution of

[5] $|g_i\rangle$ is the gradient of the function 4.2 evaluated at $|x_i\rangle$.

[6] for $\{d_i\}_{i=0}^{i=n} \in \mathbb{R}^n$, a sequence of nonzero vectors that are conjugate with respect to $\hat{A}$, using

Eqn. 4.1 in exactly n iterations, which means $x^* = x_n$. Using this information, we can get an expression for α_k in terms of the gradient at $|x_k\rangle$ for some $k < n$.

For any $|x_0\rangle \in \mathbb{R}^n$ we note that

$$|x^* - x_0\rangle = \alpha_0 |d_0\rangle + ... + \alpha_{n-1} |d_{n-1}\rangle$$

For same set of α'. Now multiplying this by $\hat{A}$ and taking the scalar product with $\langle d_k|$ gives

$$\alpha_k = \frac{\left\langle d_k \middle| \hat{A} \middle| (x^* - x_0) \right\rangle}{\left\langle d_k \middle| \hat{A} \middle| d_k \right\rangle} \tag{4.6}$$

For the first k steps of the iterations we have,

$$|x_k - x_0\rangle = \alpha_0 |d_0\rangle + ... + \alpha_{k-1} |d_{k-1}\rangle \tag{4.7}$$

The conjugacy of the $|d_k\rangle$s implies

$$\frac{\left\langle d_k \middle| \hat{A} \middle| (x_k - x_0) \right\rangle}{\left\langle d_k \middle| \hat{A} \middle| d_k \right\rangle} = 0 \tag{4.8}$$

Hence Eqn. 4.6 becomes

$$\begin{aligned} \alpha_k = \frac{\left\langle d_k \middle| \hat{A} \middle| (x^* - x_k) \right\rangle}{\left\langle d_k \middle| \hat{A} \middle| d_k \right\rangle} &= \frac{\left\langle d_k \middle| \hat{A} \middle| (x_n - x_k) \right\rangle}{\left\langle d_k \middle| \hat{A} \middle| d_k \right\rangle} \\ \hat{A}(|x_n\rangle - |x_k\rangle) &= |b\rangle - \hat{A}(|x_k\rangle \\ \alpha_k = -\frac{|d_k\rangle (\hat{A} |x_k\rangle - b)}{\left\langle d_k \middle| \hat{A} \middle| d_k \right\rangle} &= -\frac{\langle g_k \,|\, d_k \rangle}{\left\langle d_k \middle| \hat{A} \middle| d_k \right\rangle}, \end{aligned} \tag{4.9}$$

(4.10)

$|x_0\rangle \in \mathbb{R}^n$ a sequence $\{x_k\}$ generated according to $|x_{k+1}\rangle = |x_k\rangle + \alpha_k |d_k\rangle$, where $\alpha_k = -\frac{\langle g_k \,|\, d_k \rangle}{\langle d_k \,|\, A \,|\, d_k \rangle}$ and $|g_k\rangle = \hat{A}|x_k\rangle - |b\rangle$, converges to the unique solution x^*, of $\hat{A}\,|x\rangle = |b\rangle$ after n steps making $x^* = x_n$.

since $|g_k\rangle = \hat{A}|x_k\rangle - |b\rangle$

Below are the steps of the iterative algorithm for conjugate gradient method, which one can use to find the minimum of a function $f(x)$ [64].

Initial conditions:

For some arbitrary $|x_0\rangle \in \mathbb{R}^n$ taken as the starting point and $|d_0\rangle = -|g_0\rangle = b - \hat{A}|x_0\rangle$

Iterative steps:

$$\begin{aligned} |x_{k+1}\rangle &= |x_k\rangle + \alpha_k |d_k\rangle \\ \alpha_k &= -\frac{\langle g_k \,|\, d_k\rangle}{\langle d_k \,|\, A \,|\, d_k\rangle} \\ |d_{k+1}\rangle &= -|g_{k+1}\rangle + \beta_k |d_k\rangle \\ \beta_k &= -\frac{\langle g_{k+1} \,|\, A \,|\, d_k\rangle}{\langle d_k \,|\, A \,|\, d_k\rangle} \end{aligned} \tag{4.11}$$

Here, α_k has the property that $|x_k\rangle$ minimizes $f(x)$ on the line $|x_k\rangle = |x_{k-1}\rangle + \alpha_{k-1}|d_{k-1}\rangle$[7].

Nonlinear case

For a nonlinear equation, it becomes more difficult to find an α that minimizes $f(x)$ on a line. Hence some other algorithm must be used to find α. Bracketing, parabolic interpolation and Brent's method are examples of such procedures that

[7]This is the *Expanding Subspace Theorem* : for $\{d_i\}_{i=0}^{i=n} \in \mathbb{R}^n$, a sequence of nonzero vectors that are conjugate with respect to $\hat{A}$, using $|x_0\rangle \in \mathbb{R}^n$ a sequence $\{x_k\}$ generated according to $|x_{k+1}\rangle = |x_k\rangle + \alpha_k|d_k\rangle$, where $\alpha_k = -\frac{\langle g_k \,|\, d_k\rangle}{\langle d_k \,|\, A \,|\, d_k\rangle}$ has the property that minimizes $f(x) = \frac{1}{2}\left\langle x \middle| \hat{A} \middle| x \right\rangle - \langle b|\,|x\rangle$ on the line $|x_k\rangle = |x_{k-1}\rangle + \alpha_{k-1}|d_{k-1}\rangle$, -$\infty < \alpha < \infty$. [64]

track down the minimum of a polynomial. Further, the Newton-Raphson and the Secant methods are two general purpose iterative algorithms that can be used to find α in each step. Also for the linear case many choices of β exist and they all are equivalent. However for the nonlinear case they produce different results. Two of the most commonly used expressions in the later case are,

- Fletcher-Reeves formula:

$$\beta_{k+1} = \frac{\langle g_{k+1} \,|\, g_{k+1} \rangle}{\langle g_k \,|\, g_k \rangle}$$

- Polak-Ribiere formula:

$$\beta_{k+1} = \frac{\langle g_{k+1} \,|\, (g_{k+1} - g_k) \rangle}{\langle g_k \,|\, g_k \rangle}$$

Unlike the linear conjugate gradient method, the nonlinear method is not expected to converge to the solution in exactly n steps (for a problem in n dimensions). Hence after every n iterations the gradient is set to the negative gradient at that point and the process is restarted. An outline of the iterative steps in the nonlinear conjugate gradient method is as follows [63]:

$$|d_0\rangle = |g_0\rangle \;=\; -\vec{\nabla} f(x_0) \tag{4.12}$$

find α_k that minimizes $f(x_k + \alpha_k |d_k\rangle)$

$$|x_{k+1}\rangle \;=\; |x_k\rangle + \alpha_k |d_k\rangle$$

$$|g_{k+1}\rangle \;=\; -\vec{\nabla} f(x_{k+1})$$

$$\beta_{k+1} = \frac{\langle g_{k+1} \,|\, g_{k+1}\rangle}{\langle g_k \,|\, g_k\rangle} \quad or \quad \beta_{k+1} \;=\; \frac{\langle g_{k+1} \,|\, (g_{k+1} - g_k)\rangle}{\langle g_k \,|\, g_k\rangle}$$

$$|d_{k+1}\rangle \;=\; -\,|g_{k+1}\rangle + \beta_{k+1} |d_k\rangle$$

4.4 Bracketing a minimum

Bracketing a minimum is somewhat similar to finding roots of a function in one-dimension using the bisection method. In general, a root of a function can be bracketed by two numbers (a,b) if the function changes its sign going from one to the other. In contrast, to bracket a minimum there should be at least three numbers a, b, c such that $a > b > c$ (or $c > b > a$) with $f(b)$ less than both $f(a)$ and $f(c)$. In the bisection method, when a root is initially bracketed between points (a,b), the next bracketing interval is calculated by bisecting the interval into two equal segments and evaluating the function at this midpoint, x for optimal convergence. Then the smaller of the two bracketing intervals, either (a,x) or (b,x) is chosen as the next or the new bracket and this procedure is repeated until the length of the bracketting interval is very small.

In bracketing a minimum, since there is a triplet of abscissa values, the bisection

needs to chose a point either between (a,b) or (b,c). After choosing one of the two intervals, the function is evaluated at the new bisecting point x. Here the bisecting point is taken as the symmetric point to b. That is the distance to x measured from c should be the same as that from a to b. Further, this puts x in the larger segment between (a,b) and (b,c). Then if $f(x) > f(b)$, (a,b,x) is considered as the new bracket. Else if $f(x) < f(b)$ the new bracketing interval will be (a,x,c). Always in the sequence, the middle value is the abscissa whose ordinate corresponds to the best minimum found to that point. This procedure is repeated until the distance between the two outer points become less than a specified tolerance. The smallest value to set as the limit of tolerance should be the square root of the machine precision [59].

Since the total energy of the system is not exactly quadratic, we used the nonlinear conjugate gradient mechanism along with the bracketing formalism to find the α that minimizes $f(x)$ along a line or at each iteration. Ref. [59] suggests that it is best to use Brent's method to calculate a better minimum after bracketing the minimum. Brent's method uses parabolic interpolation near the minimum on sufficiently smooth functions or which are parabolic near the minimum. We used the code given for bracketing and then used the subroutine given for Brent's method to obtain a better minimum. However in our case, the improvement of the minimum from the Brent's method over the bracketing was minimal. It might be that our energy function is not smooth enough. Hence only the bracketing subroutine was used inside the nonlinear conjugate gradient method to isolate the minimum.

Appendix

A Description of the data fields belonging to struct objects

Table A1: Struct objects used in the simulation

Object	Datatype	Field name	Description
rod	double	xspos[stk][8]	Starting x-position of a rod
	double	zspos[stk]	Starting z-position of a rod
	double	xepos[stk]	Ending x-position of a rod
	double	zepos[stk]	Ending z-positon of a rod
	double	length[stk]	Length of a rod
	double	angle[stk]	Angle of a rod measured from the z-direction
	double	subunit[stk]	Number of subunits in a rod
	double	fx[stk]	x-component of the total force on a rod
	double	fz[stk]	z- component of the total force on a rod
	int	slink	link at the starting point of a rod
	int	elink	link at the ending point of a rod

Continued on next page

[8] stk defines the stack size. These fields are declared as arrays so that the initial configuration of the network is stored in index 0 and final configuration in index 1 and etc.

Table A1 – continued from previous page

Object	Data type	Field name	Description
	int	snb	neighbor rod at the starting point of a rod
	int	enb	neighbor rod at the ending point of a rod
	int	origin	index of the filament the rod belongs
	int	polarity	polarity of the rod/filament
	int	active	A flag used during treadmilling
	int	flag	A flag used during calculation of stretching forces
	int	myoflag	Indicate if a mini-filament is attached or not
mrod[9]	double	xspos1[stk]	starting x-position of rod segment 1 [10]
	double	zspos1[stk]	starting z-position of rod segment 1
	double	xepos1[stk]	ending x-position of rod segment 1
	double	zepos1[stk]	ending z-position of rod segment 1
	double	xspos2[stk]	starting x-position of rod segment 2 [11]
	double	zspos2[stk]	starting z-position of rod segment 2
	double	xepos2[stk]	ending x-position of rod segment 2
	double	zepos2[stk]	ending z-position of rod segment 2
	double	angle1[stk]	angle of the rod segment 1
	double	length1[stk]	length of the rod segment 1
	double	angle2[stk]	angle of the rod segment 2
	double	length2[stk]	length of the rod segment 2
	double	fx1	x-component of the total force on rod segment 1

Continued on next page

[9] mrods refers to the rod segments resulting due to the attachment of a mini-filament. Each rod is divided into two rod segments and named rod segment 1 and rod segment 2

[10] "rod segment 1" refers to the rod segment with the barbed end of the rod

[11] "rod segment 2" refers to the rod segment with the pointed end of the rod

Table A1 – continued from previous page

Object	Data type	Field name	Description
	double	fz1	z-component of the total force on rod segment 1
	double	fx2	x-component of the total force on rod segment 2
	double	fz2	z-component of the total force on rod segment 2
	double	subunit[stk]	Number of subunits in rod segment 1
	double	Ntot	total number of subunits in the rod
	int	slink1	starting link of the rod segment 1
	int	elink1	ending link of the rod segment 2
	int	slink2	starting link of the rod segment 1
	int	elink2	endting link of the rod segment 2
	int	snb1	starting neighbor rod of rod segment 1
	int	enb1	ending neighbor rod of rod segment 1
	int	snb2	starting neighbor rod of rod segment 2
	int	enb2	endting neighbor rod of rod segment 2
	int	polarity	Polarity of the original rod/filament
link	double	xpos[stk]	x-position of a link
	double	zpos[stk]	z-position of a link
	double	fx	x-component of the total force on a link
	double	fz	z-component of the total force on a link
	int	nbs	total number of rods intersect at the link
	int	nbname[4]	index of rods that intersect at the link
	int	nborder[4]	whether the starting point or ending point of the rod is at the link
	int	active	flag used during treadmilling
mlink [12]	double	xpos[stk]	x-position of a mlink
	double	zpos[stk]	x-position of a mlink

Continued on next page

[12]mlinks are the crosslinking points between mini-filaments and rods. Each mini-filament generates two mlinks

Table A1 – continued from previous page

Object	Data type	Field name	Description
	double	fx	x-component of the total force on a link
	double	fz	x-component of the total force on a link
	double	dEdn	derivative of elastic energy with respect to change in subunit number for that mlink
	double	dsub	change in subunit number from initial position
	int	stop	flag to indicate the end of the mini-filament attached to this mlink has stopped
	int	onbname	index of the rod the mlink is on
	int	nborder[3]	whether the starting point or the ending point is at the mlink for each component[13]
	int	myonum	index of the mini-filament attached at the mlink
	int	active	flag used during treadmilling
myo	double	xspos[stk]	starting x-position of a mini-filament
	double	zspos[stk]	starting z-position of a mini-filament
	double	xepos[stk]	ending x-position of a mini-filament
	double	zepos[stk]	ending z-position of a mini-filament
	double	angle[stk]	angle of a mini-filament measured from the z-direction
	double	length[stk]	length of a mini-filament
	double	fx	x-component of the total force on a mini-filament

Continued on next page

[13]mlink has two mrods and a mini-filament attached at that point

Table A1 – continued from previous page

Object	Data type	Field name	Description
	double	fz	x-component of the total force on a mini-filament
	int	active	flag used during treadmilling
	int	srod	index of the rod the starting point of the mini-filament is attached to
	int	erod	index of the rod the starting point of the mini-filament is attached to

Chapter 5

Conclusion

In this study we have shown that the directional movement of the myosin mini-filaments along actin filaments toward low energy configurations generates contractile forces in both random actin networks and bundles. The mechanism relies on the ability of the mini-filaments to rotate and orient into low energy contractile configurations. It was evident that actin filament bending helped accommodate such transitions. Tensile force chains carry the stress generated inside the networks to walls. The network geometry seemed to play an important role in the stress generated; our results show that bundles generate higher stresses compared to networks. Considering the notion of force chains this observation can be explained as follows: in a bundle almost all the force chains run directly to the two opposing walls and are nearly perpendicular at the point of contact but in a network, force chains disperse along four directions and can act on walls at an angle, reducing the total inward contractile force. The

network structure being sufficiently rigid to support well-dened minilament energy extrema was the main requirement for contractility.

Future work in this direction could incorporates several types of extensions. These include extending our model to three dimensions, and allowing actin filaments to form closely packed parallel bundles. (Usually single actin filaments are not observed in *in vivo* and/or *in vitro* systems. A few of them aggregate and with the aid of crosslinking proteins, they form "super filaments".) Including a more realistic cellular geometry and incorporating phenomena like cell edge oscillations, retrogade flow and cellular adhesions are also important. Finally a better treatment of the effects of complete continuous renewal of the actin filaments (treadmilling) and of dynamic crosslinkers in the system are essential. However including all these effects together might not be practical, but adding one or two properties at a time can make the system and the updates more manageable to handle. Each update will require more and more computer power and increasingly sophisticated mathematical and computational tools to handle the complex system. Novel experiments will also be needed to validate the model and input and its outputs.

Moving onto three dimensions is an extension that requires very powerful computational resources. The number of degrees of freedom grows quickly in three dimensions and the energy minimization procedure will also become slower compared to the two dimensional case. Further, the subroutines can become more complex. For example, finding crosslink points in a three-dimensional network will be much more complex

because the filaments will have to be moved to find each other. Also, it might be necessary to simulate a considerable volume of the cytoskeleton to obtain meaningful information, and the simulation volume could contain many more actin filaments and myosin mini-filaments than a two-dimensional system. These high computational and time requirements prevented us from moving on to three dimensions in the current work. Despite its difficulty to achieve, it is a very important extension to work on, and it will be more straightforward to compare results generated in three dimensions with experimental data.

One important phenomena present in real cells is edge oscillations. There is recent work suggesting that these cell edge oscillations or membrane waves and ruffles are directly affected by actomyosin contractility [65]. To be exact, they showed that actomyosin contraction coupled with actin polymerization and membrane curvature gave rise to transverse membrane waves and the velocity of these waves was proportional to the myosin activity. Implementation of our simulation for this system would require at least the consideration of membrane curvature and actin protrusion in addition to actomyosin contractility.

Another important possible extension is to treat the effects of actomyosin contractility in the presence of focal adhesions. There are many experiments that have been conducted and measured the traction forces [66, 67, 68]. Usually these measurements are done by allowing the cells to move on polyacrylamide gels that have fluorescently labeled nanobeads where the displacement field is computationally extracted from

the fluorescence data [69], or on polydimethylsiloxane micro-posts whose tip displacements are analyzed using imaging techniques [70]. Implementation of such systems requires the introduction of adhesion sites to our model. This can be achieved, for example, by allowing crosslinks on selected patches on the network to be immobile or static and treating the total force experienced by such an aggregation as the force on a single adhesion site and having many such areas rather than having a fixed boundary as in the current model. It has been found experimentally that the F-actin retrograde flow speed in cells is inversely proportional to traction stress in the extracellular matrix close to the cell edge [71]. Such observations can be used to directly compare the results produced and more importantly to validate the applicability of the developed model to real systems.

Another limitation of the current method is that, there is a condition that only one mini-filament can bind to a particular pair of actin filaments at a given time. This condition was imposed to maintain simplicity in handling the mini-filaments. There is substantial evidence that shows this is not the case in the cell or in reconstituted networks [24, 40]. For example, Ref. [40] reports that in their reconstituted bundles, there were more than 4 mini-filaments attached per actin filament. Hence the current simulation should be updated to allow more than one mini-filament to attach to a single actin filament. Along these lines [72] observed that clumps of myosin II motors forming during the ring formation in cytokinesis of fission yeast. Similarly, [11] reports reconstituted bundles forming bud-like regions in the middle. In our

networks or bundles, we did not see this, perhaps due to the limitation on mini-filament attachments. In addition, the maximum number of mini-filaments we had for a bundle of length 10 μm was 5. To see an effect like this we might need to ramp up the total number of mini-filaments in the network.

Ref. [11] observed that actin filaments become sorted according to their polarity before mini-filament aggregation occurs. For this to occur filaments should be more dynamic. With static crosslinks and constrained treadmilling imposed in our simulation, actin filaments are almost immobile, hence it is not surprising that we did not see such effects. Therefore a major and an important improvement to our model will be to make treadmilling more complete and more realistic. As it stands now, it does not allow actin filaments to depolymerize beyond a crosslink and the network is made static in a region close to the wall in order to prevent the bundle from disintegrating. Allowing filaments to treadmill at any point is straightforward. However to maintain the integrity of the network and to keep the filament density constant during the course of simulation, the code will have to be modified. One could for example, impose periodic boundary conditions for treadmilling filaments at the walls. Further to make the system more dynamic, one can allow the crosslinks to detach with a certain probability. Ref. [73, 74, 75] show that cross-linker dynamics, mainly dissociation rates, are an important determinant for the mechanical properties of actin filament gels. Hence including this will directly affect the results obtained for stress generated in such a system.

Another recent experimental observation that involves actomyosin contractility is disassembly of cytoskeletal structures. Recent cryo-TEM experiments show that formation and growth of actin bundles crosslinked by fascin is inhibited above a certain threshold of myosin II. It is observed that the disintegration of the bundles occurs in two steps, first unbundling of the actin bundles into individual filaments and then depolymerization of actin filaments [76]. When dynamical crosslinks and complete treadmilling of actin is implemented, this is another observation that one can evaluate. Such simulations will help interpret the observations in a critical manner.

In conclusion, the significance of this work lies in the predictions it could make despite the simplicity of the model. Although the model was simple, the most of the assumptions we have made here are well justified. The understanding that we have obtained by analyzing the results obtained by varying various properties of this simple system is very encouraging. In fact, with these findings we have demonstrated the generality of actomyosin contraction for the first time. This general behavior was found to exist in both random and bundle geometries. With the addition of further extensions, if we understand actomyosin contractility better it may lead to some important practical outcomes. For example, we could use it to design a biomimetic cell that moves by actomyosin contraction. Perhaps these could be used to deliver drugs to specific organs or even to track bacteria or viruses, similar to tracking by white blood cells. Also very importantly, existing anticancer drugs work by inhibiting mitosis, the division of the cell nucleus. If one had a better understanding of myosin

contractility it might enable us to treat cancer by cytokinesis inhibition as well.

Bibliography

[1] Ludovic R. Otterbein, Philip Graceffa, and Roberto Dominguez. The crystal structure of uncomplexed actin in the adp state. *Science*, 293(5530):708–711, 2001.

[2] M Vicente-Manzanares, X Ma, R S Adelstein, and A R Horwitz. Non-muscle myosin ii takes centre stage in cell adhesion and migration. *Nat Rev Mol Cell Biol*, 10(11):778 – 790, 2009.

[3] Michael A. Geeves and Kenneth C. Holmes. The molecular mechanism of muscle contraction. In John M. Squire and David A. D. Parry, editors, *Fibrous Proteins: Muscle and Molecular Motors*, volume 71 of *Advances in Protein Chemistry*, pages 161 – 193. Academic Press, 2005.

[4] R Niederman and T D Pollard. Human platelet myosin. ii. in vitro assembly and structure of myosin filaments. *The Journal of Cell Biology*, 67(1):72–92, 1975.

[5] Jeffrey T. Finer and James A. Simmons, Robert M. andSpudich. Single myosin molecule mechanics: piconewton forces and nanometre steps.

[6] Charles Mallery. Muscle fibers - biology 150 , introductory biology for majors. [Accessed: 08/08/2012].

[7] Biology Forum. The role of calcium, tropomyosin, troponin in cross-bridge cycle. [Accessed: 08/08/2012].

[8] K. Kruse and F. Julicher. Actively contracting bundles of polar filaments. *Phys. Rev. Lett.*, 85(4):1778–1781, 2000.

[9] Martin Lenz, Margaret L Gardel, and Aaron R Dinner. Requirements for contractility in disordered cytoskeletal bundles. *New Journal of Physics*, 14(3):033037, 2012.

[10] P.M. Bendix, G.H. Koenderink, D. Cuvelier, Z. Dogic, B. N. Koeleman, W. M. Brieher, C. M. Field, L. Mahadevan, and D. A. Weitz. A quantitative analysis of contractility in active cytoskeletal protein networks. *Biophys J.*, 94:3136, 2008.

[11] Y. Tanaka-Takiguchi, T. Kakei, A. Tanimura, A. Takagi, M. Honda, H. Hotani, and k. Takiguchi. The elongation and contraction of actin bundles are induced by double-headed myosins in a motor concentration-dependent manner. *J. Mol. Biol.*, 6(341):467–476, 2004.

[12] Anne-Cecile Reymann, Rajaa Boujemaa-Paterski, Jean-Louis Martiel, Christophe Guérin, Wenxiang Cao, Harvey F. Chin, Enrique M. De La Cruz,

Manuel Thery, and Laurent Blanchoin. Actin network architecture can determine myosin motor activity. *Science*, 336(6086):1310–1314, 2012.

[13] T. D. Pollard and W. C. Earnshaw. *Cell Biology*. Elsevier Science, USA, first edition, 2002.

[14] Beta Bugyi and Marie-France Carlier. Control of actin filament treadmilling in cell motility. *Annual Review of Biophysics*, 39(1):449–470, 2010.

[15] T. Svitkina, A. B. Verkhovsky, K. M. McQuade, and G. G. Borisy. Analysis of the actin-myosin ii system in fish epidermal keratocytes: mechanism of cell body translocation. *J. Cell. Biol.*, 139(2):397–415, 1997.

[16] S. Schaub, S. Bohnet, V. M. Laurent, J. J. Meister, and A. B. Verkhovsky. Comparative maps of motion and assembly of filamentous actin and myosin ii in migrating cells. *Mol. Biol. Cell*, 18(10):3723–32, 2007.

[17] M. F. Fournier, R. Sauser, D. Ambrosi, J. J. Meister, and A. B. Verkhovsky. Force transmission in migrating cells. *J. Cell. Biol.*, 188(2):287–97, 2010.

[18] Thomas D Pollard and Gary G Borisy. Cellular motility driven by assembly and disassembly of actin filaments. *Cell*, 112(4):453–465, 2003.

[19] Dimitrios Vavylonis, Qingbo Yang, and Ben O'Shaughnessy. Actin polymerization kinetics, cap structure, and fluctuations. *Proceedings of the National Academy of Sciences of the United States of America*, 102(24):8543–8548, 2005.

[20] Thekla Ohm and Albrecht Wegner. Mechanism of atp hydrolysis by polymeric actin. *Biochimica et Biophysica Acta (BBA) - Protein Structure and Molecular Enzymology*, 1208(1):8 – 14, 1994.

[21] D Pantaloni, T L Hill, M F Carlier, and E D Korn. A model for actin polymerization and the kinetic effects of atp hydrolysis. *Proceedings of the National Academy of Sciences*, 82(21):7207–7211, 1985.

[22] M M Brunett and A E Carlsson. Quantitative analysis of approaches to measuring cooperative phosphate dissociation in polymerized actin. *Biophysical journal*, 103(11):2369–2378, 2012.

[23] Thomas Lecuit, Pierre-Franois Lenne, and Edwin Munro. Force generation, transmission, and integration during cell and tissue morphogenesis. *Annual Review of Cell and Developmental Biology*, 27(1):157–184, 2011.

[24] Maria Shutova, Changsong Yang, Jury M. Vasiliev, and Tatyana Svitkina. Functions of nonmuscle myosin ii in assembly of the cellular contractile system. *PLoS ONE*, 7(7):e40814, 07 2012.

[25] James R Sellers. Myosins: a diverse superfamily. *Biochimica et Biophysica Acta (BBA) - Molecular Cell Research*, 1496(1):3 – 22, 2000.

[26] Eric H. Lee. The titin/telethonin complex - theoretical and computational biophysics group at uiuc, 2006. [Online; accessed 9-August-2012].

[27] Larissa Tskhovrebova and John Trinick. Titin: properties and family relationships. *Nat Rev Mol Cell Biol*, 4:679– 689, 2003.

[28] Henk L. Granzier and Siegfried Labeit. The giant protein titin. *Circulation Research*, 94(3):284–295, 2004.

[29] James A Spudich. The myosin swinging cross-bridge model. *Nat Rev Mol Cell Biol*, 2(5):387–392, 2001.

[30] Wikipedia. Sarcomere — wikipedia, the free encyclopedia, 2012. [Online; accessed 8-August-2012].

[31] M Glotzer. Amnimal cell cytokinesis. *Annual Review of Cell and Developmental Biology*, 17(1):351–386, 2001.

[32] P. Martin and J. Lewis. Actin cables and epidermal movement in embryonic wound healing. *Nature*, 360(6400):179–183, 1992/11/12/print.

[33] K. Kruse and F. Julicher. Self-organization and mechanical properties of active filament bundles. *Phys. Rev. E*, 67:051913, 2003.

[34] M. Lenz, T. Thoresen, M. L. Gardel, and A.R. Dinner. Contractile units in disordered actomyosin bundles arise from f-actin buckling. *Phys. Rev. Lett.*, 108(238107), 2012.

[35] A. E. Carlsson. Contractile stress generation by actomyosin gels. *Phys. Rev. E*, 74(051912), 2006.

[36] Jian-Qiu Wu and Thomas D. Pollard. Counting cytokinesis proteins globally and locally in fission yeast. *Science*, 310(5746):310–314, 2005.

[37] I. Weber, G. Gerisch, C. Heizer, J. Murphy, K. Badelt, A. Stock, J.-M. Schwartz, and J. Faix. Cytokinesis mediated through the recruitment of cortexillins into the cleavage furrow. *EMBO J*, 18:586–594, 1999.

[38] D. Mizuno, C. Tardin, C. F. Schmidt, and F. C. MacKintosh. Nonequilibrium mechanics of active cytoskeletal networks. *Science*, 315(370), 2007.

[39] G. H. Koenderink, Z. Dogic, F. Nakamura, P. M. Bendix, F. C. Mackintosh, J. H. Hartwig, T. P. Stossel, and D. A. Weitz. An active biopolymer network controlled by molecular motors. *PNAS*, 106(36):15192–15197, 2009.

[40] T. Thoresen, M. Lenz, and M. L. Gardel. Reconstitution of contractile actomyosin bundles. *Biophysical journal*, 100:2698 – 2705.

[41] E. D. Korn and J. A. Hammer. Myosins of nonmuscle cells. *Ann. Rev. Biophys. Biophys. Chem*, 17:23–45, 1988.

[42] A. J. Levine and F. C. MacKintosh. Non-equilibrium mechanics and dynamics of motor-activated gelsgeneral mechanism of actomyosin contractility. *Phys. Rev. Lett.*, 100(018104), 2008.

[43] P. Chen and V. B. Shenoy. Strain stiffening induced by molecular motors in active crosslinked biopolymer networks. *Soft Matter*, 7:355–358, 2011.

[44] A. Zemel and A Mogilner. Motor-induced sliding of microtubule and actin bundles. *Phys. Chem. Chem. Phys.*, 11:4821–4833, 2009.

[45] T. B. Liverpool, M. C. Marchetti, J.-F. Joanny, and J. Prost. *Europhys. Lett.*, 85:18007, 2009.

[46] D. A. Head, A. J. Levine, and F. C. Mackintoch. Distinct regimes of elastic response and deformation modes of cross-linked cytoskeletal and semiflexible polymer networks. *Phys. Rev. Lett.*, 68(061907), 2003.

[47] H. Kojima, A. Ishijima, and T. Yanagida. Direct measurement of stiffness of single actin filaments with and without tropomyosin by in vitro nanomanipulation. *Proc. Natl. Acad. Sci.*, 91:12962–12966, 1994.

[48] L. D. Landau and E. M. Lifshitz. *Theory of Elasticity*. Pergamon press, Newyork, third edition, 1986.

[49] M. L. Gardel, M. T. Valentine, J. C. Crocker, A. R. Bausch, and D. A. Weitz. Microrheology of entangled f-actin solutions. *Phys. Rev. Lett.*, 91:158302, Oct 2003.

[50] R. P. Diensthuber, M. Muller, S. M. Heissler, M. H. Taft, I. Chizhov, and D. J. Manstein. Phalloidin perturbs the interaction of human non-muscle myosin isoforms 2a and 2c1 with f-actin. *FEBS Lett.*, 585:767–771, 2011.

[51] T. S. Fraley, C. B. Pereira, T. C. Tran, C. A. Singleton, and J. A. Greenwood. Phosphoinositide binding regulates alpha-actinin dynamics: mechanism for modulating cytoskeletal remodeling. *J. Biol. Chem.*, 280(15):15479–15482, 2005.

[52] D. Vignjevic, S. Kojima, Y. Aratyn, O. Danciu, T. Svitkina, and G. G. Borisy. Role of fascin in filopodial protrusion. *J. Cell. Biol.*, 174(6):863–875, 2006.

[53] R.B. Phillips, J. Kondev, and J. Theriot. *Physical Biology of the Cell.* Garland Science, 2009.

[54] M. L. Gardel, K. E. Kasza, C. P. Brangwynne, J. Liu, and D. A. Weitz. Biophysical tools for biologists, volume two: In vivo techniques. *Methods in Cell. Biol.*, 89:487–519, 2008.

[55] D. Mizuno, C.Tardin, C. F. Schmidt, and F. C. MacKintosh. Nonequilibrium mechanics of active cytoskeletal networks. *Science*, 315, 2007.

[56] L. W. Janson, J. Kolega, and D. L. Taylor. The role of solation-contraction coupling in regulating stress fiber dynamics in nonmuscle cells. *J. Cell. Biol.*, 114:1005–1015, 1991.

[57] A.C. Reymann, R. Boujemaa-Paterski, J.-L. Martiel, C. Guerin, W. Cao, H. F. Chin, E. M. De La Cruz, M. Thery, and L. Blanchoin. Actin network architecture can determine myosin motor activity. *Science*, 336:1310–1314, 2012.

[58] N. L. Dasanayake, P. J. Michalski, and A. E. Carlsson. General mechanism of actomyosin contractility. *Phys. Rev. Lett.*, 107:118101, 2011.

[59] W. H. Press, S.A. Teukolsky, W. T. Vetterling, and B. P. Flannery. *Numerical Recipes in C*. Cambridge University Press, Cambridge, second edition, 1992.

[60] A. Mogilner and G Oster. Cell motility driven by actin polymerization. *Biophys. J.*, 71:3030–3045, 1996.

[61] Q. Yang, X.-F. Zhang, T. D. Pollard, and P. Forscher. Arp2/3 complexdependent actin networks constrain myosin ii function in driving retrograde actin flow. *J. Cell Biol*, 2012.

[62] C. Storm, J. J. Pastore, F. C. MacKintosh, T. C. Lubensky, and P. A. Janmey. Nonlinear elasticity in biological gels. *Nature*, 435(191-194), 2005.

[63] J. R. Shewchuk. An introduction to the conjugate gradient method without the agonizing pain. 1994.

[64] D. G. Luenberger. *Linear and Nonlinear Programing*. Springer, USA, second edition, 2005.

[65] R. Shlomovitz and N. S. Gov. Membrane waves driven by actin and myosin. *Phys. Rev. Lett.*, 98:168103, Apr 2007.

[66] Margaret L. Gardel, Ian C. Schneider, Yvonne Aratyn-Schaus, and Clare M. Waterman. Mechanical integration of actin and adhesion dynamics in cell migration.

[67] B. Geiger, J. P. Spatz, and A. D. Bershadsky. Environmental sensing through focal adhesions. *Nat Rev Mol Cell Biol*, 10:21–33, 2009.

[68] Olivier M Rossier, Nils Gauthier, Nicolas Biais, Wynn Vonnegut, Marc-Antoine Fardin, Philip Avigan, Evan R Heller, Anurag Mathur, Saba Ghassemi, Michael S Koeckert, James C Hone, and Michael P Sheetz. Force generated by actomyosin contraction builds bridges between adhesive contacts.

[69] G.C.H.Chua M. Dembo R. S. Adelstein C. Lo, D. B. Buxton and Y. Wang. Nonmuscle myosin iib is involved in the guidance of fibroblast migration. *Mol. Biol. Cell*, 15:982–989, March 2004.

[70] Y. Cai, N. Biais, G. Giannone, M. Tanase, G. Jiang, J. M. Hofman, C. H. Wiggins, P. Silberzan, A. Buguin, B. Ladoux, and M. P. Sheetz. Nonmuscle myosin iia-dependent force inhibits cell spreading and drives f-actin flow. *Biophysical journal*, 91:3907–3920, Novemner 2006.

[71] Margaret L. Gardel, Benedikt Sabass, Lin Ji, Gaudenz Danuser, Ulrich S. Schwarz, and Clare M. Waterman. Traction stress in focal adhesions correlates biphasically with actin retrograde flow speed. *The Journal of Cell Biology*, 183(6):999–1005, 2008.

[72] Damien Laporte, Nikola Ojkic, Dimitrios Vavylonis, and Jian-Qiu Wu. α-actinin and fimbrin cooperate with myosin ii to organize actomyosin bundles during contractile-ring assembly. *Molecular Biology of the Cell*, 23(16):3094–3110, 2012.

[73] M. L. Gardel, F. Nakamura, J. H. Hartwig, J. C. Crocker, T. P. Stossel, and D. A. Weitz. Prestressed f-actin networks cross-linked by hinged filamins replicate mechanical properties of cells. *Proceedings of the National Academy of Sciences of the United States of America*, 103(6):1762–1767, 2006.

[74] Tseng Y, An KM, and Esue Oand Wirtz D. The bimodal role of filamin in controlling the architecture and mechanics of f-actin networks. *J Biol Chem.*, 279(3):1819–1826, 2004.

[75] Xu J, D. Wirtz, and T. D. Pollard. Dynamic cross-linking by ?-actinin determines the mechanical properties of actin filament networks. *J Biol Chem.*, 273(16):95709576, 1998.

[76] Lior Haviv, David Gillo, Frederic Backouche, and Anne Bernheim-Groswasser. A cytoskeletal demolition worker: Myosin ii acts as an actin depolymerization

agent. *Journal of Molecular Biology*, 375(2):325 – 330, 2008.